Interference Mitigation and Alignment for Interference-Limited Communication Systems

by

Md. Jahidur Rahman

M. E. Sc., The University of Western Ontario, 2010
B. Sc. Engg., Khulna University of Engineering and Technology, 2006

A THESIS SUBMITTED IN PARTIAL FULFILLMENT OF
THE REQUIREMENTS FOR THE DEGREE OF

DOCTOR OF PHILOSOPHY

in

The Faculty of Graduate and Postdoctoral Studies

(Electrical and Computer Engineering)

THE UNIVERSITY OF BRITISH COLUMBIA
(Vancouver)

December 2017

Abstract

With limited availability of the communication spectrum and ever-increasing demands for high-data-rate services, it is natural to reuse the same time-frequency resource to the greatest degree possible. Depending on the nature of transmission and reception of the users, this leads to different instances of interference, e.g., inter-user interference in an interference network and self-interference in a Full-Duplex (FD) transmission. With a goal to mitigate such interference, in this thesis we investigate emerging interference-limited communication systems, such as FD, Device-to-Device (D2D), and Power Line Communication (PLC). To this end, we propose advanced solutions, namely self-interference mitigation and Interference Alignment (IA).

With an objective to reduce the power consumption, we study transceiver design for FD multi-cell Multi-Input Multi-Output (MIMO) systems with guaranteed Quality of Service (QoS). Considering realistic self-interference models and robustness against Channel State Information (CSI) uncertainty, our numerical results reveal transmission scenarios and design parameters for which replacing half-duplex with FD systems is beneficial in terms of power minimization. If the system is not power-constrained, however, a natural objective is to optimize the total throughput given a power budget. Nonetheless, throughput maximization underserves the users that experience poor channels, which leads to QoS unfairness. Therefore, we propose a fair transceiver design for FD multi-cell MIMO systems, which can be implemented in a distributed manner. We further extend our design to enforce robustness against

CSI uncertainty. As a second contribution within this design theme, the concept of robust fair transceiver design is also extended for D2D communications, where unlike the self-interference in FD transmission, the users suffer from strong inter-user interference.

Recognizing that simultaneous multiple connections in PLC contribute to (inter-user) interference-limited communication, we introduce IA techniques for PLC networks, for which the results confirm a significant sum-rate improvement. To overcome the implementation burden of CSI availability for IA techniques, we then study Blind Interference Alignment (BIA) for PLC X-network, and show that the characteristics of the PLC channel thwart simple implementation of this technique via impedance modulation. We therefore resort to a transmission scheme with multiple receiving ports, which can achieve the maximum multiplexing gain for this network.

Lay Summary

The transmission and reception nature of the communication users may lead to different interference scenarios, such as inter-user interference in an interference network and self-interference in a Full-Duplex (FD) transmission. As such, the system performance becomes interference-limited. In this thesis, we investigate emerging interference-limited communication systems, such as FD, Device-to-Device (D2D), and Power Line Communication (PLC), where we exploit advanced solutions, namely self-interference mitigation and Interference Alignment (IA).

The general objective of this research is to devise robust, power-efficient, and fair resource allocation schemes for interference-limited communication systems. To this end, we consider design challenges, such as Channel State Information (CSI) uncertainty, power-efficiency, and Quality of Service (QoS) fairness, which are practically relevant to these communication systems. The contributions of this thesis will advance the next generation communication technologies to meet a variety of communication needs and services.

Preface

The material presented in this thesis is based on research performed by myself under the supervision of Prof. Lutz Lampe in the Department of Electrical and Computer Engineering at the University of British Columbia, Vancouver, Canada.

A co-author of published contributions, Dr. Ali Cagatay Cirik, introduced me to the topic of full-duplex communication, assisted me towards a problem formulation in a publication related to Chapter 3, and also provided feedback on the manuscripts related to full-duplexing in Chapters 2 and 3.

The contributions made by another co-author, Dr. Hamidreza Ebrahimzadeh Saffar, which studies diversity in power line communication reported in a publication related to Chapter 4 is not part of this thesis.

Below is a list of publications related to the work presented in this thesis.

Publications Related to Chapter 2

- Md. Jahidur Rahman, Ali Cagatay Cirik, and Lutz Lampe, "Power-Efficient Transceiver Design for Full-Duplex MIMO Multi-Cell Systems with CSI Uncertainty," *IEEE Access*, vol. 5, pp. 22689-22703, 2017.

Publications Related to Chapter 3

- Ali Cagatay Cirik*, Md. Jahidur Rahman*, and Lutz Lampe, "Robust Fairness Transceiver Design for a Full-Duplex MIMO Multi-Cell System," *in press, IEEE Transactions on Communications*, Nov. 2017. (*equal contribution, listed according to the authors' last name)

- Md. Jahidur Rahman and Lutz Lampe, "Robust Transceiver Optimization for Underlay Device-to-Device Communications," in *Proceedings of IEEE International Conference on Communications (ICC), Track: Signal Processing for Communications*, pp. 7695–7700, Sept. 2015.

Publications Related to Chapter 4

- Md. Jahidur Rahman and Lutz Lampe, "Interference Alignment in Power Line Communications," *in press, Invited contribution in Encyclopedia of Wireless Networks (Section: Interference Characterization and Mitigation)*, S. Shen, X. Lin, and K. Zhang, Eds. Germany: Springer, 2017.

- Md. Jahidur Rahman and Lutz Lampe, "Rate Improvement in MIMO Power Line Communications Through Interference Alignment," *Submitted*, 2017.

- Md. Jahidur Rahman and Lutz Lampe, "Interference Alignment for MIMO Power Line Communications," in *Proceedings of IEEE International Symposium on Power Line Communications and Its Applications (ISPLC)*, pp. 71–76, Apr. 2015.

- Lutz Lampe, Md. Jahidur Rahman, and Hamidreza Ebrahimzadeh Saffar, "Characteristics of Power Line Networks: Diversity and Interference Align-

ment," in *Proceedings of IEEE International Symposium on Power Line Communications and Its Applications (ISPLC)*, pp. 1–6, Apr. 2017.**(Best Paper Award)**

Additional publications from Ph.D. research (not included in this thesis) are provided in Appendix A.

Table of Contents

List of Tables

List of Figures

List of Abbreviations

3GPP	Third Generation Partnership Project
5G	Fifth Generation
ADC	Analog-to-Digital Converter
AWGN	Additive White Gaussian Noise
BIA	Blind Interference Alignment
BS	Base Station
CDF	Cumulative Distribution Function
CPU	Central Processing Unit
CSI	Channel State Information
D2D	Device-to-Device
DAC	Digital-to-Analog Converter
DCP	Difference of Convex Function Programming
DL	Downlink
DoF	Degrees of Freedom
DR	Dynamic Range
ETSI	European Telecommunications Standards Institute
FD	Full-Duplex
FDD	Frequency-Division Duplex
FDMA	Frequency Division Multiple access
HD	Half-Duplex

IA	Interference Alignment
IEEE	Institute of Electrical and Electronics Engineers
LNA	Low Noise Amplifier
LO	Local Oscillator
LOS	Line Of Sight
LTE	Long Term Evolution
LTE-A	LTE-Advanced
Max-SINR	Maximum Signal-to-Interference-Plus-Noise Ratio
MIMO	Multi-Input Multi-Output
Min-IL	Minimum Interference Leakage
MISO	Multi-Input Single-Output
MMSE	Minimum Mean-Squared Error
MS	Mobile Station
MSE	Mean Squared Error
MSR	Maximum Sum-Rate
MU-MIMO	Multi-User MIMO
MUI	Multi-User Interference
NLOS	Non Line Of Sight
OFDM	Orthogonal Frequency Division Multiplexing
PA	Power Amplifier
PLC	Power Line Communication
PSD	Power Spectral Density
PU	Primary User
QoS	Quality of Service
RAM	Random Access Memory

RCP	Remote Centralized Processor
RF	Radio Frequency
SCA	Successive Convex Approximation
SDP	Semidefinite Programming
SDR	Semidefinite Relaxation
SIMO	Single-Input Multi-Output
SINR	Signal-to-Interference-Plus-Noise Ratio
SISO	Single-Input Single-Output
SNR	Signal-to-Noise Ratio
SOCP	Second Order Cone Programming
SU	Secondary User
TDD	Time-Division Duplex
TDMA	Time Division Multiple Access
UL	Uplink
WMMSE	Weighted Minimum Mean-Squared Error
WSR	Weighted Sum-Rate

Notations

$\boldsymbol{A}$	Matrix
$\boldsymbol{a}$	Vector
$\mathbf{I}_N$	N by N identity matrix
$[\mathbf{A}]_{nn}$	n-th row and n-th column of matrix $\mathbf{A}$
$\mathbf{0}_{N\times M}$	N by M zero matrix
$\lvert\cdot\rvert$	Absolute value of a complex number
$(\cdot)^T$	Transpose
$(\cdot)^H$	Hermitian transpose
$\mathrm{vec}(\cdot)$	Vectorization
$\mathcal{CN}(\mu, \sigma^2)$	A complex Gaussian distribution with mean μ and variance σ^2
$\mathbb{C}^{N\times M}$	The set of complex matrices with a dimension of N by M
$\mathbb{E}(\cdot)$	Statistical expectation operator
$\otimes$	Kronecker product
$\lVert\cdot\rVert_2$	l_2-norm
$\lVert\cdot\rVert_F$	Frobenius norm
$\mathrm{diag}(\mathbf{A})$	A diagonal matrix with the same diagonal elements as $\mathbf{A}$
$\mathrm{Tr}(\cdot)$	Trace of a matrix
$\mathrm{rank}(\cdot)$	Rank of a matrix
$\lceil\cdot\rceil$	Upper bound
$\perp$	Statistical independence

$\circ$	Hadamard product or element-wise multiplication
$\lvert\mathcal{S}\rvert$	The cardinality of set $\mathcal{S}$

Acknowledgments

First and foremost, I would like to thank Allah, the Almighty, for giving me the strength, knowledge, and ability to undertake the research in this thesis.

I would like to express my sincere gratitude to my advisor Prof. Lutz Lampe for the support during the course of my Ph.D. His knowledge, work ethic and perseverance are truly inspiring and his guidance has helped me in every stage of my research.

I thank the members of my examining committee at UBC, Professors Vijay K. Bhargava, Vincent Wong, Md. Jahangir Hossain (UBC Okanagan), Karthik Pattabiraman, and Ryozo Nagamune (Mechanical Engineering), for their time and insightful comments. Special thanks go to Professor Rodney Vaughan at the Simon Fraser University for serving as the external examiner, and also for physically participating in the final exam.

I am grateful to Natural Science and Engineering Research Council of Canada and the University of British Columbia for supporting this research partially through an Alexander Graham Bell Canada Graduate Scholarship and a Four Year Doctoral Fellowship, respectively.

My sincere thank goes to Dr. Ali Cagatay Cirik, who was a postdoctoral fellow in our research group, for his time and many fruitful discussions. I also thank my fellow colleagues, to name a few, Naveen, Ayman, Gautham, Hao, in the Communication Theory Lab for numerous technical conversations. Finally, I would like to thank my

mother and my wife, who have been the biggest support during the course of this journey.

Dedication

To my father (who left us on January 11, 2003), my mother and my wife.

Chapter 1

Introduction

1.1 Interference and Noise

Interference and noise are two key performance-limiting factors in many communications systems. Unlike noise, which can be generated internally as well as externally of the communication systems, different instances of interference arise depending on the nature of transmission and reception of the participating users over a given communication medium. One important difference between noise and interference is the fact that interference usually suffers from the same propagation disturbances as the useful signal while the noise level is typically constant, at least over a short time interval [1].

The nature of noise and interference have deep implications on the performance of communication systems. In a noise-limited communication system, such as space communications, performance degradation due to underlying noise cannot be avoided, since generally we do not have control over the noise sources. In contrast, for an interference-limited communication system, as in cellular communications, the very nature of interference facilitate the mitigation and/or cancellation of the same phenomenon via intelligent manipulation over time, space, frequency, or combination of these domains. In this thesis, we focus on intelligent manipulations of different instances of interference so as to improve the performance of interference-limited communication systems.

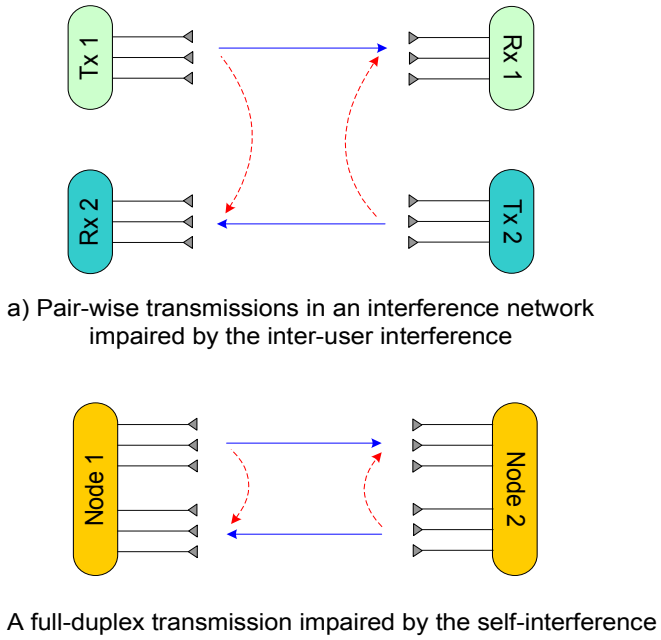

Figure 1.1: Illustrations of interference mechanisms in an interference network and full-duplex transmission.

1.2 Different Interference Mechanisms in Communication Systems

Continuing the discussions from the previous section, here we provide two specific instances of interference that arise due to the nature of transmission and reception over a common communication medium. A commonly studied scenario is an interference network, where transmitters and receivers communicate on a pair basis over a common communication medium. Naturally, the transmission of any given pair will interfere the reception of the other pairs, hence they experience the inter-user interference. As such, the system capacity of these networks is limited by this inter-user interference [2].

Interference may also arise due to simultaneous transmission and reception by

a user over the same frequency band, e.g., in Full-Duplex (FD) transmission. This form of interference is known as the self-interference [3]. More specifically, the self-interference refers to the interference that a transmitting terminal causes to the reception of the desired signal by that terminal. Therefore, the system capacity is limited by the self-interference for this communications scenario. These are illustrated in Figs. 1.1 (a) and (b), which highlight detrimental interference for the data transmission in interference networks and FD communications, respectively.

1.3 Emerging Interference-Limited Communication Systems

With ever-increasing demands for high-data-rate services and limited spectrum, it is natural to aim at transmitting (and/or receiving) at the same time-frequency resource. As presented above, this leads to communication scenarios where users experience different forms of interference in the network. In what follows, we discuss three emerging communication techniques in the context of both wireless and wireline communication systems, where users communicate in the same time-frequency resource leading to inference-limited system performance.

1.3.1 Full-Duplex Transmission

Communication in cellular networks occurs in multipoint-to-point, i.e., users to Base Station (BS), and point-to-multipoint, i.e., BS to users, which are commonly known as uplink and downlink transmissions. This is usually achieved via orthogonalizing the channel, i.e., the BS communicates with users in separate time-frequency resources. Obviously, higher rates could be achieved if the BS and users are able to

communicate (i.e., transmit and receive) simultaneously in the same frequency band. This can be achieved through FD communication [4]. Conventional wireless communication systems that operate in Half-Duplex (HD) transmission mode–commonly known as Time-Division Duplex (TDD) or Frequency-Division Duplex (FDD), employ two orthogonal channels to transmit and receive. Therefore, these transmission techniques cannot achieve the maximal spectral efficiency. FD transceivers have the capability of transmission and reception at the same time over the same frequency band [5, 6], and thus hold the promise to double the link capacity or increase the spectral efficiency due to more flexible access control and networking [7, 8].

While FD communication has been known for many decades, only recently it has attracted renewed attention. One key reason behind this that the traditional approaches to increase spectral efficiency through advanced techniques, such as modulation, coding, multiplexing are thought to be exhausted [5]. Therefore, much research efforts have been put into non-traditional approaches, such as FD communication. However, the major stumbling block for the exploitation of the FD ability of communication devices is the strong self-interference. This is particularly pronounced in conventional cellular systems with large cell sizes, which require a higher transmit power (i.e., causing a stronger self-interference) to compensate for the higher cell-edge path losses. Therefore, the exploitation of the FD ability requires sophisticated interference mitigation techniques to reap the potential benefit of doubling the spectral efficiency.

1.3.2 Device-to-Device Communication

Device-to-Device (D2D) communication enables direct communication between two or more users in cellular networks, with less intervention from the BS or the core

network. In a traditional cellular network, all communications between two users must go through the BS. This protocol suits the scenario in which users are not usually close enough to establish a direct communication between them. However, mobile users these days demand high-data-rate services, such as video sharing. These services can be facilitated with low latency if they could be in range for D2D communications. Therefore, D2D communications in such scenarios can increase the spectral and energy efficiencies of the cellular network by offloading traffic from the core network [9,10]. Furthermore, supported by the trend of proximity-based services for commercial purposes and public safety needs, recently the D2D communication has gained considerable attention from the network operators and the research community [11]. In D2D communications, the interference may result from simultaneous transmissions of other D2D users within the same cell, and possibly from transmissions of D2D users in neighboring cells (e.g., in a multi-cell D2D communication scenario), in addition to the interference originating from conventional cellular transmissions [12]. It is apparent that the system performance of the D2D communication is limited by the underlying inter-user interference in the network, which motivates the study of interference mitigation techniques for this new communication paradigm.

1.3.3 Power Line Communication

Data transmission over power lines is an attractive solution for providing communication services, even in hard-to-reach areas through the reuse of existing power grid infrastructures [13, 14]. The technique permits the seamless implementation of a communication system without the need for an additional wiring infrastructure.

A closer look at the signal transmission over power lines would reveal that the data communication is essentially an unintended broadcast transmission, since the

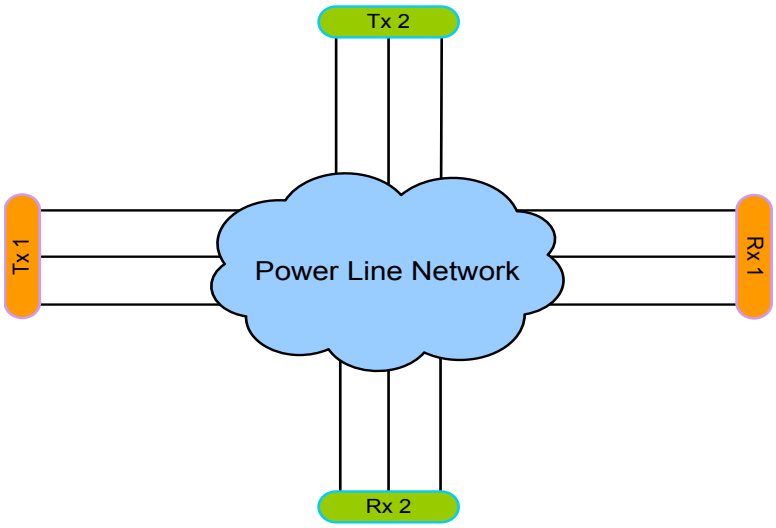

Figure 1.2: An illustration of the PLC interference network, where each transmitter (Tx 1 and Tx 2) communicate to its paired-receiver (Rx 1 and Rx 2, respectively).

communication signals can travel through the electricity grid. As it is illustrated in Fig. 1.2, simultaneous pair-wise data communication (i.e., at the same time-frequency resource) in a PLC network resembles data transmission and interference scenarios in wireless interference networks, similar to the illustration in Fig. 1.1(a). Another communication protocol is illustrated in Fig. 1.3, where each transmit port may have signals intended for each of the receive ports in the network. This is alike the data communication over the wireless X-network [15]. Due to the underlying inter-user interference in the PLC network, the system performance (e.g., sum-rate) becomes interference-limited. These inter-user interference has not been dealt with advanced techniques for PLC networks, such as Interference Alignment (IA) [16–18], which we investigate in this thesis.

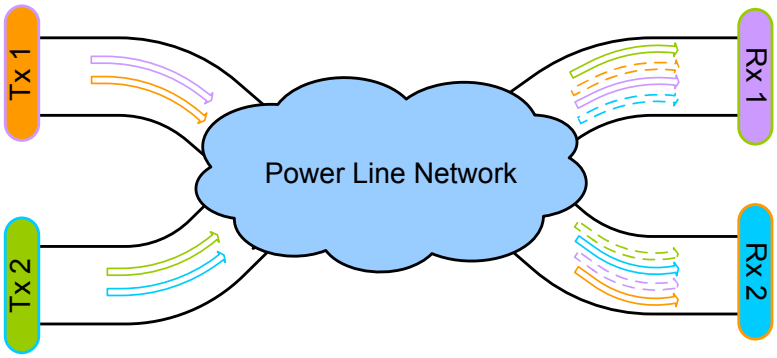

Figure 1.3: An illustration of the PLC X-network, where each transmitter (Tx 1 and Tx 2) has data to transmit to each of the two receivers (Rx 1 and Rx 2) in the network. Solid and dashed arrows denote desired signal and interference, respectively.

1.4 Solutions to Mitigate Interference

While in FD communication the interfering signal may be perfectly known from its own transmission, this is not the case in an interference network, i.e, the other users' signal is not known. Despite knowing the interfering signal, the self-interference in FD communication cannot be canceled completely, mainly due to the channel estimation error and limited Dynamic Range (DR) of the associated components in the transceiver. Therefore, in the case of FD, the (residual) self-interference is the performance limiting factor, while in the interference network it is the inter-user interference that limits the system performance. In the sequel, we discuss two solutions to deal with the self-interference and the inter-user interference in communication networks.

1.4.1 Self-Interference Mitigation

The deployment of the FD communication is facilitated by the recent emergence of short-range communication systems (e.g., small-cell systems), which incurs a lower cell-edge path loss compared to traditional cellular systems. Therefore, the mitigation or reduction of the detrimental self-interference becomes much more manageable [5].

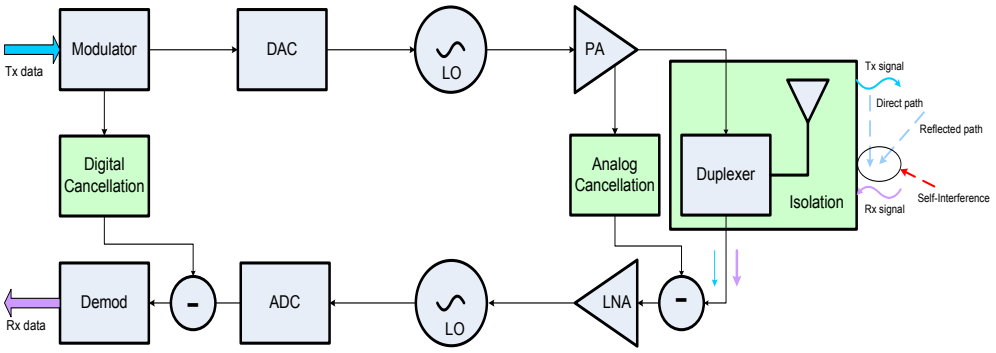

Figure 1.4: An illustration of the self-interference mitigation through interference cancellations at different stages of the FD communication system.

As illustrated in Fig. 1.4, the general idea of the self-interference mitigation is to suppress (e.g., through isolation in the propagation domain) and subtract the dominant part of the self-interference signal in the Radio Frequency (RF) analog domain, so that the remaining signal can be processed for further interference reduction in the baseband, i.e., digital domain [19–22].

As shown in Fig. 1.5, for a small-cell BS which transmits at 24 dBm, and assuming a typical -100 dBm receiver noise floor with 15 dB isolation between the BS transmit and receive antennas, the BS's self-interference will be 109 dB above the noise floor. Obviously, systems with larger cell sizes will suffer a higher self-interference level due to requirement of the increased transmit power. Considering a typical 14-bit Analog-to-Digital Converter (ADC) which results in a DR of 54 dB [5], the system suffers from a residual self-interference of -45 dBm even with a perfect digital domain cancellation, which is 55 dB above the noise floor. This strong self-interference is a major drawback for the exploitation of the FD ability of communication devices.

In recent years, specialized self-interference cancellation techniques along with

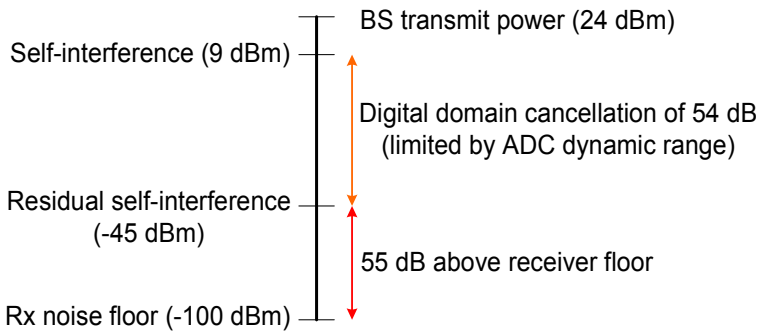

Figure 1.5: An illustration of the residual self-interference due to limited ADC dynamic range in a typical small-cell full-duplex communication.

promising results from experimental research have demonstrated adequate levels of isolation between transmitting and receiving signals [23–25]. Nevertheless, such techniques are far from perfect owing to imperfections of associated radio components, such as non-ideal Power Amplifier (PA) and Low Noise Amplifier (LNA), Local Oscillator (LO), ADC and Digital-to-Analog Converter (DAC) [26]. Further challenges arise due to inaccurate Channel State Information (CSI) in the interference paths, which makes complete cancellation of the self-interference unattainable [27].

1.4.2 Interference Alignment

Generally, there are three common ways to deal with the inter-user interference in communication networks. First, if the interference is strong, the interfering signal can be decoded, and hence the desired signal can be separated [28]. Second, when the interference is weak, the interfering signal can be treated as an additional noise [29]. On the other hand, when the strength of the interference is comparable to the desired signal, the conventional wisdom is to avoid the interference by orthogonalization of the communication medium either in time or frequency domain. An extensive

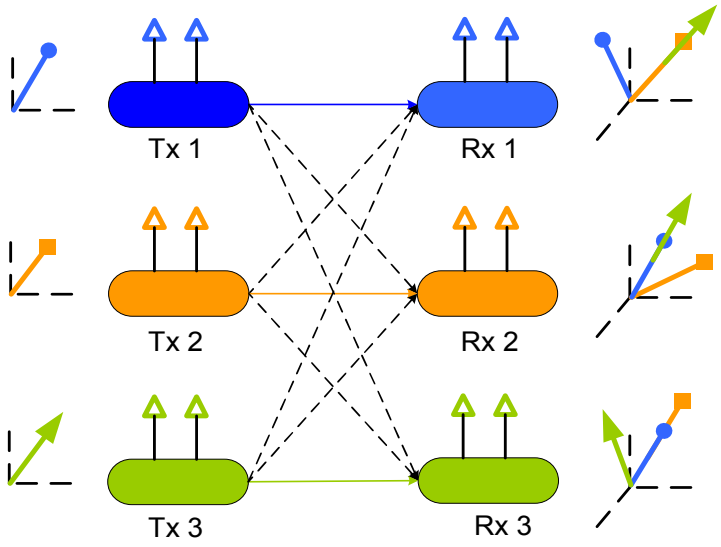

Figure 1.6: An illustration of the interference alignment for a 3-user MIMO wireless interference network over two spatial signaling dimensions.

use of this technique is found in time or frequency division multiple access based communication systems [30, 31]. Such an orthogonal medium access makes sure that multiple users can access the channel without creating interference to each other. The access mechanism can be considered as a cake-cutting measure, where each user gets only a portion of the communication resources depending on the number of participating users. For example, if there are K participating user-pairs in the network, they can only receive $\frac{1}{K}$ portion of the total communication resources. On the other hand, if they communicate at the same time-frequency resource as in an interference network, there will be $K-1$ interfering signals. In general, K signaling dimensions will be needed to recover the desired signal. The fundamental question is, how many signaling dimensions are really needed to resolve the desired signal from the remaining $K-1$ interfering signals? Alternatively, is it possible to recover the desired signal within a reduced signaling dimensions?

In order to circumvent the above under-determined problem, the notion of IA was introduced as an approach to maximize interference-free signal space for the desired user [16–18]. If the interference signals could be consolidated into a smaller subspace so that they do not span the entire signal space at the receiver and at the same time, the desired signal could avoid falling into the interference space, it may be possible to recover the desired signal interference-free. This is done via the technique of IA. In essence, IA allows interfering users to transmit simultaneously by consolidating the space spanned by the interference at receivers within a small number of signaling dimensions, while keeping the desired signals separable from interference so that they can be projected into the null space of interference, and recovered interference-free. The alignment of the interference can be obtained in time domain (e.g., via symbol extension), in frequency domain (e.g., over multiple subchannels), or in spatial domain (e.g., via multiple antennas) [32]. For example, Fig. 1.6 illustrates the IA for a 3-user Multi-Input Multi-Output (MIMO) wireless interference network over two spatial signaling dimensions. The idea is considered to be a breakthrough since now the interference networks, such as D2D and power line communications considered in this thesis, can achieve a much higher rate employing the technique of IA.

1.5 Design Challenges

In this section, we highlight relevant design challenges for emerging interference-limited communication systems that we investigate in this thesis. To this end, we focus on design aspects that are pertinent to practical implementations of these communications systems.

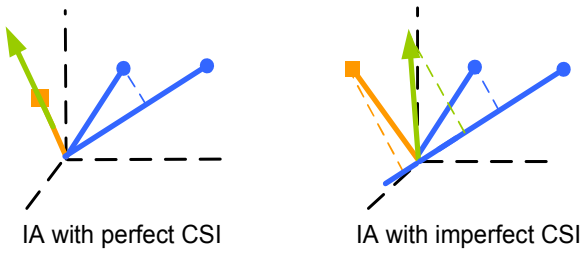

Figure 1.7: An illustration of the impact of imperfect CSI on the performance of IA.

1.5.1 Imperfect CSI

The availability of CSI greatly simplifies the design of communication systems. As for IA, it is essential to precode the transmitted signals such that the interfering signals are aligned at the corresponding receivers, while the desired signal can be decoded interference-free. This necessitates the availability of the CSI, as such, the performance of IA is limited by quality of the CSI. As it is illustrated on the left side of Fig. 1.7, the IA design with perfect CSI would facilitate exact alignment of two interfering signals in one dimension, and therefore, the desired signal can be recovered inference-free on the second dimension (i.e., no projection of the interfering signals onto the signal subspace). On the other hand, imperfect CSI would lead to transmit and receive filters not being designed properly. As shown on the right side of Fig. 1.7, this will cause the interference signals projection onto the signal subspace, which results in a degradation of the Signal-to-Interference-Plus-Noise Ratio (SINR) [33]. Similarly, the performance gains offered by FD communication depend on the availability of the CSI. In particular, the availability of the CSI will determine the quality of the self-interference cancellation, and hence the overall performance gain over an HD system [34].

Depending on whether the quality of CSI is limited by estimation or quantization,

one of two models of CSI uncertainty is usually adopted to develop robust transmission techniques [35]. A Bayesian model assumes that the statistics of the CSI error due to estimation noise are known. Different from this, bounded models consider that the error belongs to a predefined bounded uncertainty region, with no further assumption on the statistical properties.

1.5.2 Power-Efficiency

Transmit power is an important design parameter to evaluate the overall system performance, especially in power-constrained applications [36]. This has also been emphasized for interference-limited communication systems (e.g., in cellular communications), since reducing transmit power has obvious benefits, such as reduced interference for wireless networks and lower cost for wireless devices [37, 38]. These are even more pronounced for FD wireless devices as they consume more power due to additional components and processing involved with the self-interference mitigation [27, 39]. With increasing emphasis on incorporating energy awareness in Fifth Generation (5G) communication systems [40], in which the FD communication is also considered as a key technology [41], in this thesis we study power-efficient resource allocation techniques for FD communications.

1.5.3 Fairness

For cellular communications, the total throughput maximization is optimal if the goal is to maximize combined sum-rates of the uplink and downlink transmissions. One giveaway of this approach is that users that experience good channels will be allocated all the resources [42–45]. For example, in an FD cellular system, as the self-interference power increases, it starts overwhelming the desired signals coming from

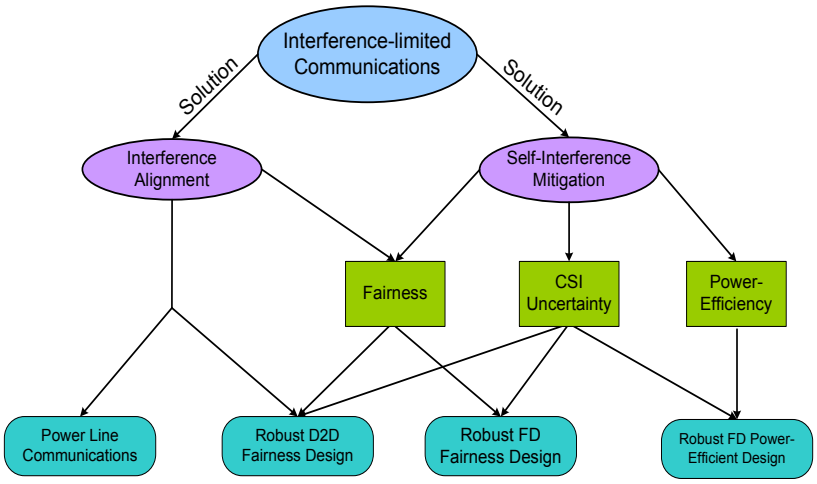

Figure 1.8: A flow diagram of research problems addressed in this thesis (denoted by rounded rectangles) for interference-limited communication systems considering practical design challenges (denoted by rectangles) through the interference alignment and self-interference mitigation techniques.

the uplink users, which reduces the achievable rate in the uplink channel. Therefore, reducing the transmit power in the uplink channel and concentrating on the downlink channel is more beneficial to optimize the system sum-rate. In this case, uplink users are not served, i.e., all the resources are devoted for the downlink transmission, which results in unfairness. The situation is compounded in multi-cell FD systems, where additional interference sources exist, which will degrade the performance of the users, especially for the ones at the cell-edge. Therefore, it is important to ensure satisfactory performance among all the users in the network, which motivates us to consider fairness design in emerging FD and D2D communications.

1.6 Major Contributions and Thesis Outline

The general objective of this research is to devise robust, power-efficient, and fair resource allocation schemes for interference-limited communication systems. As de-

picted in Fig. 1.8, we are concerned with interference-limited communications systems, specifically FD, D2D, and power line communications. To this end, we consider design challenges, such as CSI uncertainty, power-efficiency, and fairness considerations, which are practically relevant to these communication systems. As for solutions, we concentrate on two sophisticated techniques, i.e., self-interference mitigation and interference alignment. Where possible, we strive to devise low-complexity solutions for optimizing the system performance.

1.6.1 Major Contributions of the Thesis

Our contributions in this thesis are summarized as follows.

- **Power-Efficient Transceiver Design for FD Communication Systems.** Motivated by reducing power consumption for FD wireless devices, we explore power-efficient transmit and receiver beamforming designs for an FD MIMO multi-cell system. In particular, we assume that BSs operating in FD transmission mode serve multiple FD mobile users at the same time over the same frequency band. To guarantee a certain Quality of Service (QoS), we enforce maintenance of a minimum SINR for each user. Concerning these design constraints together with realistic FD self-interference models, we investigate the transmit and receive beamforming designs that minimize the joint transmission power of BSs and users. The non-convex precoder design problem is posed as a Difference of Convex Function Programming (DCP), which can be efficiently solved via Successive Convex Approximation (SCA). Owing to the FD transmission both at BSs and users, our design approach considers a comprehensive system model that includes I) the self-interference at each FD BS and FD user, II) the interference among adjacent BSs, i.e., inter-BS interference, and III) the

interference among all the mobile users in all cells, where other cellular communication scenarios can be derived as a subset of this system model. In order to account for practical design aspects, we consider modeling of the CSI uncertainties to propose both statistical and worst-case designs. Our contributions toward this research theme has been published in [46].

- **Fairness Considerations in FD and D2D Communication Systems.** Performance fairness is an important design consideration in interference-limited communication systems. We realize that the existing works on FD cellular systems focus on the maximization of overall throughput, which results in unfairness between uplink and downlink channels depending on the self-interference power and inter-user interference levels. Therefore, we consider the transmit and receive beamforming designs that maximize the SINRs in the uplink and downlink channels to introduce fairness among the users in an FD MIMO multi-cell system. To this end, we formulate the fairness problem as a harmonic-sum maximization approach, in an attempt to draw a balance between total user throughput and fairness, and the solution allows for distributed computations of the beamformers. In order to address practical design aspects, we consider the transceiver design that enforces robustness against imperfect CSI while providing fair performance among FD users. The robust fairness design problem is handled via a low-complexity iterative algorithm based on alternating optimization and the Semidefinite Relaxation (SDR) technique. Our contribution toward this design theme has been accepted for publication in [47].

  As a second contribution within this design theme, we study robust fairness transceiver design for another emerging interference-limited communication system, such as D2D communications, where the main challenge lies in dealing with

the inter-user interference. To this end, we assume the D2D users employ IA to mitigate the inter-user interference. We consider that the multi-antenna D2D users in the cellular network operate as secondary users via underlay cognitive transmission, where its transmission is constrained by the interference power constraint that is enforced by the primary network (i.e., macrocell). Similar to the previous design problem for FD communications, this design problem is tackled via an alternating optimization and the SDR technique. We claim that this study is the first to investigate a robust transceiver design in the context of underlay D2D communications. Our research work in this regard has been published in [48].

- **Interference Alignment for Power Line Communications.** With complete lack of advanced interference mitigation techniques in the context of PLC, we focus on investigating IA techniques for this interference-limited communication system, where the system performance is limited by the underlying inter-user interference. We claim that this thesis is the first to consider such advanced interference mitigation techniques in the context of PLC networks. To begin with, we consider different MIMO PLC interference networks to study the feasibility of IA and evaluate the performance in terms of system sum-rate for these setups in the presence of Additive White Gaussian Noise (AWGN). However, unlike most communications, noise in MIMO PLC is often found to be spatially correlated. Concerning this, we also study the performance of the IA for MIMO PLC networks in the presence of practical measured noise, and specifically investigate the impact of spatial noise correlation. Another contribution toward this research direction is to study the Blind Interference Alignment (BIA) for PLC X-networks, which works without requiring CSI at the transmitter. In

particular, we investigate network configurations, where seemingly simple realization of the BIA through impedance modulation is not achievable for the PLC X-network. This is followed by proposal of a transmission scheme that enables the implementation of the BIA for the PLC X-networks. Our contribution toward this research direction has been submitted for publication in [49] and accepted/published in [50–52].

1.6.2 Organization of the Thesis

The thesis is structured around the list of contributions in the previous section and is organized as follows.

In Chapter 1, we provide essential backgrounds on interference-limited communication systems and also introduce a few emerging instances of such systems that are investigated in this thesis. We then discuss design challenges in the specific context of these interference-limited communication systems to motivate our research. This is followed by introduction of relevant solutions so as to mitigate interference in these communication systems.

Chapter 2 focuses on the design of a power-efficient resource allocation technique for FD communication systems. To guarantee a certain QoS and considering realistic FD self-interference models, we investigate joint sum-power minimization of BSs and users. Noting that the resulting optimization problem is NP-hard, we then divide this optimization problem into separate receive and transmit beamforming design steps, which can be solved iteratively. Practical design aspects are taken into account by way of stochastic and bounded uncertainties. Based on simulation parameters from the Third Generation Partnership Project (3GPP) standardization body, numerical results suggest that FD systems generally outperform HD ones under a wide range

of QoS constraints and transceiver distortions.

Chapter 3 considers the fairness problem in both FD and D2D communications. We begin by considering an FD MIMO multi-cell system to provide fairness in the form of SINR maximization in the uplink and downlink channels. We then propose an alternating optimization algorithm to tackle the problem. Thereafter, we consider the worst-case transceiver design under bounded CSI uncertainty. Numerical results verify the improved fairness performance when compared with other algorithms and confirm the robustness against the CSI uncertainty.

In the second part of this chapter, we study robust transceiver optimization for D2D communications that aims for SINR fairness among D2D users, similar to the previous robust design problem for FD communications. Numerical simulations demonstrate the performance of the proposed transceiver compared to the benchmark case of an IA system without primary network/macrocell (non-cognitive). We observe that at low SNR and high CSI error with relaxed interference power constraint, the worst-case stream data rate of the D2D users are close to that of the users in non-cognitive IA system but performance degrades significantly with stringent interference power constraint.

In Chapter 4, we study IA techniques for different PLC networks. Assuming AWGN, we first consider different MIMO PLC interference networks and exploit iterative Minimum Interference Leakage (Min-IL) and Maximum Signal-to-Interference-Plus-Noise Ratio (Max-SINR) algorithms to study the IA feasibility and sum-rate performances. Our results show that the sum-rate of the PLC networks can be significantly improved through the exploitation of Max-SINR algorithm. In particular, it is found that at high Signal-to-Noise Ratio (SNR) the performance gain in terms of sum-rate with IA over orthogonal transmission techniques is around 30% for a 3-user

2×2 MIMO PLC network. We then study the performance of the IA for MIMO PLC networks with practical measured noise, and also investigate the impact of spatial noise correlation. To this end, we choose Max-SINR as a candidate algorithm which is known to offer the best performance in terms of sum-rate, but susceptible to noise statistics. Unlike channel correlation in MIMO communications, our results suggest that noise correlation actually helps to improve the system performance. We then focus on the BIA to study its feasibility and propose a transmission scheme that facilitates the implementation of this technique for PLC X-networks. The results suggest that the maximum multiplexing gain can be achieved exploiting the proposed transmission scheme.

Finally, the conclusions and potential avenues for further research related to topics studied in this thesis are presented in Chapter 5. To this end, we stress on decentralized algorithm designs for FD communication systems. We then emphasize studying more inclusive communication scenarios for the D2D communication. Finally, in this chapter we discuss relevance and potential benefits of CSI feedback reduction for IA in PLC networks.

Chapter 2

Power Minimization in Full-Duplex Communication Systems

2.1 Introduction

While the potential benefits of FD systems are easy to foresee, the implementation of these systems poses significant challenges. For example, since an FD system relies on simultaneous transmission and reception, one major drawback for the exploitation of FD ability is the strong self-interference at the front-end of the receiver caused by the signal leakage from the transmit antennas to its receive antennas. Although sophisticated self-interference cancellation techniques may achieve certain levels of isolation between transmitting and receiving signals [20,21], they are far from perfect due to imperfections of radio components, such as amplifier non-linearity and oscillator phase noise [26]. Furthermore, due to inherent inaccuracy in the CSI estimation of the associated interference paths, the complete cancellation of the self-interference cannot be achieved [34]. Therefore, the system optimization in the context of FD communications under the residual self-interference were studied in [53–56], and the references therein.

Owing to increased spectral efficiency and recent advances in hardware design, FD communication has been investigated for point-to-point MIMO systems in [34,55–59] and for single-cell systems in [60–63]. However, these studies assumed HD users and

did not account for the signal distortion caused by non-ideal amplifiers, oscillators, ADCs, and DACs. FD communication has also been studied for multi-cell MIMO systems [64–67]. The works [64–66] focused on the optimization of system sum-rate while [67] considered user selection with power control. The minimization of transmit power has not been a design criterion, e.g., in [64–67].

As we discussed in Chapter 1, the reduction of transmit power of the wireless devices is beneficial since it also translates to the reduction of associated interference in wireless networks and lower cost of production for these devices [37, 38]. In the specific context of FD communications, the mitigation of the self-interference requires additional components and processing power, hence FD devices consume relatively more power [27, 39]. As there is an increasing emphasis on the design approach that incorporates energy awareness [11], the design of power-efficient FD transceivers has recently been studied considering the sum-power minimization in the context of interference channels [58, 59] and relay networks [34]. In this chapter, we consider the sum-power minimization design approach for FD MIMO multi-cell systems. In particular, we investigate the problem of minimizing the joint transmit power at BSs and users while meeting QoS requirements in the form of SINR. As illustrated in Fig. 2.1, because of the FD transmission both at BSs and users, our design approach considers I) the self-interference at each FD BS and FD user, II) the interference among adjacent BSs, i.e., inter-BS interference, and III) the interference among all the mobile users in all cells. In addition, we consider transmitter and receiver distortions caused by non-ideal amplifiers, oscillators, ADCs, and DACs in our study. Although the resulting optimization problem is non-convex and NP-hard, we can represent it as a DCP, which can be solved via SCA [68–71]. While the global optimality cannot be guaranteed, the objective value in SCA converges monotonically as it is improved

with each iteration. Within this context, in the first part of this chapter, our goal is to understand under what conditions replacing HD systems with FD ones may be beneficial for the power minimization.

This will be expanded in the second part of the chapter to consider the CSI uncertainty, similar to previous studies on FD communications in the context of cognitive radio [72, 73], physical layer security [74–76], point-to-point MIMO communication [77], and single-cell multi-user system [78]. To this end, we present robust designs for the power-minimization FD operation considering both stochastic and bounded CSI uncertainties. Numerical results confirm that the proposed FD designs achieve power savings compared to an HD setup and a non-robust design, under a wide range of QoS constraints and signal distortions at the transceiver.

The rest of this chapter is organized as follows. The system model is presented in Section 2.2. The power-minimization FD transceiver design assuming perfect CSI is derived in Section 2.3. This is extended to the case of imperfect CSI in Section 2.4. Numerical results and discussions are provided in Section 2.5. Finally, we summarize our findings in Section 2.6.

2.2 System Model

In this section, we discuss the system model for an FD MIMO multi-cell system.

2.2.1 Signal Model

We consider an FD cellular communication scenario having K cells, where cell k has one BS k, $k = 1, \ldots, K$, as illustrated in Fig. 2.1. We assume that each BS, k is equipped with M_k transmit and N_k receive antennas, and serves I_k users in its cell. We denote i_k to be the ith user in cell k, equipped with M_{i_k} transmit

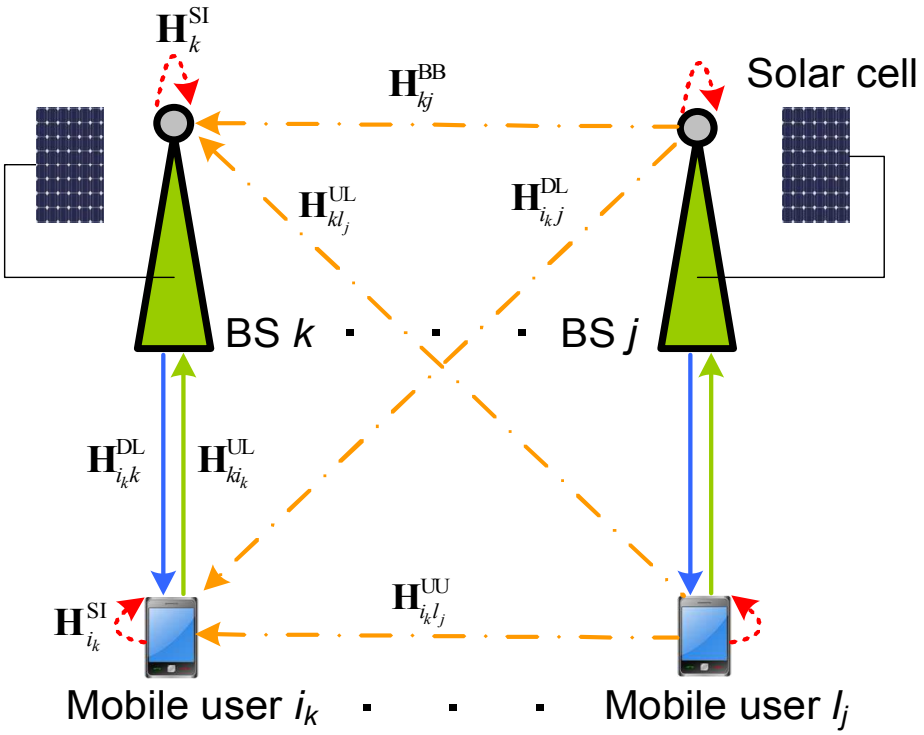

Figure 2.1: An illustration of a power-constrained FD MIMO multi-cell system with solar-powered BSs. Dashed arrows denote the self-interference and dash-dotted arrows denote the interference between different nodes. Solid lines denote the desired signals in the uplink and downlink transmissions.

and N_{i_k} receive antennas. We define the set of BSs as $\mathcal{K} = \{1, \ldots, K\}$ and users as $\mathcal{I} = \{i_k \mid k \in \{1, 2, \ldots, K\},\ i \in \{1, 2, \ldots, I_k\}\}$. We view $\mathbf{H}_{i_kj}^{\mathrm{DL}} \in \mathbb{C}^{N_{i_k} \times M_j}$ as the channel between BS j and user i_k in the downlink transmission, $\mathbf{H}_{kl_j}^{\mathrm{UL}} \in \mathbb{C}^{N_k \times M_{l_j}}$ as the channel between BS k and user l_j in the uplink transmission, $\mathbf{H}_{i_kl_j}^{\mathrm{UU}} \in \mathbb{C}^{N_{i_k} \times M_{l_j}}$ as the interference channel from the user l_j to the user i_k, $\mathbf{H}_{kj}^{\mathrm{BB}} \in \mathbb{C}^{N_k \times M_j}$ as the interference channel from the BS j to the BS k, $\mathbf{H}_k^{\mathrm{SI}} \in \mathbb{C}^{N_k \times M_k}$ and $\mathbf{H}_{i_k}^{\mathrm{SI}} \in \mathbb{C}^{N_{i_k} \times M_{i_k}}$ as the self-interference channel from the transmit antennas to the receive antennas for the BS k and user i_k, respectively.

The availability of the CSI is crucial in maximizing the gains offered by the FD transmission. We note that there are three types of CSI involved in the system

design, i.e., I) BSs to users ($\mathbf{H}^{\mathrm{DL}}_{i_k j}$) or users to BSs ($\mathbf{H}^{\mathrm{UL}}_{k l_j}$) channels, II) BSs to BSs ($\mathbf{H}^{\mathrm{BB}}_{kj}$) channels, and III) users to users ($\mathbf{H}^{\mathrm{UU}}_{i_k l_j}$) channels. Considering, for example a 3GPP Long Term Evolution (LTE) system, each BS broadcasts the cell-specific reference signal, including its cell identity [79]. Therefore, BSs to users channels can be estimated from the received reference signal at each user. Users then report the CSI via control and/or shared channels to the BSs [79]. Hence, type I channels can be estimated, e.g., assuming channel reciprocity. The same cell-specific reference signal can be used at other BSs to estimate the type II channels [67]. The type III channels are difficult to obtain as there is no direct signaling between users. However, the channel estimation between users can be facilitated via neighbor discovery at each user through the use of sounding reference signal in 3GPP LTE system [80]. Similar mechanisms to estimate channels between users have been proposed for D2D communications [81].

2.2.2 Precoding

Each user i_k in the uplink and downlink channels sends symbols, $\mathbf{s}^{\mathrm{UL}}_{i_k} \in \mathbb{C}^{d^{\mathrm{UL}}_{i_k} \times 1}$ and $\mathbf{s}^{\mathrm{DL}}_{i_k} \in \mathbb{C}^{d^{\mathrm{DL}}_{i_k} \times 1}$, respectively, where $d^{\mathrm{UL}}_{i_k}$ and $d^{\mathrm{DL}}_{i_k}$ are the number of data streams in the respective direction. We assume that the symbols are independent and identically distributed (i.i.d.) with unit power, i.e., $\mathbb{E}\left[\mathbf{s}^{\mathrm{UL}}_{i_k}\left(\mathbf{s}^{\mathrm{UL}}_{i_k}\right)^H\right] = \mathbf{I}_{d^{\mathrm{UL}}_{i_k}}$ and $\mathbb{E}\left[\mathbf{s}^{\mathrm{DL}}_{i_k}\left(\mathbf{s}^{\mathrm{DL}}_{i_k}\right)^H\right] = \mathbf{I}_{d^{\mathrm{DL}}_{i_k}}$, for the uplink and downlink transmissions, respectively. Together with the transmit beamforming matrices $\mathbf{V}^{\mathrm{UL}}_{i_k} = \left[\mathbf{v}^{\mathrm{UL}}_{i_k,1}, \ldots, \mathbf{v}^{\mathrm{UL}}_{i_k,d^{\mathrm{UL}}_{i_k}}\right] \in \mathbb{C}^{M_{i_k} \times d^{\mathrm{UL}}_{i_k}}$ and $\mathbf{V}^{\mathrm{DL}}_{i_k} = \left[\mathbf{v}^{\mathrm{DL}}_{i_k,1}, \ldots, \mathbf{v}^{\mathrm{DL}}_{i_k,d^{\mathrm{DL}}_{i_k}}\right] \in \mathbb{C}^{M_k \times d^{\mathrm{DL}}_{i_k}}$ in the uplink and downlink channels, the transmitted signals of the user i_k and BS k can be written as, $\mathbf{x}^{\mathrm{UL}}_{i_k} = \mathbf{V}^{\mathrm{UL}}_{i_k}\mathbf{s}^{\mathrm{UL}}_{i_k}$ and $\mathbf{x}^{\mathrm{DL}}_{k} = \sum_{i=1}^{I_k} \mathbf{V}^{\mathrm{DL}}_{i_k}\mathbf{s}^{\mathrm{DL}}_{i_k}$, respectively. For convenience, we collect all beamforming vectors, $\mathbf{v}^{X}_{i_k,m},\ i_k \in \mathcal{I},\ m \in \mathcal{M},\ X \in \{\mathrm{UL}, \mathrm{DL}\}$ in the stacked vector $\mathbf{v}$, where $\mathcal{M}$ denotes

the set of the data streams.

2.2.3 Received Signals

As mentioned earlier, we take into account the limited DR at FD nodes [26], which has also been applied in [53, 54, 56, 57, 65]. Essentially, non-ideal components, such as amplifiers, oscillators, ADCs and DACs contribute to limited DR. To model the limited receiver DR, an additive white Gaussian receiver distortion with a variance equal to β times the power of the undistorted received signal is injected at each receive antenna [82]. Similarly, an additive white Gaussian transmitter noise with a variance equal to κ times the power of the intended transmit signal is injected at each transmit antenna to model the limited transmitter DR [83]. Considering the limited DR, the signals received by the BS k and that received by the user i_k, can be respectively written as

$$\mathbf{y}_k^{\mathrm{UL}} = \sum_{j=1}^{K}\sum_{l=1}^{I_j} \mathbf{H}_{kl_j}^{\mathrm{UL}}\mathbf{x}_{l_j}^{\mathrm{UL}} + \mathbf{H}_k^{\mathrm{SI}}\left(\mathbf{x}_k^{\mathrm{DL}} + \mathbf{c}_k^{\mathrm{DL}}\right) + \sum_{j=1, j\neq k}^{K} \mathbf{H}_{kj}^{\mathrm{BB}}\mathbf{x}_j^{\mathrm{DL}} + \mathbf{e}_k^{\mathrm{UL}} + \mathbf{n}_k^{\mathrm{UL}}, \quad (2.1)$$

$$\mathbf{y}_{i_k}^{\mathrm{DL}} = \sum_{j=1}^{K} \mathbf{H}_{i_k j}^{\mathrm{DL}}\mathbf{x}_j^{\mathrm{DL}} + \mathbf{H}_{i_k}^{\mathrm{SI}}\left(\mathbf{x}_{i_k}^{\mathrm{UL}} + \mathbf{c}_{i_k}^{\mathrm{UL}}\right) + \sum_{(l,j)\neq(i,k)} \mathbf{H}_{i_k l_j}^{\mathrm{UU}}\mathbf{x}_{l_j}^{\mathrm{UL}} + \mathbf{e}_{i_k}^{\mathrm{DL}} + \mathbf{n}_{i_k}^{\mathrm{DL}}, \quad (2.2)$$

where $\mathbf{n}_k^{\mathrm{UL}} \in \mathbb{C}^{N_k\times 1}$ and $\mathbf{n}_{i_k}^{\mathrm{DL}} \in \mathbb{C}^{N_{i_k}\times 1}$ denote the AWGN vector with zero mean and unit covariance matrix at the BS k and user i_k, respectively. In (2.2), $\mathbf{c}_{i_k}^{\mathrm{UL}} \in \mathbb{C}^{M_{i_k}\times 1}$ is the signal distortion at the transmitter antennas of user i_k, which models the effect of limited DR to account for transmitter chain inaccuracies. Unlike the thermal noise components, the covariance matrix of $\mathbf{c}_{i_k}^{\mathrm{UL}}$ depends on the power of the transmit antenna. It is modeled as $\mathbf{c}_{i_k}^{\mathrm{UL}} \sim \mathcal{CN}\left(\mathbf{0}, \kappa\,\mathrm{diag}\left(\mathbf{V}_{i_k}^{\mathrm{UL}}\left(\mathbf{V}_{i_k}^{\mathrm{UL}}\right)^H\right)\right), \mathbf{c}_{i_k}^{\mathrm{UL}} \perp \mathbf{x}_{i_k}^{\mathrm{UL}}$ [26].

In (2.2), $\mathbf{e}_{i_k}^{\mathrm{DL}} \in \mathbb{C}^{N_{i_k}\times 1}$ is the additive receiver distortion at the receiver antennas of user i_k. Similar to the transmitter side, it models the effect of lim-

ited DR to account for the receiver chain inaccuracies, and modeled as $\mathbf{e}_{i_k}^{\mathrm{DL}} \sim \mathcal{CN}\left(\mathbf{0}, \beta \mathrm{diag}\left(\mathbf{\Phi}_{i_k}^{\mathrm{DL}}\right)\right), \mathbf{e}_{i_k}^{\mathrm{DL}} \perp \mathbf{\Theta}_{i_k}^{\mathrm{DL}}$ [26], where $\mathbf{\Phi}_{i_k}^{\mathrm{DL}} = \mathrm{Cov}\{\mathbf{\Theta}_{i_k}^{\mathrm{DL}}\}$ and $\mathbf{\Theta}_{i_k}^{\mathrm{DL}}$ is the undistorted received vector at the user i_k, i.e., $\mathbf{\Theta}_{i_k}^{\mathrm{DL}} = \mathbf{y}_{i_k}^{\mathrm{DL}} - \mathbf{e}_{i_k}^{\mathrm{DL}}$. In (2.1), $\mathbf{c}_k^{\mathrm{DL}}$ and $\mathbf{e}_k^{\mathrm{UL}}$ are the transmitter and receiver distortion at the BS k, respectively, which are modeled similarly. Furthermore, we note that as the FD nodes know their own transmit signals and the self-interference channel, the terms $\mathbf{H}_k^{\mathrm{SI}}\mathbf{x}_k^{\mathrm{DL}}$ and $\mathbf{H}_{i_k}^{\mathrm{SI}}\mathbf{x}_{i_k}^{\mathrm{UL}}$ can be cancelled from the received signal $\mathbf{y}_k^{\mathrm{UL}}$ at the kth BS and $\mathbf{y}_{i_k}^{\mathrm{UL}}$ at the i_kth user, respectively [26]. We denote the self-interference free received signals as $\tilde{\mathbf{y}}_k^{\mathrm{UL}}$ and $\tilde{\mathbf{y}}_{i_k}^{\mathrm{UL}}$, respectively.

2.2.4 Decoding

We make use of linear decoders, $\mathbf{U}_{i_k}^{\mathrm{UL}} = \left[\mathbf{u}_{i_k,1}^{\mathrm{UL}}, \ldots, \mathbf{u}_{i_k,d_{i_k}^{\mathrm{UL}}}^{\mathrm{UL}}\right] \in \mathbb{C}^{N_k \times d_{i_k}^{\mathrm{UL}}}$, and $\mathbf{U}_{i_k}^{\mathrm{DL}} = \left[\mathbf{u}_{i_k,1}^{\mathrm{DL}}, \ldots, \mathbf{u}_{i_k,d_{i_k}^{\mathrm{DL}}}^{\mathrm{DL}}\right] \in \mathbb{C}^{N_{i_k} \times d_{i_k}^{\mathrm{DL}}}$, to process the received signals at the BS k and user i_k, respectively. Then the estimates of data streams of user i_k in the uplink and downlink channels are obtained as, $\hat{\mathbf{s}}_{i_k}^{\mathrm{UL}} = \left(\mathbf{U}_{i_k}^{\mathrm{UL}}\right)^H \tilde{\mathbf{y}}_k^{\mathrm{UL}}$ and $\hat{\mathbf{s}}_{i_k}^{\mathrm{DL}} = \left(\mathbf{U}_{i_k}^{\mathrm{DL}}\right)^H \tilde{\mathbf{y}}_{i_k}^{\mathrm{DL}}$, respectively. Again, for convenience, we collect all decoding vectors, $\mathbf{u}_{i_k,m}^X,\ i_k \in \mathcal{I},\ m \in \mathcal{M},\ X \in \{\mathrm{UL}, \mathrm{DL}\}$ in the stacked vector $\mathbf{u}$.

2.2.5 Uplink and Downlink SINRs

With estimated data streams, the SINR values of the m-th stream associated with the user i_k in the uplink and downlink channels can be expressed as in (2.3) and (2.4), respectively, shown at the bottom of the following page. Here, $\mathbf{\Sigma}_{i_k}^{\mathrm{UL}}(\mathbf{v})\left(\mathbf{\Sigma}_{i_k}^{\mathrm{DL}}(\mathbf{v})\right)$ denote the covariance matrix of the aggregate interference-plus-noise for the user i_k in the uplink (downlink) channel, and can be approximated, under $\beta \ll 1$ and $\kappa \ll 1$, as in (2.5) and (2.6), respectively, given on the following page as well. We note that

$\mathbf{\Sigma}_{i_k}^{\mathrm{UL}}(\mathbf{v})$ and $\mathbf{\Sigma}_{i_k}^{\mathrm{DL}}(\mathbf{v})$ depend on non-local parameters, such as channel matrices and pre-coding matrices at other links. However, they can be determined locally provided that there is a sufficient coherence time window within which all channel and pre-coding matrices do not change [84–86].

We note that our system model considers the most general communication scenario, where the FD BSs communicate with the FD users in a multi-cell environment. The other communication scenarios, e.g., I) FD BSs and HD users in a multi-cell, II) FD BS and FD users in a single-cell, III) FD BS and HD users in a single cell, and IV) HD BSs and HD users in single and multi-cell environments, can be recovered as special cases.

$$\gamma_{i_k,m}^{\mathrm{UL}}\left(\mathbf{v},\mathbf{u}_{i_k,m}^{\mathrm{UL}}\right)=\frac{\left|\left(\mathbf{u}_{i_k,m}^{\mathrm{UL}}\right)^{H}\mathbf{H}_{ki_k}^{\mathrm{UL}}\mathbf{v}_{i_k,m}^{\mathrm{UL}}\right|^{2}}{\left(\mathbf{u}_{i_k,m}^{\mathrm{UL}}\right)^{H}\underbrace{\left(\mathbf{\Sigma}_{i_k}^{\mathrm{UL}}(\mathbf{v})+\sum_{n=1}^{d_{i_k}^{\mathrm{UL}}}\mathbf{H}_{ki_k}^{\mathrm{UL}}\mathbf{v}_{i_k,n}^{\mathrm{UL}}\left(\mathbf{v}_{i_k,n}^{\mathrm{UL}}\right)^{H}\left(\mathbf{H}_{ki_k}^{\mathrm{UL}}\right)^{H}\right)}_{\mathbf{Q}_{i_k}^{\mathrm{UL}}(\mathbf{v})}\mathbf{u}_{i_k,m}^{\mathrm{UL}}-\left|\left(\mathbf{u}_{i_k,m}^{\mathrm{UL}}\right)^{H}\mathbf{H}_{ki_k}^{\mathrm{UL}}\mathbf{v}_{i_k,m}^{\mathrm{UL}}\right|^{2}},\tag{2.3}$$

$$\gamma_{i_k,m}^{\mathrm{DL}}\left(\mathbf{v},\mathbf{u}_{i_k,m}^{\mathrm{DL}}\right)=\frac{\left|\left(\mathbf{u}_{i_k,m}^{\mathrm{DL}}\right)^{H}\mathbf{H}_{i_kk}^{\mathrm{DL}}\mathbf{v}_{i_k,m}^{\mathrm{DL}}\right|^{2}}{\left(\mathbf{u}_{i_k,m}^{\mathrm{DL}}\right)^{H}\underbrace{\left(\mathbf{\Sigma}_{i_k}^{\mathrm{DL}}(\mathbf{v})+\sum_{n=1}^{d_{i_k}^{\mathrm{DL}}}\mathbf{H}_{i_kk}^{\mathrm{DL}}\mathbf{v}_{i_k,n}^{\mathrm{DL}}\left(\mathbf{v}_{i_k,n}^{\mathrm{DL}}\right)^{H}\left(\mathbf{H}_{i_kk}^{\mathrm{DL}}\right)^{H}\right)}_{\mathbf{Q}_{i_k}^{\mathrm{DL}}(\mathbf{v})}\mathbf{u}_{i_k,m}^{\mathrm{DL}}-\left|\left(\mathbf{u}_{i_k,m}^{\mathrm{DL}}\right)^{H}\mathbf{H}_{i_kk}^{\mathrm{DL}}\mathbf{v}_{i_k,m}^{\mathrm{DL}}\right|^{2}}.\tag{2.4}$$

2.3 Sum-Power Minimization with Perfect CSI

In this section, our goal is to study the joint sum-power minimization of the FD BSs and users assuming that perfect CSI is available at the FD transmitters while enforcing an SINR constraint for each data stream. The corresponding optimization

---

$$\mathbf{\Sigma}_{i_k}^{\mathrm{UL}}(\mathbf{v}) = \sum_{(l,j)\neq(i,k)} \sum_{n=1}^{d_{l_j}^{\mathrm{UL}}} \mathbf{H}_{kl_j}^{\mathrm{UL}} \mathbf{v}_{l_j,n}^{\mathrm{UL}} \left(\mathbf{v}_{l_j,n}^{\mathrm{UL}}\right)^H \left(\mathbf{H}_{kl_j}^{\mathrm{UL}}\right)^H + \sum_{j=1,j\neq k}^{K} \sum_{l=1}^{I_j} \sum_{n=1}^{d_{l_j}^{\mathrm{DL}}} \mathbf{H}_{kj}^{\mathrm{BB}} \mathbf{v}_{l_j,n}^{\mathrm{DL}} \left(\mathbf{v}_{l_j,n}^{\mathrm{DL}}\right)^H$$
$$\left(\mathbf{H}_{kj}^{\mathrm{BB}}\right)^H + \mathbf{I}_{N_k} + \sum_{l=1}^{I_k} \sum_{n=1}^{d_{l_k}^{\mathrm{DL}}} \kappa \mathbf{H}_k^{\mathrm{SI}} \mathrm{diag}\left(\mathbf{v}_{l_k,n}^{\mathrm{DL}} \left(\mathbf{v}_{l_k,n}^{\mathrm{DL}}\right)^H\right) \left(\mathbf{H}_k^{\mathrm{SI}}\right)^H + \beta \sum_{j=1}^{K} \sum_{l=1}^{I_j} \sum_{n=1}^{d_{l_j}^{\mathrm{UL}}} \mathrm{diag}\left(\mathbf{H}_{kl_j}^{\mathrm{UL}}\right.$$
$$\left.\mathbf{v}_{l_j,n}^{\mathrm{UL}} \left(\mathbf{v}_{l_j,n}^{\mathrm{UL}}\right)^H \left(\mathbf{H}_{kl_j}^{\mathrm{UL}}\right)^H\right) + \beta \sum_{j=1,j\neq k}^{K} \sum_{l=1}^{I_j} \sum_{n=1}^{d_{l_j}^{\mathrm{DL}}} \mathrm{diag}\left(\mathbf{H}_{kj}^{\mathrm{BB}} \mathbf{v}_{l_j,n}^{\mathrm{DL}} \left(\mathbf{v}_{l_j,n}^{\mathrm{DL}}\right)^H \left(\mathbf{H}_{kj}^{\mathrm{BB}}\right)^H\right)$$
$$+ \beta \sum_{l=1}^{I_k} \sum_{n=1}^{d_{l_k}^{\mathrm{DL}}} \mathrm{diag}\left(\mathbf{H}_k^{\mathrm{SI}} \mathbf{v}_{l_k,n}^{\mathrm{DL}} \left(\mathbf{v}_{l_k,n}^{\mathrm{DL}}\right)^H \left(\mathbf{H}_k^{\mathrm{SI}}\right)^H\right), \tag{2.5}$$

$$\mathbf{\Sigma}_{i_k}^{\mathrm{DL}}(\mathbf{v}) = \sum_{(l,j)\neq(i,k)} \sum_{n=1}^{d_{l_j}^{\mathrm{DL}}} \mathbf{H}_{i_kj}^{\mathrm{DL}} \mathbf{v}_{l_j,n}^{\mathrm{DL}} \left(\mathbf{v}_{l_j,n}^{\mathrm{DL}}\right)^H \left(\mathbf{H}_{i_kj}^{\mathrm{DL}}\right)^H + \sum_{(l,j)\neq(i,k)} \sum_{n=1}^{d_{l_j}^{\mathrm{UL}}} \mathbf{H}_{i_kl_j}^{\mathrm{UU}} \mathbf{v}_{l_j,n}^{\mathrm{UL}} \left(\mathbf{v}_{l_j,n}^{\mathrm{UL}}\right)^H$$
$$\left(\mathbf{H}_{i_kl_j}^{\mathrm{UU}}\right)^H + \mathbf{I}_{N_{i_k}} + \kappa \mathbf{H}_{i_k}^{\mathrm{SI}} \sum_{n=1}^{d_{i_k}^{\mathrm{UL}}} \mathrm{diag}\left(\mathbf{v}_{i_k,n}^{\mathrm{UL}} \left(\mathbf{v}_{i_k,n}^{\mathrm{UL}}\right)^H\right) \left(\mathbf{H}_{i_k}^{\mathrm{SI}}\right)^H + \beta \sum_{j=1}^{K} \sum_{l=1}^{I_j} \sum_{n=1}^{d_{l_j}^{\mathrm{DL}}} \mathrm{diag}\left(\mathbf{H}_{i_kj}^{\mathrm{DL}}\right.$$
$$\left.\mathbf{v}_{l_j,n}^{\mathrm{DL}} \left(\mathbf{v}_{l_j,n}^{\mathrm{DL}}\right)^H \left(\mathbf{H}_{i_kj}^{\mathrm{DL}}\right)^H\right) + \beta \sum_{(l,j)\neq(i,k)} \sum_{n=1}^{d_{l_j}^{\mathrm{UL}}} \mathrm{diag}\left(\mathbf{H}_{i_kl_j}^{\mathrm{UU}} \mathbf{v}_{l_j,n}^{\mathrm{UL}} \left(\mathbf{v}_{l_j,n}^{\mathrm{UL}}\right)^H \left(\mathbf{H}_{i_kl_j}^{\mathrm{UU}}\right)^H\right)$$
$$+ \beta \sum_{n=1}^{d_{i_k}^{\mathrm{UL}}} \mathrm{diag}\left(\mathbf{H}_{i_k}^{\mathrm{SI}} \mathbf{v}_{i_k,n}^{\mathrm{UL}} \left(\mathbf{v}_{i_k,n}^{\mathrm{UL}}\right)^H \left(\mathbf{H}_{i_k}^{\mathrm{SI}}\right)^H\right). \tag{2.6}$$

problem can be formulated as

$$\min_{\mathbf{v},\mathbf{u}} \quad \sum_{k=1}^{K}\sum_{i=1}^{I_k}\sum_{m=1}^{d_{i_k}^{\mathrm{UL}}} \left(\mathbf{v}_{i_k,m}^{\mathrm{UL}}\right)^H \mathbf{v}_{i_k,m}^{\mathrm{UL}} + \sum_{k=1}^{K}\sum_{i=1}^{I_k}\sum_{m=1}^{d_{i_k}^{\mathrm{DL}}} \left(\mathbf{v}_{i_k,m}^{\mathrm{DL}}\right)^H \mathbf{v}_{i_k,m}^{\mathrm{DL}} \tag{2.7}$$

$$\text{s.t.} \quad \gamma_{i_k,m}^{X}\left(\mathbf{v},\mathbf{u}_{i_k,m}^{X}\right) \geq \gamma_{\mathrm{th}}^{X}, \;\; i_k \in \mathcal{I}, \; m \in \mathcal{M}, \; X \in \{\mathrm{UL},\mathrm{DL}\}, \tag{2.8}$$

where $\gamma_{\mathrm{th}}^{X},\ X \in \{\mathrm{UL},\mathrm{DL}\}$ is the QoS constraint.

The above problem is not jointly convex in $\mathbf{v}$ and $\mathbf{u}$, and it is known to be NP-hard [87]. In what follows, we show that an approximation of the original problem can be solved efficiently.

2.3.1 Approximated Problem

The original problem in (2.7)-(2.8) can be solved (suboptimally) in an iterative manner where the sum-power converges. To this end, the problem is divided into separate transmit and receive beamforming designs which can be solved alternatively. We note that with fixed transmit beamformers, the linear minimum mean-squared error (MMSE) receiver is optimal in the sense that it maximizes the per-stream SINR [88, 89]. In this regard, the optimal MMSE receiver that maximizes the per-stream SINR can be expressed as

$$\mathbf{u}_{i_k,m}^{X} = \left(\mathbf{H}_{i_k}^{X}\mathbf{V}_{i_k}^{X}\left(\mathbf{V}_{i_k}^{X}\right)^H\left(\mathbf{H}_{i_k}^{X}\right)^H + \mathbf{\Sigma}_{i_k}^{X}(\mathbf{v})\right)^{-1}\mathbf{H}_{i_k}^{X}\mathbf{v}_{i_k,m}^{X}. \tag{2.9}$$

When MMSE receivers are applied to recover the data streams, it leads to the following well-known relationship [89]

$$(\Gamma_{i_k,m}^{X})^{-1} = 1 + \gamma_{i_k,m}^{X}, \tag{2.10}$$

where $\Gamma^X_{i_k,m}$ and $\gamma^X_{i_k,m}$ are the Mean Squared Error (MSE) and SINR, respectively, and it is assumed that an MMSE receiver is applied to recover each stream of the user, $i_k \in \mathcal{I},\ m \in \mathcal{M},\ X \in \{\mathrm{UL}, \mathrm{DL}\}$. The corresponding MSE function can be computed as

$$\Gamma^X_{i_k,m}\left(\mathbf{v}, \mathbf{u}^X_{i_k,m}\right) = |(\mathbf{u}^X_{i_k,m})^H \mathbf{H}^X_{i_k} \mathbf{v}^X_{i_k,m} - 1|^2 + (\mathbf{u}^X_{i_k,m})^H \left\{ \mathbf{\Sigma}^X_{i_k}(\mathbf{v}) + \sum_{n=1, n\neq m}^{d^{\mathrm{X}}_{i_k}} \mathbf{H}^{\mathrm{X}}_{i_k} \mathbf{v}^{\mathrm{X}}_{i_k,n} \left(\mathbf{v}^{\mathrm{X}}_{i_k,n}\right)^H \left(\mathbf{H}^{\mathrm{X}}_{i_k}\right)^H \right\} \mathbf{u}^X_{i_k,m}. \tag{2.11}$$

Assuming that the uplink and downlink transmissions employ certain QoS constraints, γ^X_{th}, the precoder design problem can be written as

$$\min_{\mathbf{v}} \quad P_{\mathrm{BS+UE}} \tag{2.12}$$

$$\text{s.t.} \quad (\Gamma^X_{i_k,m})^{-1}\left(\mathbf{v}, \mathbf{u}^X_{i_k,m}\right) \geq \gamma^X_{\mathrm{th}} + 1, \tag{2.13}$$

where $P_{\mathrm{BS+UE}}$ is given by

$$P_{\mathrm{BS+UE}} = \sum_{k=1}^{K} \sum_{i=1}^{I_k} \sum_{m=1}^{d^{\mathrm{UL}}_{i_k}} \left(\mathbf{v}^{\mathrm{UL}}_{i_k,m}\right)^H \mathbf{v}^{\mathrm{UL}}_{i_k,m} + \sum_{k=1}^{K} \sum_{i=1}^{I_k} \sum_{m=1}^{d^{\mathrm{DL}}_{i_k}} \left(\mathbf{v}^{\mathrm{DL}}_{i_k,m}\right)^H \mathbf{v}^{\mathrm{DL}}_{i_k,m}.$$

The above non-convex problem can be formulated as a DCP with the introduction of an upper bounding constraint for each MSE term, i.e., $\Gamma^X_{i_k,m} \leq f(\theta^X_{i_k,m})$, where $f(\theta^X_{i_k,m})$ is a monotonic log-concave function and $\theta^X_{i_k,m}$ is an auxiliary variable, $i_k \in \mathcal{I},\ m \in \mathcal{M},\ X \in \{\mathrm{UL}, \mathrm{DL}\}$. To that end, we assume $f(\theta^X_{i_k,m}) = c^{-\theta^X_{i_k,m}}$, where $c > 1$. For later results, we choose $c = 2$ as suggested in [70].

With this approximation, the problem in (2.12)-(2.13) can be reformulated as

$$\min_{\mathbf{v},\theta} \quad P_{\mathrm{BS+UE}} \tag{2.14}$$

$$\text{s.t.} \quad \Gamma^X_{i_k,m}\left(\mathbf{v}, \mathbf{u}^X_{i_k,m}\right) \leq c^{\theta^X_{i_k,m}}, \tag{2.15}$$

$$\theta^X_{i_k,m} \geq \frac{\log_e(\gamma^X_{\text{th}} + 1)}{\log_e c}, \tag{2.16}$$

Note that the above problem in still non-convex due to MSE upper bounding constraint in (2.15).

2.3.2 Solving the Approximated Problem

The non-convex part of the above MSE constraint, $f(\theta^X_{i_k,m}) = c^{-\theta^X_{i_k,m}}$, can be linearly approximated at a given point, $\theta^{X_\tau}_{i_k,m}$, by the first-order Taylor series

$$\begin{aligned} f(\theta^X_{i_k,m}, \theta^{X_\tau}_{i_k,m}) &= f(\theta^{X_\tau}_{i_k,m}) + (\theta^X_{i_k,m} - \theta^{X_\tau}_{i_k,m}) f'(\theta^{X_\tau}_{i_k,m}) \\ &= -a^{X_\tau}_{i_k,m}\theta^X_{i_k,m} + b^{X_\tau}_{i_k,m}, \end{aligned} \tag{2.17}$$

where τ is the iteration index, $a^{X_\tau}_{i_k,m}$ and $b^{X_\tau}_{i_k,m}$ are the coefficients of the linear approximation, $f'(\theta^{X_\tau}_{i_k,m})$ is the first-order partial derivative with respect to $\theta^X_{i_k,m}$. Taking the first-order partial derivative, we have

$$\begin{aligned} f(\theta^X_{i_k,m}, \theta^{X_\tau}_{i_k,m}) &= c^{-\theta^{X_\tau}_{i_k,m}} + (\theta^X_{i_k,m} - \theta^{X_\tau}_{i_k,m})(-c^{-\theta^{X_\tau}_{i_k,m}} \log_e c) \\ &= -\theta^X_{i_k,m} c^{-\theta^{X_\tau}_{i_k,m}} \log_e c + c^{-\theta^{X_\tau}_{i_k,m}}(1 + \theta^{X_\tau}_{i_k,m} \log_e c). \end{aligned} \tag{2.18}$$

Therefore, we arrive at

$$a^{X_\tau}_{i_k,m} = c^{-\theta^{X_\tau}_{i_k,m}} \log_e c, \tag{2.19}$$

$$b^{X_\tau}_{i_k,m} = c^{-\theta^{X_\tau}_{i_k,m}}(1 + \theta^{X_\tau}_{i_k,m} \log_e c). \tag{2.20}$$

At iteration τ with fixed $\theta^{X_\tau}_{i_k,m},\ i_k \in \mathcal{I},\ m \in \mathcal{M}, X \in \{\text{UL}, \text{DL}\}$, the optimization

problem in (2.14)-(2.16) can be written as

$$\min_{\mathbf{v},\theta} \quad P_{\text{BS+UE}} \tag{2.21}$$

$$\text{s.t.} \quad \Gamma^{X}_{i_k,m}\left(\mathbf{v}, \mathbf{u}^{X}_{i_k,m}\right) \leq -a^{X_\tau}_{i_k,m}\theta^{X}_{i_k,m} + b^{X_\tau}_{i_k,m}, \tag{2.22}$$

$$\theta^{X}_{i_k,m} \geq \log_c(\gamma^{X}_{\text{th}} + 1). \tag{2.23}$$

In the above optimization problem, all constraints are convex due to the linear approximations. After solving the above optimization problem at each iteration, the next point can be computed using an exact line search method i.e., $\theta^{X_{\tau+1}}_{i_k,m} = \theta^{X_\tau}_{i_k,m}$ or based on the equality of the MSE constraint, $\theta^{X_{\tau+1}}_{i_k,m} = -\log_2(\Gamma^{X_{\tau+1}}_{i_k,m})$ [70].

The problem is solved in a way that the sum-power converges by alternating between the receive and transmit beamforming designs. The iterative transmit beamformers are optimized by repeatedly computing the linear approximation and then solving the above reformulated optimization problem in (2.21)-(2.23). The steps for solving the optimization problem is summarized in Algorithm 1.

Algorithm 1 Sum-Power Minimization with Perfect CSI.

1: Initialize the transmit beamforming vectors $\mathbf{v}^{X}_{i_k,m}$ and $\theta^{X_\tau}_{i_k,m}$, $i_k \in \mathcal{I}$, $m \in \mathcal{M}, X \in \{\text{UL}, \text{DL}\}$. Set $\tau = 0$.
2: **repeat**
3: Calculate the MMSE receive beamforming vectors $\mathbf{u}$ from (2.9).
4: **repeat**
5: Calculate the linear approximation coefficients, $a^{X_\tau}_{i_k,m}$ and $b^{X_\tau}_{i_k,m}$, $i_k \in \mathcal{I}$, $m \in \mathcal{M}$, $X \in \{\text{UL}, \text{DL}\}$ from (2.19) and (2.20), respectively.
6: Calculate $\mathbf{v}$ from (2.21)-(2.23).
7: Update $\theta^{X_\tau}_{i_k,m}$, $i_k \in \mathcal{I}$, $m \in \mathcal{M}$, $X \in \{\text{UL}, \text{DL}\}$ using line search. Set $\tau = \tau + 1$.
8: **until** Convergence (inner) of the objective function in (2.21) or a predefined number of iterations is reached.
9: **until** Convergence (outer) of the objective function in (2.21) or a predefined number of iterations is reached.

2.3.3 Convergence Analysis

The Algorithm 1 is guaranteed to converge if it can be proved that the objective function in (2.21) decreases monotonically at each optimization step and it is bounded below. We note that the original optimization problem in (2.7)-(2.8) and the approximated optimization problem in (2.21)-(2.23) have the same objective function. Furthermore, the optimization variables in (2.21)-(2.23) satisfy the same QoS constraint in (2.7)-(2.8). Therefore, it is sufficient to show that the sum-power converges following Algorithm 1 and the objective function is bounded below. It is apparent that the sum-power is bounded below, i.e., $P_{\text{BS+UE}} > 0$.

We note the MMSE receive filter update at step 3 of Algorithm 1 minimizes the per-stream MSE, which means that less (or equal) transmit power will be needed to satisfy that per-stream MSE. This leads to decreased required sum-power [88, 89]. Furthermore, the SCA optimization related to the transmit beamformers converges monotonically due to the fact that the point of approximation is included in the approximated convex problem via the update of $\theta_{i_k,m}^{X_\tau},\ i_k \in \mathcal{I},\ m \in \mathcal{M},\ X \in \{\text{UL}, \text{DL}\}$, as presented in Section 2.3.2 [68, 70, 71]. Therefore, the objective function is guaranteed to converge.

We further note that we deal with a convex problem at each optimization step, which can be solved efficiently [90]. However, the above convergence proof only holds for the monotonically decreasing convergence to a limit point of the objective function. Since the original problem in (2.7)-(2.8) is non-convex, generally the global optimality cannot be ensured.

Table 2.1: Comparison of the Run-Time (in seconds) for Algorithm 1

Setting 1	Setting 2	Setting 3
16.63	30.91	39.95

2.3.4 Complexity Analysis

The computational complexity is determined by the problem size, i.e, number and size of the optimization variables and constraints. Assuming the same number of transmit antennas (M), receive antennas (N) and same number of data streams (d) at each node, in this section, we analyze the computational complexity of the proposed algorithm. Since the proposed algorithm relies on iterative update, we provide per-iteration complexity. We do so by omitting linear constraints since their impact on overall complexity can be considered negligible.

Given the number of users, $|\mathcal{I}|$ and assuming interior point method for convex quadratic programming [90], the total complexity of the each iteration of the optimization problem involves $\mathcal{O}(M^3)+|\mathcal{I}|\left(MNd+M^2d+N^2d\right)+N\left(NM+Md+N^2\right)$ calculations [84]. We note that calculations of some terms in the covariance matrices can be reused. For example, the second term in (2.5) can be reused to calculate the sixth term as it incurs the diagonalization of the same matrix.

2.3.5 Run-Time Analysis

The run-time of an algorithm depends on the problem size, the convergence accuracy desired from the optimization problem, and the machine on which the algorithm is running. In our case, we use a consumer grade computer machine with 1.6 GHz processor, 8 GB of Random Access Memory (RAM), and a 8-core Central Processing Unit (CPU). The algorithm was tested when the computer had some other activities running in the background. To this end, we consider three different antenna settings,

such as $\{M_k = N_k = 4, M_{i_k} = N_{i_k} = 2, d_{i_k}^X = 1\}$, $\{M_k = N_k = 8, M_{i_k} = N_{i_k} = 4, d_{i_k}^X = 2\}$, $\{M_k = N_k = 12, M_{i_k} = N_{i_k} = 6, d_{i_k}^X = 3\}$, $i_k \in \mathcal{I}$, $X \in \{\text{UL}, \text{DL}\}$, termed as settings 1, 2, and 3, respectively. Table 2.1 presents the average run time (in seconds) with different antenna settings for a convergence accuracy of 10^{-5}, which is a reasonable time for the convergence.

2.4 Sum-Power Minimization with CSI Uncertainty

The realization of the full potential for FD communications relies on the quality of the CSI available at the transceiver. The CSI can be obtained at each transmitter via channel estimation through the pilot signals or it can be fed back to the transmitter using quantized feedback signaling [35]. Nonetheless, due to inevitable estimation error involved with the channel estimation process or limited capacity of the feedback channel, the assumption of the perfect CSI availability is idealistic. In order to account for this design challenge, in the following we study the sum-power minimization problem under the imperfect CSI scenario considering both stochastic and bounded uncertainties.

2.4.1 Sum-Power Minimization with Stochastic CSI Uncertainty

In this section, we incorporate the stochastic CSI uncertainty into our design, where the uncertainty is usually modeled as a complex random matrix with normally distributed elements, and the transmitter is assumed to know the distribution type and corresponding parameters [91–94]. The statistical CSI uncertainty model is expressed

as

$$\mathbf{H} \in \mathcal{H} = \left\{ \tilde{\mathbf{H}} + \mathbf{\Delta} : \mathbf{\Delta} \sim \mathcal{CN}(\mathbf{0}, \sigma_\delta \boldsymbol{I}) \right\}, \tag{2.24}$$

where $\tilde{\mathbf{H}}$, $\mathbf{\Delta}$, and σ_δ denote the estimated CSI, the channel error matrix, and the variance of the CSI uncertainty, respectively. The estimated CSI and the channel error matrix are assumed to be statistically independent.

Applying the model (2.24) to the respective channels, $\mathbf{H}^{\mathrm{UL}}_{kl_j}$, $\mathbf{H}^{\mathrm{DL}}_{i_k j}$, $\mathbf{H}^{\mathrm{UU}}_{i_k l_j}$, $\mathbf{H}^{\mathrm{BB}}_{kj}$, $\mathbf{H}^{\mathrm{SI}}_{k}$, and $\mathbf{H}^{\mathrm{SI}}_{i_k}$ in the FD multi-cell system, we have the corresponding distributions for the channel error matrices given by

$$\mathbf{\Delta}^{\mathrm{UL}}_{\boldsymbol{kl_j}} \sim \mathcal{CN}(\mathbf{0}, \sigma^{\mathrm{ul}}_\delta \boldsymbol{I}), \tag{2.25}$$

$$\mathbf{\Delta}^{\mathrm{DL}}_{\boldsymbol{i_k j}} \sim \mathcal{CN}(\mathbf{0}, \sigma^{\mathrm{dl}}_\delta \boldsymbol{I}), \tag{2.26}$$

$$\mathbf{\Delta}^{\mathrm{UU}}_{\boldsymbol{i_k l_j}} \sim \mathcal{CN}(\mathbf{0}, \sigma^{\mathrm{uu}}_\delta \boldsymbol{I}), \tag{2.27}$$

$$\mathbf{\Delta}^{\mathrm{BB}}_{\boldsymbol{kj}} \sim \mathcal{CN}(\mathbf{0}, \sigma^{\mathrm{bb}}_\delta \boldsymbol{I}), \tag{2.28}$$

$$\mathbf{\Delta}^{\mathrm{SI}}_{\boldsymbol{k}} \sim \mathcal{CN}(\mathbf{0}, \sigma^{\mathrm{si,b}}_\delta \boldsymbol{I}), \tag{2.29}$$

$$\mathbf{\Delta}^{\mathrm{SI}}_{\boldsymbol{i_k}} \sim \mathcal{CN}(\mathbf{0}, \sigma^{\mathrm{si,u}}_\delta \boldsymbol{I}). \tag{2.30}$$

The above variance terms can be further modeled as [95]

$$\sigma_\delta = \lambda \rho^{-\eta}. \tag{2.31}$$

The model captures the effect of the channel uncertainties pertaining to the estimation accuracy. According to this model, the error variance for the associated channel depends on the nominal SNR, ρ, unless $\eta = 0$. The parameters $\lambda > 0$ and $\eta \geq 0$ are meant to capture a variety of communication scenarios. For example,

the case of perfect CSI can be obtained with $\lambda = 0$. Reciprocal channels and CSI feedback can be captured with $\eta = 1$ and $\eta = 0$, respectively.

Considering the CSI uncertainty, the optimization problem that we want to solve can be written as

$$\min_{\mathbf{v},\mathbf{u}} \quad \sum_{k=1}^{K}\sum_{i=1}^{I_k}\sum_{m=1}^{d_{i_k}^{\mathrm{UL}}} \left(\mathbf{v}_{i_k,m}^{\mathrm{UL}}\right)^H \mathbf{v}_{i_k,m}^{\mathrm{UL}} + \sum_{k=1}^{K}\sum_{i=1}^{I_k}\sum_{m=1}^{d_{i_k}^{\mathrm{DL}}} \left(\mathbf{v}_{i_k,m}^{\mathrm{DL}}\right)^H \mathbf{v}_{i_k,m}^{\mathrm{DL}} \tag{2.32}$$

$$\text{s.t.} \quad \tilde{\gamma}_{i_k,m}^{X}\left(\mathbf{v}, \mathbf{u}_{i_k,m}^{X}\right) \geq \gamma_{\mathrm{th}}^{X}, \;\; i_k \in \mathcal{I}, \; m \in \mathcal{M}, \; X \in \{\mathrm{UL}, \mathrm{DL}\}, \tag{2.33}$$

where $\tilde{\gamma}_{i_k,m}^{X}\left(\mathbf{v}, \mathbf{u}_{i_k,m}^{X}\right), \; i_k \in \mathcal{I}, \; m \in \mathcal{M}, \; X \in \{\mathrm{UL}, \mathrm{DL}\}$ is the SINR that accounts for the stochastic CSI uncertainty, and computed as in (2.35) and (2.36) for the uplink and downlink transmissions, respectively. Under the assumption of the stochastic CSI uncertainty, it is intuitive that all nodes have access to $\tilde{\mathbf{H}}$ and the statistics about the CSI uncertainty, instead of $\mathbf{H}$. With the above modeling of the stochastic CSI uncertainty, the interference plus noise covariance matrices in (2.5) and (2.6) can be approximated as in (2.37) and (2.38), respectively. We obtain this approximation by omitting terms that involve multiplication of the CSI uncertainty associated with each channel, since their products are negligibly small. Furthermore, $\tilde{\mathbf{\Sigma}}_{i_k}^{\mathrm{UL}}(\mathbf{v})$ and $\tilde{\mathbf{\Sigma}}_{i_k}^{\mathrm{DL}}(\mathbf{v})$ are obtained by directly replacing all instances of $\mathbf{H}$ by $\tilde{\mathbf{H}}$ in (2.5) and (2.6) for the uplink and downlink transmissions, respectively.

As in the previous section, at iteration τ and for a fixed $\tilde{\theta}_{i_k,m}^{X_\tau}, \; i_k \in \mathcal{I}, \; m \in \mathcal{M}, \; X \in \{\mathrm{UL}, \mathrm{DL}\}$, the optimization problem in (2.32)-(2.33) can be cast as below

$$\min_{\mathbf{v},\theta} \quad \tilde{P}_{\mathrm{BS+UE}} \tag{2.39}$$

$$\text{s.t.} \quad \tilde{\Gamma}_{i_k,m}^{X}\left(\mathbf{v}, \mathbf{u}_{i_k,m}^{X}\right) \leq -\tilde{a}_{i_k,m}^{X_\tau}\tilde{\theta}_{i_k,m}^{X} + \tilde{b}_{i_k,m}^{X_\tau}, \tag{2.40}$$

$$\tilde{\theta}_{i_k,m}^{X} \geq \log_c(\gamma_{\mathrm{th}}^{X} + 1), \tag{2.41}$$

$$\tilde{\gamma}_{i_k,m}^{\mathrm{UL}}\left(\mathbf{v},\mathbf{u}_{i_k,m}^{\mathrm{UL}}\right)=\frac{\left|\left(\mathbf{u}_{i_k,m}^{\mathrm{UL}}\right)^H\tilde{\mathbf{H}}_{ki_k}^{\mathrm{UL}}\mathbf{v}_{i_k,m}^{\mathrm{UL}}\right|^2}{\left(\mathbf{u}_{i_k,m}^{\mathrm{UL}}\right)^H\left(\tilde{\mathbf{\Sigma}}_{i_k,\delta}^{\mathrm{UL}}\left(\mathbf{v}\right)+\sum_{n=1}^{d_{i_k}^{\mathrm{UL}}}\tilde{\mathbf{H}}_{ki_k}^{\mathrm{UL}}\mathbf{v}_{i_k,n}^{\mathrm{UL}}\left(\mathbf{v}_{i_k,n}^{\mathrm{UL}}\right)^H\left(\tilde{\mathbf{H}}_{ki_k}^{\mathrm{UL}}\right)^H\right)\mathbf{u}_{i_k,m}^{\mathrm{UL}}-\left|\left(\mathbf{u}_{i_k,m}^{\mathrm{UL}}\right)^H\tilde{\mathbf{H}}_{ki_k}^{\mathrm{UL}}\mathbf{v}_{i_k,m}^{\mathrm{UL}}\right|^2},\tag{2.35}$$

$$\tilde{\gamma}_{i_k,m}^{\mathrm{DL}}\left(\mathbf{v},\mathbf{u}_{i_k,m}^{\mathrm{DL}}\right)=\frac{\left|\left(\mathbf{u}_{i_k,m}^{\mathrm{DL}}\right)^H\tilde{\mathbf{H}}_{i_kk}^{\mathrm{DL}}\mathbf{v}_{i_k,m}^{\mathrm{DL}}\right|^2}{\left(\mathbf{u}_{i_k,m}^{\mathrm{DL}}\right)^H\left(\tilde{\mathbf{\Sigma}}_{i_k,\delta}^{\mathrm{DL}}\left(\mathbf{v}\right)+\sum_{n=1}^{d_{i_k}^{\mathrm{DL}}}\tilde{\mathbf{H}}_{i_kk}^{\mathrm{DL}}\mathbf{v}_{i_k,n}^{\mathrm{DL}}\left(\mathbf{v}_{i_k,n}^{\mathrm{DL}}\right)^H\left(\tilde{\mathbf{H}}_{i_kk}^{\mathrm{DL}}\right)^H\right)\mathbf{u}_{i_k,m}^{\mathrm{DL}}-\left|\left(\mathbf{u}_{i_k,m}^{\mathrm{DL}}\right)^H\tilde{\mathbf{H}}_{i_kk}^{\mathrm{DL}}\mathbf{v}_{i_k,m}^{\mathrm{DL}}\right|^2}.\tag{2.36}$$

$$\begin{aligned}\tilde{\mathbf{\Sigma}}_{i_k,\delta}^{\mathrm{UL}}\left(\mathbf{v}\right)\approx\tilde{\mathbf{\Sigma}}_{i_k}^{\mathrm{UL}}\left(\mathbf{v}\right)+\Bigg\{&\sigma_\delta^{\mathrm{ul}}\sum_{j=1}^{K}\sum_{l=1}^{I_j}\sum_{n=1}^{d_{l_j}^{\mathrm{UL}}}\mathrm{tr}\left(\mathbf{v}_{l_j,n}^{\mathrm{UL}}\left(\mathbf{v}_{l_j,n}^{\mathrm{UL}}\right)^H\right)+\sigma_\delta^{\mathrm{bb}}\sum_{j=1}^{K}\sum_{l=1}^{I_j}\sum_{n=1}^{d_{l_j}^{\mathrm{DL}}}\mathrm{tr}\left(\mathbf{v}_{l_j,n}^{\mathrm{DL}}\right.\\&\left.\left(\mathbf{v}_{l_j,n}^{\mathrm{DL}}\right)^H\right)+\sigma_\delta^{\mathrm{si,b}}\kappa\sum_{l=1}^{I_k}\sum_{n=1}^{d_{l_k}^{\mathrm{DL}}}\mathrm{tr}\left(\mathbf{v}_{l_k,n}^{\mathrm{DL}}\left(\mathbf{v}_{l_k,n}^{\mathrm{DL}}\right)^H\right)+\beta\sigma_\delta^{\mathrm{ul}}\sum_{j=1}^{K}\sum_{l=1}^{I_j}\sum_{n=1}^{d_{l_j}^{\mathrm{UL}}}\mathrm{tr}\left(\mathbf{v}_{l_j,n}^{\mathrm{UL}}\left(\mathbf{v}_{l_j,n}^{\mathrm{UL}}\right)^H\right)\\&+\sigma_\delta^{\mathrm{bb}}\beta\sum_{j=1}^{K}\sum_{l=1}^{I_j}\sum_{n=1}^{d_{l_j}^{\mathrm{DL}}}\mathrm{tr}\left(\mathbf{v}_{l_j,n}^{\mathrm{DL}}\left(\mathbf{v}_{l_j,n}^{\mathrm{DL}}\right)^H\right)+\sigma_\delta^{\mathrm{si,b}}\beta\sum_{l=1}^{I_k}\sum_{n=1}^{d_{l_k}^{\mathrm{DL}}}\mathrm{tr}\left(\mathbf{v}_{l_k,n}^{\mathrm{DL}}\left(\mathbf{v}_{l_k,n}^{\mathrm{DL}}\right)^H\right)\Bigg\}\mathbf{I}_{N_k},\end{aligned}\tag{2.37}$$

$$\begin{aligned}\tilde{\mathbf{\Sigma}}_{i_k,\delta}^{\mathrm{DL}}\left(\mathbf{v}\right)\approx\tilde{\mathbf{\Sigma}}_{i_k}^{\mathrm{DL}}\left(\mathbf{v}\right)+\Bigg\{&\sigma_\delta^{\mathrm{dl}}\sum_{j=1}^{K}\sum_{l=1}^{I_j}\sum_{n=1}^{d_{l_j}^{\mathrm{DL}}}\mathrm{tr}\left(\mathbf{v}_{l_j,n}^{\mathrm{DL}}\left(\mathbf{v}_{l_j,n}^{\mathrm{DL}}\right)^H\right)+\sigma_\delta^{\mathrm{uu}}\sum_{j=1}^{K}\sum_{l=1}^{I_j}\sum_{n=1}^{d_{l_j}^{\mathrm{UL}}}\mathrm{tr}\left(\mathbf{v}_{l_j,n}^{\mathrm{UL}}\right.\\&\left.\left(\mathbf{v}_{l_j,n}^{\mathrm{UL}}\right)^H\right)+\sigma_\delta^{\mathrm{si,u}}\kappa\sum_{n=1}^{d_{i_k}^{\mathrm{UL}}}\mathrm{tr}\left(\mathbf{v}_{i_k,n}^{\mathrm{UL}}\left(\mathbf{v}_{i_k,n}^{\mathrm{UL}}\right)^H\right)+\sigma_\delta^{\mathrm{dl}}\beta\sum_{j=1}^{K}\sum_{l=1}^{I_j}\sum_{n=1}^{d_{l_j}^{\mathrm{DL}}}\mathrm{tr}\left(\mathbf{v}_{l_j,n}^{\mathrm{DL}}\left(\mathbf{v}_{l_j,n}^{\mathrm{DL}}\right)^H\right)\\&+\sigma_\delta^{\mathrm{uu}}\beta\sum_{j=1}^{K}\sum_{l=1}^{I_j}\sum_{n=1}^{d_{l_j}^{\mathrm{UL}}}\mathrm{tr}\left(\mathbf{v}_{l_j,n}^{\mathrm{UL}}\left(\mathbf{v}_{l_j,n}^{\mathrm{UL}}\right)^H\right)+\sigma_\delta^{\mathrm{si,u}}\beta\sum_{n=1}^{d_{i_k}^{\mathrm{UL}}}\mathrm{tr}\left(\mathbf{v}_{i_k,n}^{\mathrm{UL}}\left(\mathbf{v}_{i_k,n}^{\mathrm{UL}}\right)^H\right)\Bigg\}\mathbf{I}_{N_{i_k}}.\end{aligned}\tag{2.38}$$

where parameters $\tilde{a}_{i_k,m}^{X_\tau}$ and $\tilde{b}_{i_k,m}^{X_\tau}$ are applicable for the design involving the stochastic CSI uncertainty, but follow the same construction as derived for the case of perfect CSI design as in (2.19) and (2.20), $\tilde{\Gamma}_{i_k,m}^{X}$ is the MSE with the stochastic CSI uncertainty, and $\tilde{P}_{\text{BS+UE}}$ is the total transmit power for the same, obtained as in (2.14). Alike the perfect CSI design, the above optimization problem is convex and can be solved iteratively following the similar steps as in Algorithm 1.

2.4.2 Sum-Power Minimization with Bounded CSI Uncertainty

Now we extend our design to deal with the bounded CSI uncertainty. To this end, we restrict the imperfect CSI within a norm-bounded deterministic (or worst-case) model, where the instantaneous CSI is assumed to be located in a known set of possible values [96–99]. The norm-bounded uncertainty model is expressed as

$$\mathbf{H} \in \mathcal{H} = \left\{ \tilde{\mathbf{H}} + \mathbf{\Delta} : \|\mathbf{\Delta}\|_F \leq \epsilon \right\}, \tag{2.42}$$

$$\hat{\gamma}_{i_k,m}^{\text{UL}}\left(\mathbf{v}, \mathbf{u}_{i_k,m}^{\text{UL}}\right)_{\text{LB}} = \frac{\left|\left(\mathbf{u}_{i_k,m}^{\text{UL}}\right)^H \tilde{\mathbf{H}}_{ki_k}^{\text{UL}} \mathbf{v}_{i_k,m}^{\text{UL}}\right|^2}{\left[\left(\mathbf{u}_{i_k,m}^{\text{UL}}\right)^H \hat{\mathbf{\Sigma}}_{i_k}^{\text{UL}}(\mathbf{v}) \mathbf{u}_{i_k,m}^{\text{UL}}\right] + \left(\mathbf{u}_{i_k,m}^{\text{UL}}\right)^H \sum_{n=1,n\neq m}^{d_{i_k}^{\text{UL}}} \tilde{\mathbf{H}}_{ki_k}^{\text{UL}} \mathbf{v}_{i_k,n}^{\text{UL}} \left(\mathbf{v}_{i_k,n}^{\text{UL}}\right)^H \left(\tilde{\mathbf{H}}_{ki_k}^{\text{UL}}\right)^H \mathbf{u}_{i_k,m}^{\text{UL}}}, \tag{2.45}$$

$$\hat{\gamma}_{i_k,m}^{\text{DL}}\left(\mathbf{v}, \mathbf{u}_{i_k,m}^{\text{DL}}\right)_{\text{LB}} = \frac{\left|\left(\mathbf{u}_{i_k,m}^{\text{DL}}\right)^H \tilde{\mathbf{H}}_{i_k k}^{\text{DL}} \mathbf{v}_{i_k,m}^{\text{DL}}\right|^2}{\left[\left(\mathbf{u}_{i_k,m}^{\text{DL}}\right)^H \hat{\mathbf{\Sigma}}_{i_k}^{\text{DL}}(\mathbf{v}) \mathbf{u}_{i_k,m}^{\text{DL}}\right] + \left(\mathbf{u}_{i_k,m}^{\text{DL}}\right)^H \sum_{n=1,n\neq m}^{d_{i_k}^{\text{DL}}} \tilde{\mathbf{H}}_{i_k k}^{\text{DL}} \mathbf{v}_{i_k,n}^{\text{DL}} \left(\mathbf{v}_{i_k,n}^{\text{DL}}\right)^H \left(\tilde{\mathbf{H}}_{i_k k}^{\text{DL}}\right)^H \mathbf{u}_{i_k,m}^{\text{DL}}}, \tag{2.46}$$

where $\tilde{\mathbf{H}}$, $\mathbf{\Delta}$, and ϵ denote the nominal value of the CSI, the channel error matrix, and the uncertainty bound, respectively. The uncertainty sizes can be made related to the quality of the channels, where the radius of the uncertainty regions can be set to $\epsilon = s\|\tilde{\mathbf{H}}\|_F,\ s \in [0,1)$ [100]. Considering the CSI uncertainty, the optimization problem that is of interest is given as below

$$\begin{aligned} \min_{\mathbf{v},\mathbf{u}} \quad & \sum_{k=1}^{K}\sum_{i=1}^{I_k}\sum_{m=1}^{d_{i_k}^{\mathrm{UL}}} \left(\mathbf{v}_{i_k,m}^{\mathrm{UL}}\right)^H \mathbf{v}_{i_k,m}^{\mathrm{UL}} + \sum_{k=1}^{K}\sum_{i=1}^{I_k}\sum_{m=1}^{d_{i_k}^{\mathrm{DL}}} \left(\mathbf{v}_{i_k,m}^{\mathrm{DL}}\right)^H \mathbf{v}_{i_k,m}^{\mathrm{DL}} \\ \text{s.t.} \quad & \min_{\mathbf{\Delta}} \gamma_{i_k,m}^{X}\left(\mathbf{v}, \mathbf{u}_{i_k,m}^{X}\right) \geq \gamma_{\mathrm{th}}^{X}, \end{aligned} \tag{2.43}$$

$$\left(\mathbf{u}_{i_k,m}^{\mathrm{UL}}\right)^H \tilde{\mathbf{\Sigma}}_{i_k}^{\mathrm{UL}}(\mathbf{v})\mathbf{u}_{i_k,m}^{\mathrm{UL}} = \sum_{(l,j)\neq(i,k)}\sum_{n=1}^{d_{l_j}^{\mathrm{UL}}} ||(\mathbf{u}_{i_k,m}^{\mathrm{UL}})^H \tilde{\mathbf{H}}_{kl_j}^{\mathrm{UL}} \mathbf{v}_{l_j,n}^{\mathrm{UL}}||_F^2 + \sum_{j=1,j\neq k}^{K}\sum_{l=1}^{I_j}\sum_{n=1}^{d_{l_j}^{\mathrm{DL}}} ||(\mathbf{u}_{i_k,m}^{\mathrm{UL}})^H \tilde{\mathbf{H}}_{kj}^{\mathrm{BB}} \mathbf{v}_{l_j,n}^{\mathrm{DL}}||_F^2$$

$$+ ||\mathbf{u}_{i_k,m}^{\mathrm{UL}}||_F^2 + \kappa \sum_{l=1}^{I_k}\sum_{n=1}^{d_{l_k}^{\mathrm{DL}}} ||(\mathbf{u}_{i_k,m}^{\mathrm{UL}})^H \tilde{\mathbf{H}}_{k}^{\mathrm{SI}} \mathrm{diag}\left(\mathbf{v}_{l_k,n}^{\mathrm{DL}}(\mathbf{v}_{l_k,n}^{\mathrm{DL}})^H\right)^{\frac{1}{2}} ||_F^2 + \beta \sum_{j=1}^{K}\sum_{l=1}^{I_j}\sum_{n=1}^{d_{l_j}^{\mathrm{UL}}} || \left(\tilde{\mathbf{H}}_{kl_j}^{\mathrm{UL}} \mathbf{v}_{l_j,n}^{\mathrm{UL}}\right)^H$$

$$\mathrm{diag}\left(\mathbf{u}_{i_k,m}^{\mathrm{UL}}(\mathbf{u}_{i_k,m}^{\mathrm{UL}})^H\right)^{\frac{1}{2}} ||_F^2 + \beta \sum_{j=1,j\neq k}^{K}\sum_{l=1}^{I_j}\sum_{n=1}^{d_{l_j}^{\mathrm{DL}}} ||\left(\tilde{\mathbf{H}}_{kj}^{\mathrm{BB}} \mathbf{v}_{l_j,n}^{\mathrm{DL}}\right)^H \mathrm{diag}\left(\mathbf{u}_{i_k,m}^{\mathrm{UL}}(\mathbf{u}_{i_k,m}^{\mathrm{UL}})^H\right)^{\frac{1}{2}} ||_F^2$$

$$+\beta \sum_{l=1}^{I_k}\sum_{n=1}^{d_{l_k}^{\mathrm{DL}}} ||\left(\tilde{\mathbf{H}}_{k}^{\mathrm{SI}} \mathbf{v}_{l_k,n}^{\mathrm{DL}}\right)^H \mathrm{diag}\left(\mathbf{u}_{i_k,m}^{\mathrm{UL}}(\mathbf{u}_{i_k,m}^{\mathrm{UL}})^H\right)^{\frac{1}{2}} ||_F^2, \tag{2.47}$$

$$\left(\mathbf{u}_{i_k,m}^{\mathrm{DL}}\right)^H \tilde{\mathbf{\Sigma}}_{i_k}^{\mathrm{DL}}\left(\mathbf{v}\right)\mathbf{u}_{i_k,m}^{\mathrm{DL}} = \sum_{(l,j)\neq(i,k)}\sum_{n=1}^{d_{l_j}^{\mathrm{DL}}} ||(\mathbf{u}_{i_k,m}^{\mathrm{DL}})^H \tilde{\mathbf{H}}_{i_kj}^{\mathrm{DL}} \mathbf{v}_{l_j,n}^{\mathrm{DL}}||_F^2 + \sum_{(l,j)\neq(i,k)}\sum_{n=1}^{d_{l_j}^{\mathrm{UL}}} ||(\mathbf{u}_{i_k,m}^{\mathrm{DL}})^H \tilde{\mathbf{H}}_{i_kl_j}^{\mathrm{UU}} \mathbf{v}_{l_j,n}^{\mathrm{UL}}||_F^2$$

$$+ ||\mathbf{u}_{i_k,m}^{\mathrm{DL}}||_F^2 + \kappa \sum_{n=1}^{d_{i_k}^{\mathrm{UL}}} ||(\mathbf{u}_{i_k,m}^{\mathrm{DL}})^H \tilde{\mathbf{H}}_{i_k}^{\mathrm{SI}} \mathrm{diag}\left(\mathbf{v}_{i_k,n}^{\mathrm{UL}}\left(\mathbf{v}_{i_k,n}^{\mathrm{UL}}\right)^H\right)^{\frac{1}{2}} ||_F^2 + \beta \sum_{j=1}^{K}\sum_{l=1}^{I_j}\sum_{n=1}^{d_{l_j}^{\mathrm{DL}}} || \left(\tilde{\mathbf{H}}_{i_kj}^{\mathrm{DL}} \mathbf{v}_{l_j,n}^{\mathrm{DL}}\right)^H$$

$$\mathrm{diag}\left(\mathbf{u}_{i_k,m}^{\mathrm{DL}}(\mathbf{u}_{i_k,m}^{\mathrm{DL}})^H\right)^{\frac{1}{2}} ||_F^2 + \beta \sum_{(l,j)\neq(i,k)}\sum_{n=1}^{d_{l_j}^{\mathrm{UL}}} || \left(\tilde{\mathbf{H}}_{i_kl_j}^{\mathrm{UU}} \mathbf{v}_{l_j,n}^{\mathrm{UL}}\right)^H \mathrm{diag}\left(\mathbf{u}_{i_k,m}^{\mathrm{DL}}(\mathbf{u}_{i_k,m}^{\mathrm{DL}})^H\right)^{\frac{1}{2}} ||_F^2$$

$$+ \beta \sum_{n=1}^{d_{i_k}^{\mathrm{UL}}} || \left(\tilde{\mathbf{H}}_{i_k}^{\mathrm{SI}} \mathbf{v}_{i_k,n}^{\mathrm{UL}}\right)^H \mathrm{diag}\left(\mathbf{u}_{i_k,m}^{\mathrm{DL}}(\mathbf{u}_{i_k,m}^{\mathrm{DL}})^H\right)^{\frac{1}{2}} ||_F^2. \tag{2.48}$$

$$i_k \in \mathcal{I},\ m \in \mathcal{M},\ X \in \{\mathrm{UL}, \mathrm{DL}\}, \|\mathbf{\Delta}\|_F \leq \epsilon. \tag{2.44}$$

Given the size of the CSI uncertainty, one way to guarantee the worst-case SINR is by obtaining its lower bound. The lower bound of the SINRs for the uplink and downlink transmissions are given in (2.45) and (2.46), respectively, where $\hat{\mathbf{\Sigma}}_{i_k}^{X}(\mathbf{v})$ includes both the estimated channel ($\tilde{\mathbf{H}}$) and the CSI uncertainty ($\mathbf{\Delta}$). Assuming the same uncertainty bound for associated CSI uncertainties, tractable upper bounds for the first terms in the denominators of (2.45) and (2.46), i.e., $(\mathbf{u}_{i_k,m}^{X})^H \hat{\mathbf{\Sigma}}_{i_k}^{X}(\mathbf{v})(\mathbf{u}_{i_k,m}^{X})$ are given in (2.49) and (2.50), for the uplink and downlink transmissions, respectively. The bound follows from the properties that $\mathrm{Tr}(A_1B_1) = \mathrm{Tr}(B_1A_1)$ for any $A_1 \in \mathbb{C}^{\bar{M}^{\mathrm{X}} \times \bar{N}^{\mathrm{X}}}$, $B_1 \in \mathbb{C}^{\bar{N}^{\mathrm{X}} \times \bar{M}^{\mathrm{X}}}$ and $\mathrm{Tr}(A_2B_2) \leq \mathrm{Tr}(A_2)\mathrm{Tr}(B_2)$ for any positive definite matrices, $A_2, B_2 \in \mathbb{C}^{\bar{N}^{\mathrm{X}} \times \bar{N}^{\mathrm{X}}}$ [101], where

$$\left(\bar{M}^{\mathrm{X}},\ \bar{N}^{\mathrm{X}}\right) = \begin{cases} (N_k,\ M_{i_k}) & \text{if X} = \mathrm{UL}, \\ (N_{i_k},\ M_k) & \text{if X} = \mathrm{DL}. \end{cases} \tag{2.51}$$

Finally, it exploits the bound on the CSI uncertainty from $\mathrm{Tr}(\Delta\Delta^H) \leq \epsilon^2$ to arrive at (2.49) and (2.50) for the uplink and downlink transmissions, respectively. A similar technique that involves obtaining tractable forms related to norm-bounded CSI uncertainty can be found in [87,102]. With the lower bound of the SINR, $\hat{\gamma}_{i_k,m}^{X}\left(\mathbf{v}, \mathbf{u}_{i_k,m}^{X}\right)_{\mathrm{LB}}$, the optimization problem can be written as below

$$\min_{\cdot \mathbf{v},\mathbf{u}} \quad \sum_{k=1}^{K}\sum_{i=1}^{I_k}\sum_{m=1}^{d_{i_k}^{\mathrm{UL}}} \left(\mathbf{v}_{i_k,m}^{\mathrm{UL}}\right)^H \mathbf{v}_{i_k,m}^{\mathrm{UL}} + \sum_{k=1}^{K}\sum_{i=1}^{I_k}\sum_{m=1}^{d_{i_k}^{\mathrm{DL}}} \left(\mathbf{v}_{i_k,m}^{\mathrm{DL}}\right)^H \mathbf{v}_{i_k,m}^{\mathrm{DL}} \tag{2.52}$$

$$\text{s.t.} \quad \hat{\gamma}_{i_k,m}^{X}\left(\mathbf{v}, \mathbf{u}_{i_k,m}^{X}\right)_{\mathrm{LB}} \geq \gamma_{\mathrm{th}}^{X},\ \ i_k \in \mathcal{I},\ m \in \mathcal{M},\ X \in \{\mathrm{UL}, \mathrm{DL}\}. \tag{2.53}$$

By obtaining the lower bound of the SINR, we can write the following one-to-one

relationship

$$\left(\hat{\Gamma}_{i_k,m}^{X}\right)_{\mathrm{UB}} = \left[1 + \left(\hat{\gamma}_{i_k,m}^{X}\right)_{\mathrm{LB}}\right]^{-1}, \tag{2.54}$$

where $\left(\hat{\Gamma}_{i_k,m}^{X}\right)_{\mathrm{UB}}$ is the upper bound of the MSE, $i_k \in \mathcal{I},\ m \in \mathcal{M},\ X \in \{\mathrm{UL}, \mathrm{DL}\}$. That is to say, we can exploit the upper bound (i.e., worst-case) of the MSE, $(\hat{\Gamma}_{i_k,m}^{X})_{\mathrm{UB}}$, to guarantee the lower bound (i.e., worst-case) of the SINR, $(\hat{\gamma}_{i_k,m}^{X})_{\mathrm{LB}}$ as a QoS

$$\begin{aligned}
\lceil (\mathbf{u}_{i_k,m}^{\mathrm{UL}})^H \hat{\mathbf{\Sigma}}_{i_k}^{\mathrm{UL}}(\mathbf{v})\, \mathbf{u}_{i_k,m}^{\mathrm{UL}} \rceil &= \underbrace{\left(\mathbf{u}_{i_k,m}^{\mathrm{UL}}\right)^H \tilde{\mathbf{\Sigma}}_{i_k}^{\mathrm{UL}}(\mathbf{v}) \mathbf{u}_{i_k,m}^{\mathrm{UL}}}_{\text{From eqn. (2.47)}} + \epsilon^2 \sum_{j=1}^{K} \sum_{l=1}^{I_j} \sum_{n=1}^{d_{l_j}^{\mathrm{UL}}} ||\mathbf{v}_{l_j,n}^{\mathrm{UL}}||_F^2 ||\mathbf{u}_{i_k,m}^{\mathrm{UL}}||_F^2 \\
&+ \epsilon^2 \sum_{j=1}^{K} \sum_{l=1}^{I_j} \sum_{n=1}^{d_{l_j}^{\mathrm{DL}}} ||\mathbf{v}_{l_j,n}^{\mathrm{DL}}||_F^2 ||\mathbf{u}_{i_k,m}^{\mathrm{UL}}||_F^2 + \epsilon^2 \kappa \sum_{l=1}^{I_k} \sum_{n=1}^{d_{l_k}^{\mathrm{DL}}} ||\mathrm{diag}\left(\mathbf{v}_{l_k,n}^{\mathrm{DL}} (\mathbf{v}_{l_k,n}^{\mathrm{DL}})^H\right)^{\frac{1}{2}}||_F^2 ||\mathbf{u}_{i_k,m}^{\mathrm{UL}}||_F^2 \\
&+ \epsilon^2 \beta \sum_{j=1}^{K} \sum_{l=1}^{I_j} \sum_{n=1}^{d_{l_j}^{\mathrm{UL}}} ||\mathbf{v}_{l_j,n}^{\mathrm{UL}}||_F^2 ||\mathrm{diag}\left(\mathbf{u}_{i_k,m}^{\mathrm{UL}} (\mathbf{u}_{i_k,m}^{\mathrm{UL}})^H\right)^{\frac{1}{2}}||_F^2 + \epsilon^2 \beta \sum_{j=1}^{K} \sum_{l=1}^{I_j} \sum_{n=1}^{d_{l_j}^{\mathrm{DL}}} ||\mathbf{v}_{l_j,n}^{\mathrm{DL}}||_F^2 || \\
&\mathrm{diag}\left(\mathbf{u}_{i_k,m}^{\mathrm{UL}} (\mathbf{u}_{i_k,m}^{\mathrm{UL}})^H\right)^{\frac{1}{2}}||_F^2 + \epsilon^2 \beta \sum_{l=1}^{I_k} \sum_{n=1}^{d_{l_k}^{\mathrm{DL}}} ||\mathbf{v}_{l_k,n}^{\mathrm{DL}}||_F^2 ||\mathrm{diag}\left(\mathbf{u}_{i_k,m}^{\mathrm{UL}} (\mathbf{u}_{i_k,m}^{\mathrm{UL}})^H\right)^{\frac{1}{2}}||_F^2
\end{aligned} \tag{2.49}$$

$$\begin{aligned}
\lceil (\mathbf{u}_{i_k,m}^{\mathrm{DL}})^H \hat{\mathbf{\Sigma}}_{i_k}^{\mathrm{DL}}(\mathbf{v})\, \mathbf{u}_{i_k,m}^{\mathrm{DL}} \rceil &= \underbrace{\left(\mathbf{u}_{i_k,m}^{\mathrm{DL}}\right)^H \tilde{\mathbf{\Sigma}}_{i_k}^{\mathrm{DL}}(\mathbf{v}) \mathbf{u}_{i_k,m}^{\mathrm{DL}}}_{\text{From eqn. (2.48)}} + \epsilon^2 \sum_{j=1}^{K} \sum_{l=1}^{I_j} \sum_{n=1}^{d_{l_j}^{\mathrm{DL}}} ||\mathbf{v}_{l_j,n}^{\mathrm{DL}}||_F^2 ||\mathbf{u}_{i_k,m}^{\mathrm{DL}}||_F^2 \\
&+ \epsilon^2 \sum_{j=1}^{K} \sum_{l=1}^{I_j} \sum_{n=1}^{d_{l_j}^{\mathrm{UL}}} ||\mathbf{v}_{l_j,n}^{\mathrm{UL}}||_F^2 ||\mathbf{u}_{i_k,m}^{\mathrm{DL}}||_F^2 + \epsilon^2 \kappa \sum_{n=1}^{d_{i_k}^{\mathrm{UL}}} ||\mathbf{u}_{i_k,m}^{\mathrm{DL}}||_F^2 ||\mathrm{diag}\left(\mathbf{v}_{i_k,n}^{\mathrm{UL}} (\mathbf{v}_{i_k,n}^{\mathrm{UL}})^H\right)^{\frac{1}{2}}||_F^2 \\
&+ \epsilon^2 \beta \sum_{j=1}^{K} \sum_{l=1}^{I_j} \sum_{n=1}^{d_{l_j}^{\mathrm{DL}}} ||\mathbf{v}_{l_j,n}^{\mathrm{DL}}||_F^2 ||\mathrm{diag}\left(\mathbf{u}_{i_k,m}^{\mathrm{DL}} (\mathbf{u}_{i_k,m}^{\mathrm{DL}})^H\right)^{\frac{1}{2}}||_F^2 + \epsilon^2 \beta \sum_{j=1}^{K} \sum_{l=1}^{I_j} \sum_{n=1}^{d_{l_j}^{\mathrm{UL}}} ||\mathbf{v}_{l_j,n}^{\mathrm{UL}}||_F^2 || \\
&\mathrm{diag}\left(\mathbf{u}_{i_k,m}^{\mathrm{DL}} (\mathbf{u}_{i_k,m}^{\mathrm{DL}})^H\right)^{\frac{1}{2}}||_F^2 + \epsilon^2 \beta \sum_{n=1}^{d_{i_k}^{\mathrm{UL}}} ||\mathbf{v}_{i_k,n}^{\mathrm{UL}}||_F^2 ||\mathrm{diag}\left(\mathbf{u}_{i_k,m}^{\mathrm{DL}} (\mathbf{u}_{i_k,m}^{\mathrm{DL}})^H\right)^{\frac{1}{2}}||_F^2
\end{aligned} \tag{2.50}$$

constraint. For given $\tilde{\mathbf{H}}_{i_k}^X,\ i_k \in \mathcal{I},\ m \in \mathcal{M},\ X \in \{\mathrm{UL}, \mathrm{DL}\}$, $(\hat{\Gamma}_{i_k,m}^X)_{\mathrm{UB}}$ can be computed as

$$(\hat{\Gamma}_{i_k,m}^X)_{\mathrm{UB}} = |(\mathbf{u}_{i_k,m}^X)^H \tilde{\mathbf{H}}_{i_k}^X \mathbf{V}_{i_k,m}^X - 1|^2 + \lceil (\mathbf{u}_{i_k,m}^X)^H \hat{\mathbf{\Sigma}}_{i_k}^X(\mathbf{v}) \mathbf{u}_{i_k,m}^X \rceil + (\mathbf{u}_{i_k,m}^X)^H \sum_{n=1,n\neq m}^{d_{i_k}^{\mathrm{X}}} \tilde{\mathbf{H}}_{i_k}^{\mathrm{X}} \mathbf{v}_{i_k,n}^{\mathrm{X}} \left(\mathbf{v}_{i_k,n}^{\mathrm{X}}\right)^H \left(\tilde{\mathbf{H}}_{i_k}^{\mathrm{X}}\right)^H \mathbf{u}_{i_k,m}^X. \tag{2.55}$$

At iteration τ and for a fixed $\hat{\theta}_{i_k,m}^{X_\tau},\ i_k \in \mathcal{I},\ m \in \mathcal{M}$, the above optimization problem can be reformulated as below

$$\min_{\mathbf{v},\theta} \quad \hat{P}_{\mathrm{BS+UE}} \tag{2.56}$$

$$\text{s.t.} \quad (\hat{\Gamma}_{i_k,m}^X)_{\mathrm{UB}} \leq -\hat{a}_{i_k,m}^{X_\tau} \hat{\theta}_{i_k,m}^X + \hat{b}_{i_k,m}^{X_\tau}, \tag{2.57}$$

$$\hat{\theta}_{i_k,m}^X \geq \log_c(\gamma_{\mathrm{th}}^X + 1), \tag{2.58}$$

where $\hat{(\cdot)}$ denotes the related variables for the case of norm-bounded design, similar to those in the stochastic uncertainty design. The optimization problem is also convex and can be solved similarly following the steps as in Algorithm 1.

2.5 Numerical Results And Discussions

Considering both perfect and imperfect CSI, in this section we investigate the performance of the proposed sum-power minimization algorithms for an FD MIMO multi-cell system through numerical simulations. We choose the simulation parameters from the 3GPP LTE specifications for small-cell deployments [103]. As discussed in Chapter 1, the small cells are suitable for deployment of the FD technology since the cell-edge path loss is less than that in conventional cellular systems, which makes the

problem of self-interference much more manageable [5, 61, 104].

In particular, our simulation setup considers an outdoor multi-cell scenario with three pico cells randomly dropped in a hexagonal macrocell. For simplicity, we assume the same number of transmit and receive antennas at each BS, i.e., $M_k = N_k = N,\ k \in \mathcal{K}$, and at each mobile user, i.e., $M_{i_k} = N_{i_k} = M,\ i_k \in \mathcal{I}$. We further assume that there are two users in each cell, where each BS is equipped with $N = 4$ transmit and receive antennas, and each user is equipped with $M = 2$ transmit and receive antennas[1]. Also, we consider that each user sends a single data stream in the uplink (UL) and downlink (DL) directions. We average our results over 500 independent channel realizations. The stochastic CSI uncertainty is generated following the model in (2.31), where the nominal SNR is calculated based on the standard transmit power of the BS and mobile users specified in [103]. The path loss model for line-of-sight (LOS) and non-line-of-sight (NLOS) communications between the BS and users are generated according to the following probability [64]

$$P_{\text{LOS}} \;=\; 0.5 - \min(0.5, 5\exp(-0.156/d)) + \min(0.5, 5\exp(-d/0.03)), \quad (2.59)$$

where d denotes the distance (km) between the BS and users.

We view $\mathbf{H}_{ki_k}^{\text{UL}} = \sqrt{\kappa_{i_k}^{\text{UL}}}\bar{\mathbf{H}}_{ki_k}^{\text{UL}}$ as the uplink channel between the user i_k and the BS k. The same model has been used in [61, 65, 66]. Here, $\bar{\mathbf{H}}_{ki_k}^{\text{UL}}$ denotes the small-scale fading following a complex Gaussian distribution with zero mean and unit variance, whereas the large-scale fading consisting of the path loss and shadowing is denoted by, $\kappa_{i_k}^{\text{UL}} = 10^{(-\text{Z}/10)},\ Z \in \{\text{LOS}, \text{NLOS}\}$, where LOS and NLOS are calculated from the specific path loss model given in Table 2.2. In the same vein, we define the

[1]Similar to studies in [26, 62], out of total $N_k + M_k$ antennas at the BS k, we assume that only N_k (M_k) antennas are used for HD transmission (reception). The same holds for the mobile users.

Table 2.2: Simulation Parameters and Corresponding Settings for an FD MIMO Multi-Cell System

Parameters	**Settings**
Cell Radius	40 m
Minimum Distance between BSs	40 m
Carrier Frequency	2 GHz
Bandwidth	10 MHz
Thermal Noise Density	-174 dBm/Hz
Noise Figure	BS: 13 dB, User: 9 dB
Path Loss (dB) between BS and users (d in km)	LOS: $103.8 + 20.9 \log_{10} d$ NLOS: $145.4 + 37.5 \log_{10} d$
Path Loss (dB) between users (d in km)	$98.45 + 20 \log_{10} d,\ d \leq 50$ m $175.78 + 40 \log_{10} d,\ d > 50$ m
Path Loss (dB) between BSs (d in km)	LOS: $89.5 + 16.9 \log_{10} d,\ d < 2/3$ km, LOS: $101.9 + 40 \log_{10} d,\ d \geq 2/3$ km, NLOS: $169.36 + 40 \log_{10} d$
Shadowing Standard Deviation between BS and users	10 dB
Shadowing Standard Deviation between users	12 dB
Shadowing Standard Deviation between BSs	6 dB

channels between the BS and DL users, and that of between the UL and DL users.

In order to simulate the self-interference channel, we adopt the model from [3].

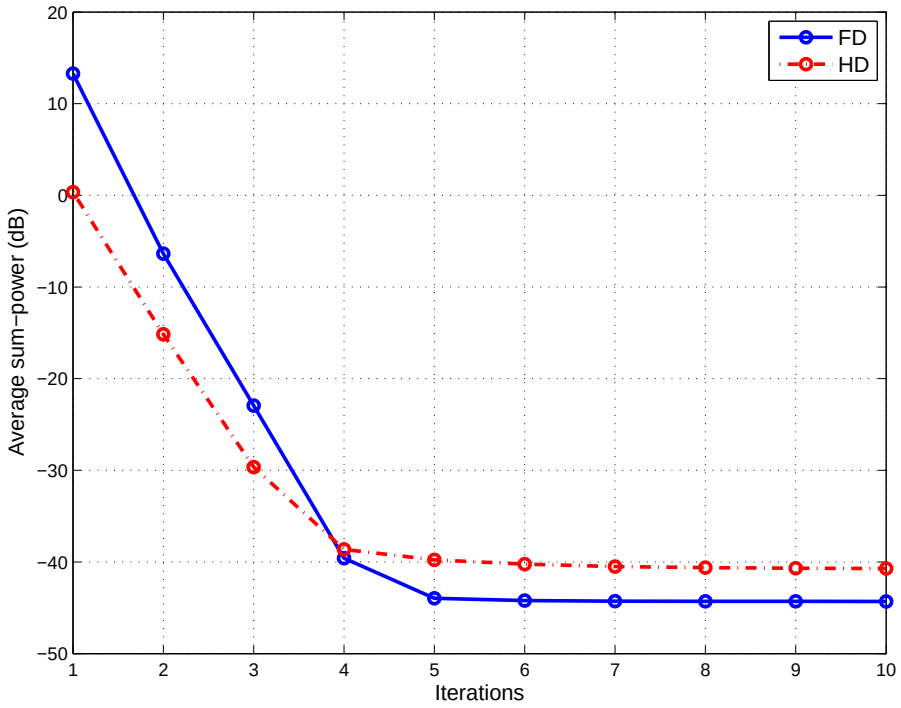

Figure 2.2: Convergence of the objective function in (2.21) for perfect CSI design with $\kappa = \beta = -120$ dB and a QoS constraint of 2.63 Mb/s.

Accordingly, at the BS k the self-interference channel is distributed as

$$\mathbf{H}_k^{\mathrm{SI}} \sim \mathcal{CN}\left(\sqrt{\frac{K_R}{1+K_R}}\bar{\mathbf{H}}_k^{\mathrm{SI}}, \frac{1}{1+K_R}\mathbf{I}_{N_k} \otimes \mathbf{I}_{M_k}\right), \tag{2.60}$$

where K_R denotes the Rician factor and $\bar{\mathbf{H}}_k^{\mathrm{SI}}$ is a deterministic matrix[2]. Table 2.2 summarizes the simulation parameters and corresponding settings. Unless stated otherwise, in our experiments we stick to the above settings of the network parameters.

In all our results, the rate is calculated as the spectral efficiency via $\log_2(1 + \Gamma_{i_k,m}^X)$, $i_k \in \mathcal{I}$, $m \in \mathcal{M}$, $X \in \{\mathrm{UL}, \mathrm{DL}\}$. We also note that our results on the power

[2]Without loss of generality, we assume $K_R = 1$ and $\bar{\mathbf{H}}_k^{\mathrm{SI}}$ is a matrix of all ones [61].

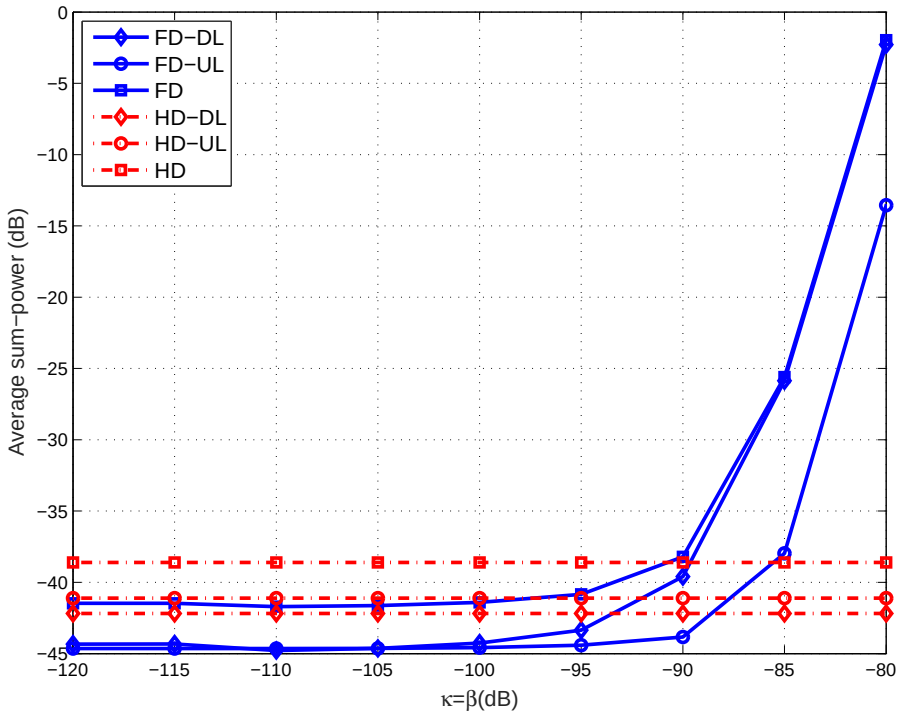

Figure 2.3: Comparison of the average power required by FD and HD systems for the perfect CSI design with a QoS constraint of 2.63 Mb/s and varying transceiver distortions.

efficiency do not account for the overhead owing to the execution of the optimization algorithms.

2.5.1 Perfect CSI Results

The proposed sum-power minimization algorithm presented in Section 2.3 relies on iterative updates of the design parameters. The iterative nature of the algorithm ensures a local optimal solution. To this end, it is desirable to observe the convergence behavior of the presented algorithm. Fig. 2.2 shows the outer convergence of the sum-power function in (2.21) for FD and HD operations. As expected, we observe strictly non-increasing behavior of the optimization objective at each iteration. Furthermore,

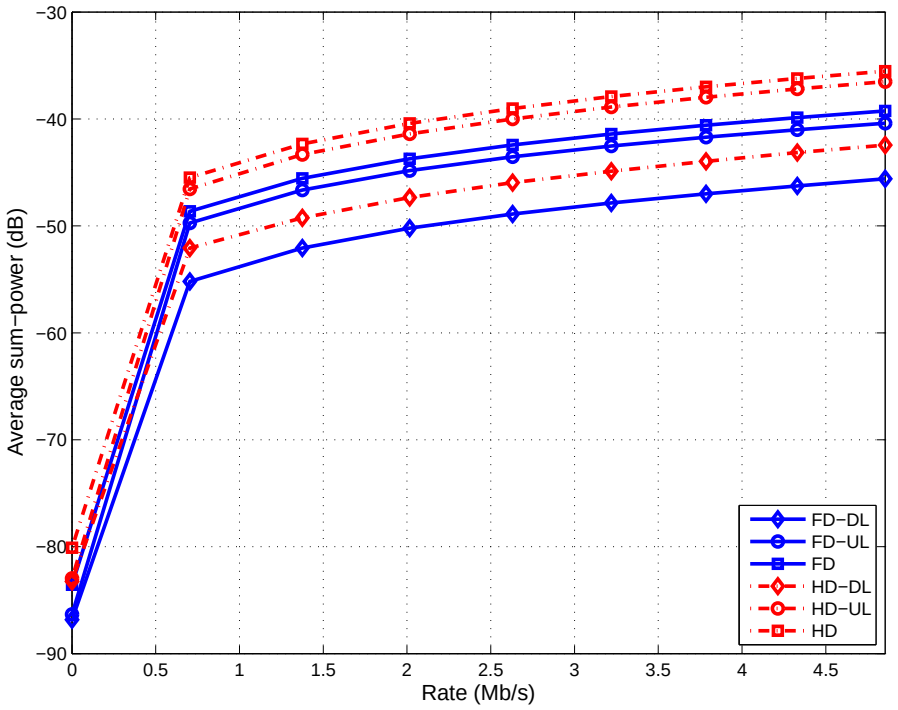

Figure 2.4: Comparison of the average power required by FD and HD systems for the perfect CSI design with $\kappa = \beta = -120$ dB and varying QoS constraints.

we notice faster convergence of the HD setup. This is because the FD system needs to consider additional self-interference in the design process, which contributes to the slower convergence of the optimization algorithm.

Fig. 2.3 provides a comparison of the average sum-power required by FD and HD systems with respect to the transceiver distortion. For the HD operation, we assume that each BS serves the same number of DL and UL users as in the FD system. As we observe from Fig. 2.3, FD and HD setups require the same average power at around $\kappa = \beta \approx -90$ dB. However, the FD transmission outperforms the HD one when $\kappa = \beta < -90$ dB. These levels of self-interference cancellation have been achieved through a recent advanced technique reported in [25]. We also note that

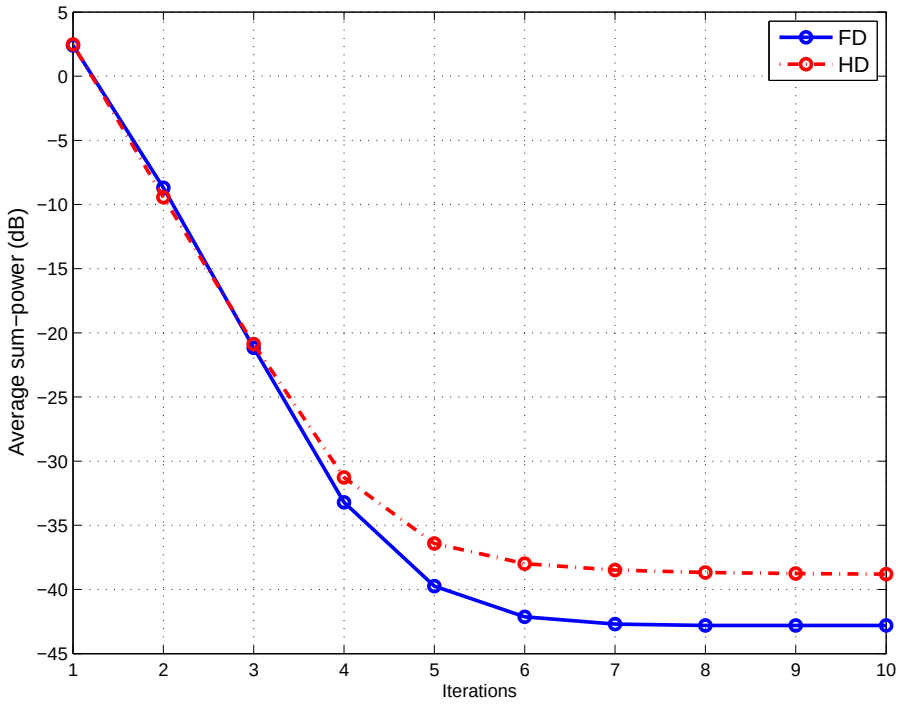

Figure 2.5: Convergence of the objective function in (2.39) for a design with stochastic CSI uncertainty, $\kappa = \beta = -120$ dB, a QoS constraint of 2.63 Mb/s, $\eta = 0.3$, and $\lambda = 0.2$.

the power efficiency gain for the FD over that of the HD transmission varies with different κ (β) values. This is due to the fact that the higher transmitter (receiver) distortion, represented by κ (β), corresponds to larger residual self-interference, which necessitates a higher required transmit power to maintain the same QoS constraint. Therefore, we generally achieve a higher power efficiency gain with smaller values of κ (β). Furthermore, FD-DL transmission tends to consume more power at higher κ (β). This is mainly due to the fact that the user has a lower noise figure, which also gets compounded at higher κ (β), i.e., more interference.

Fig. 2.4 demonstrates a comparison of the average sum-power required by FD and HD systems with varying QoS constraints. As we notice from Fig. 2.4, as the

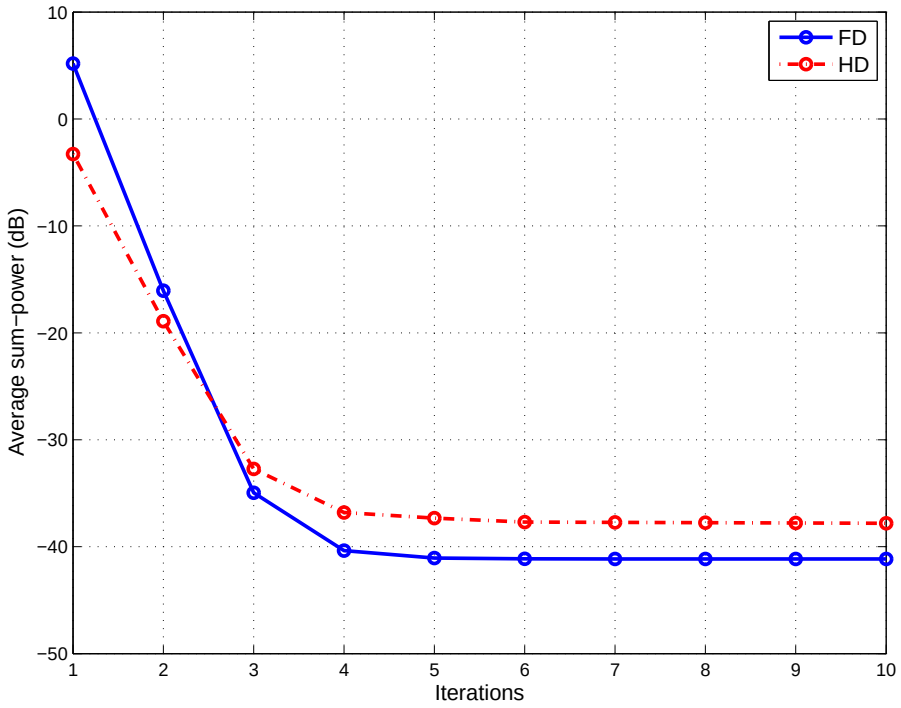

Figure 2.6: Convergence of the objective function in (2.56) for a design with norm-bounded CSI uncertainty, $\kappa = \beta = -120$ dB, a QoS constraint of 2.63 Mb/s, and $s = 0.01$.

QoS constraint increases, power requirements for both FD and HD systems increase. Furthermore, with increasing QoS constraints, the HD system requires increasingly more power, i.e., the gap between the required power for FD and HD systems tends to be larger. Also, at this level of κ (β), the power consumption is mainly determined by the interference between the nodes, which is lower between the users due to higher path losses.

2.5.2 Imperfect CSI Results

After observing the power efficiency gains offered by the FD transmission with perfect CSI, in this section we study the performance in the presence of imperfect CSI.

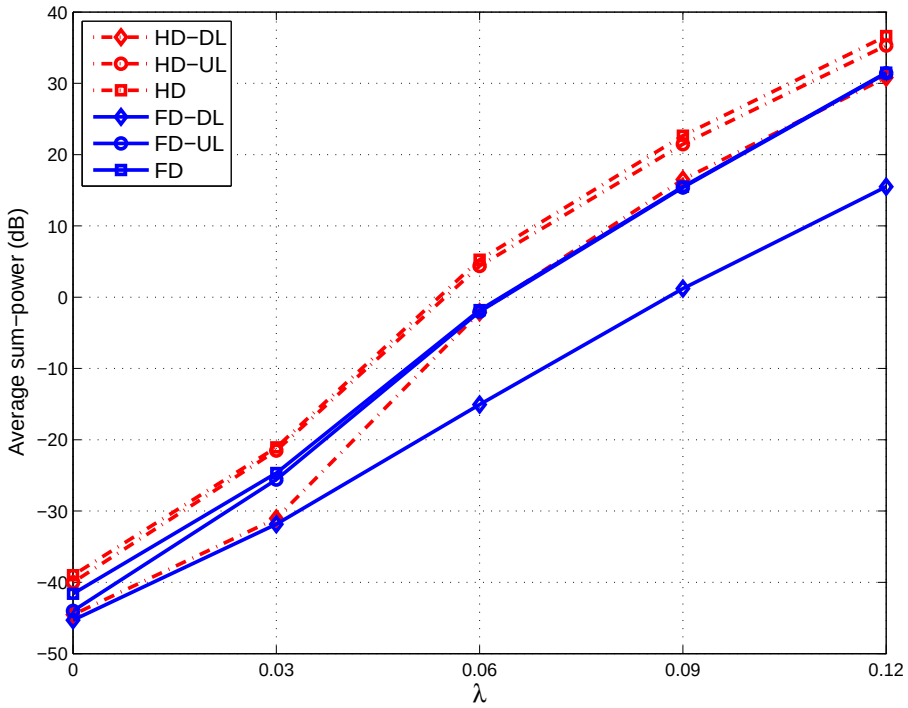

Figure 2.7: Comparison of the average power required by robust FD and HD systems with stochastic CSI uncertainty, $\kappa = \beta = -120$ dB, a QoS constraint of 2.63 Mb/s, and $\eta = 0.3$.

As discussed in Section 2.4, we consider both stochastic and norm-bounded CSI uncertainties, where either the statistics or the size of the CSI uncertainty is known to the transmitter, respectively. For the sake of simplicity, in either case we assume that the associated channel links experience the same CSI uncertainty.

Similar to the algorithm presented in Section 2.3, each of the robust algorithms in Section 2.4 also rely on iterative updates of the design parameters to arrive at a local optimum. Figs. 2.5 and 2.6 show the outer convergences of the proposed robust sum-power minimization algorithms for FD and HD setups over multiple design parameters considering the stochastic and the norm-bounded CSI uncertainties, respectively. In both cases, we observe strictly non-increasing behavior of the optimization

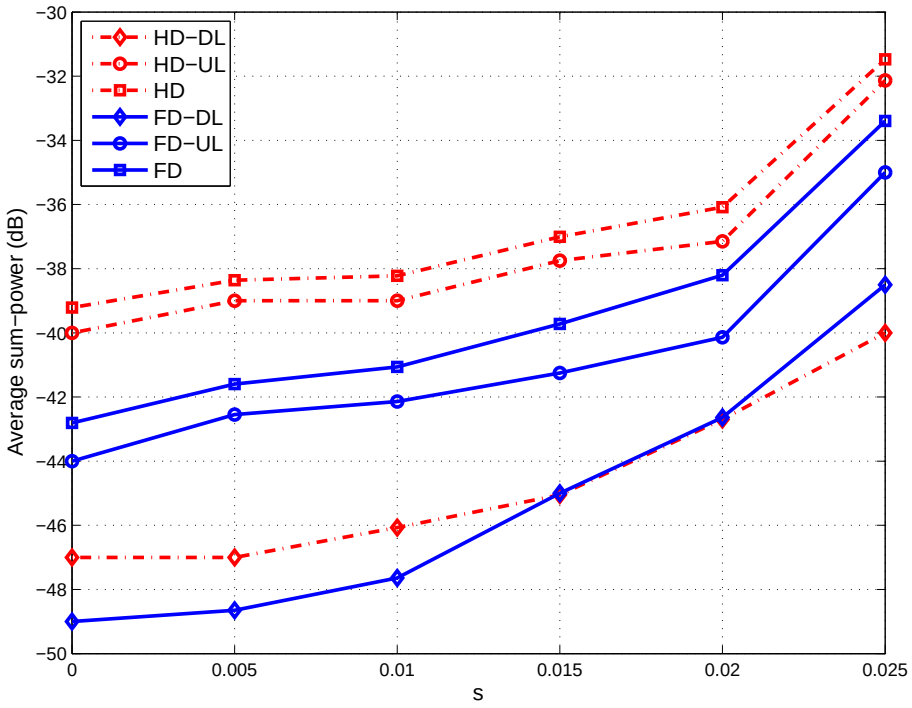

Figure 2.8: Comparison of the average power required by robust FD and HD systems with norm-bounded uncertainty, $\kappa = \beta = -120$ dB and a QoS constraint of 2.63 Mb/s.

objectives, i.e., the reduction of the sum-power with each iteration. Furthermore, as in the case of perfect CSI, the HD setup generally converges in fewer optimization iterations compared to its FD counterpart.

In Fig. 2.7, we compare the average power requirements for the robust FD and HD setups in the presence of stochastic CSI uncertainty for a given QoS constraint and transceiver distortion, where the parameters λ and η are chosen similar to those in [65, 95]. In particular, we notice that for a given η, the required transmit power for FD and HD setups increase with larger λ. This is justified because the higher CSI uncertainty means increased noise; therefore they require more power to guarantee the same QoS. We also note that the proposed FD design consumes less power to

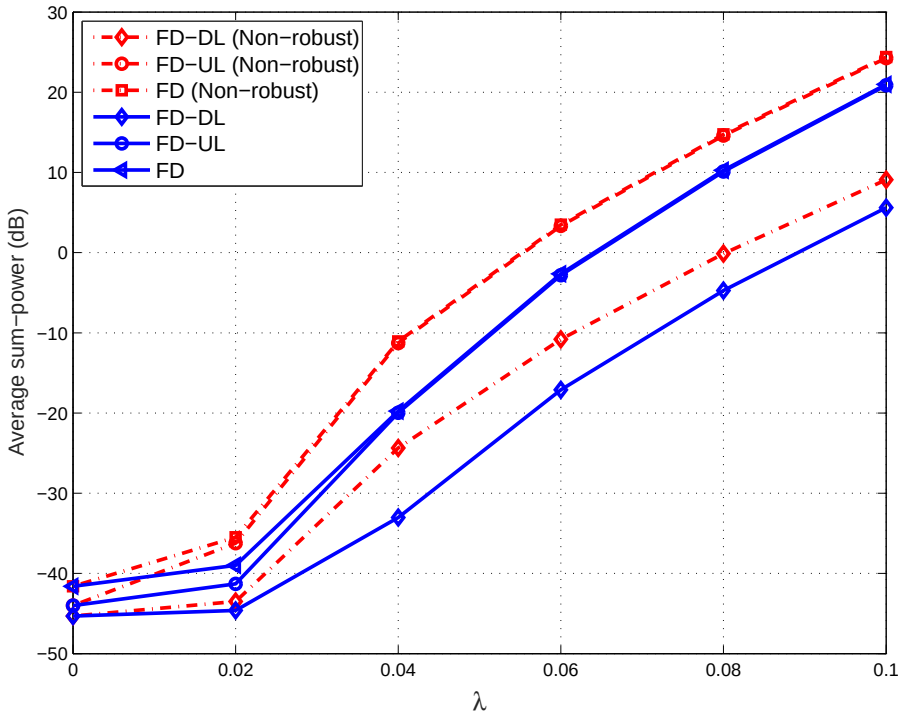

Figure 2.9: Comparison of the average power required by robust and non-robust FD systems with stochastic CSI uncertainty, $\kappa = \beta = -120$ dB, a QoS constraint of 2.63 Mb/s, and $\eta = 0.3$.

guarantee the same QoS than the HD one.

Next we compare the average power requirements for the robust FD and HD setups assuming norm-bounded CSI uncertainty for a given QoS and transceiver distortion, as depicted in Fig. 2.8. The CSI uncertainty parameter is related to the quality of the associated channels through the parameter s, whose range is chosen similar to settings in [65, 105]. We observe that the required transmit power for FD and HD setups increase with larger s. This corroborates the previous observation with the stochastic CSI uncertainty, since the noise also increases with larger CSI uncertainty. It is also apparent from the robust results that the FD system is affected slightly more by the increased CSI uncertainty than the HD one since the former

involves more channel links (i.e., associated CSI uncertainties).

Finally, in Fig. 2.9 we present the average power required by the robust and non-robust FD setups against the stochastic CSI uncertainty, measured by λ and η. This result exemplifies the benefits that can be harnessed through the robust design in the presence of CSI uncertainty. As we see from this result, as λ increases the power requirements increase for both robust and non-robust FD systems. We also observe that the non-robust FD setup requires more power in order to guarantee the same QoS since it does not consider the CSI uncertainty into the design process. Furthermore, as λ increases (i.e., with increased CSI uncertainty), the difference in required average power between the robust and non-robust FD systems tends to increases for the same reason. In particular, the robust design results in power savings that can be as high as 87% for the considered simulation scenario.

2.6 Conclusions

In this chapter, we have studied the transmit and receive beamforming designs in order to minimize the transmit power for an FD MIMO multi-cell system while maintaining a certain QoS. In addition to the limited DR at the transceivers, such a communication system also suffers from the self-interference as well as the co-channel interference from other nodes. Due to the non-convex nature of the optimization problem, we approximate this as a DCP, which is then solved via SCA. Our results demonstrate that the FD systems require less transmit power than the HD systems under low to moderate level of transceiver distortions and for increasing QoS constraints. In dealing with both stochastic and norm-bounded CSI uncertainties, our studies suggest that the proposed robust FD designs similarly require less power when compared with the HD setups. Moreover, we have quantified the transmit power that

can be saved through the robust design in comparison to a non-robust design. The results justify the importance of a robust design in power-constrained applications.

Chapter 3

Fairness Consideration in Full-Duplex and Device-to-Device Communication Systems

3.1 Introduction

In the previous chapter, we have addressed the problem of sum-power minimization for the power-constrained FD applications, with maintenance of a certain QoS. In this chapter, we address the QoS fairness problem, given a certain power constraint. There may be specific interference scenarios in communications networks, as we address in the sequel, which may skew the resource allocations in favor of users that experience good channels, i.e., weak interference, if one tries to maximize the total sum-rate of the network. In this case, it is likely that some users in the network will be underserved, which leads to unfairness among the users. One possibility to achieve network-wide fairness is to maximize the minimum SINR among all the users in the network. This is same as equalizing the SINR performance of all users, and thus it is a strategy for enforcing the desired level of fairness in the network. The authors in [106, 107] have shown that max-min problems can be solved by Second Order Cone Programming (SOCP) programs, which have a high computational com-

plexity. In this chapter, our general objective is to design low complexity algorithms that achieve the desired fairness among the users. Furthermore, we also consider practical design aspects, such as CSI uncertainty. To this end, in the sequel we address fairness considerations in the specific context of FD and D2D communications. As presented in the Chapter 1, the performance of both FD and D2D systems are interference-limited. For the former, it is the (residual) self-interference that limits the performance, while the performance is limited by the inter-user interference for the latter.

The rest of this chapter is organized as follows. In Section 3.2, we investigate the fairness design in FD multi-cell MIMO communications. We study the same design criteria for the D2D communications in Section 3.3. We summarize the findings of this chapter in Section 3.4.

3.2 Fairness in FD Communications

In Section 2.1 of Chapter 2, we discussed that the FD system suffers form the residual self-interference due to imperfections of radio components, such as amplifier non-linearity, oscillator phase noise. We also noted that the system optimization under the influence of residual self-interference has been investigated in various studies, such as [53–56].

The beamformer design for the sum-rate maximization in FD multi-cell cellular systems has been studied in [61, 65]. It has been reported that when the sum-rate maximization problems are considered in FD systems, the increasing self-interference power overwhelms the desired signals of the uplink users, which leads to reduction in achievable rate in the uplink channel. Since the objective is to maximize the total throughput, a natural solution is to reduce the transmit power in the uplink channel.

Therefore, the uplink users are underserved, since all the resources are devoted for the downlink transmission. This leads to unfairness among the users. In the context of multi-cell FD communications as it is illustrated in Fig. 3.1 and also discussed in Section 2.1 of Chapter 2, there will be additional interference owing to the FD transmission both at BSs and users, i.e., I) the self-interference at each FD BS and FD user, II) the interference among adjacent BSs, i.e., inter-BS interference, and III) the interference among all the mobile users in all cells. This interference will further degrade the performance of the cell-edge users. Therefore, in the first part of this section, we propose a transceiver design that maximizes the harmonic-sum of SINRs for MIMO systems, and derive an iterative low-complexity distributed algorithm.

In the second part of this section, we extend our design to provide resilience against inaccuracies of the CSI. To this end, the CSI errors are often modeled as Gaussian random variables [94], and the robustness can be provided in the statistical sense. Alternatively, another way to achieve robustness is by worst-case optimization, which designs the system to operate under the worst-case channel condition if the CSI uncertainty is bounded [96–98]. We adopt the second approach and propose a low complexity iterative algorithm based on SDR technique to achieve fairness.

The numerical results show that the proposed FD system outperforms the HD system under self-interference levels that have been achieved recently. In addition, we verify the advantages of incorporating important practical issues, such as CSI uncertainty and fairness performance into the transceiver design.

3.2.1 System Model

In this section, we consider an FD multi-cell multi-user MIMO system as it is illustrated in Fig. 3.1. In particular, we consider a K cell FD system, where BS

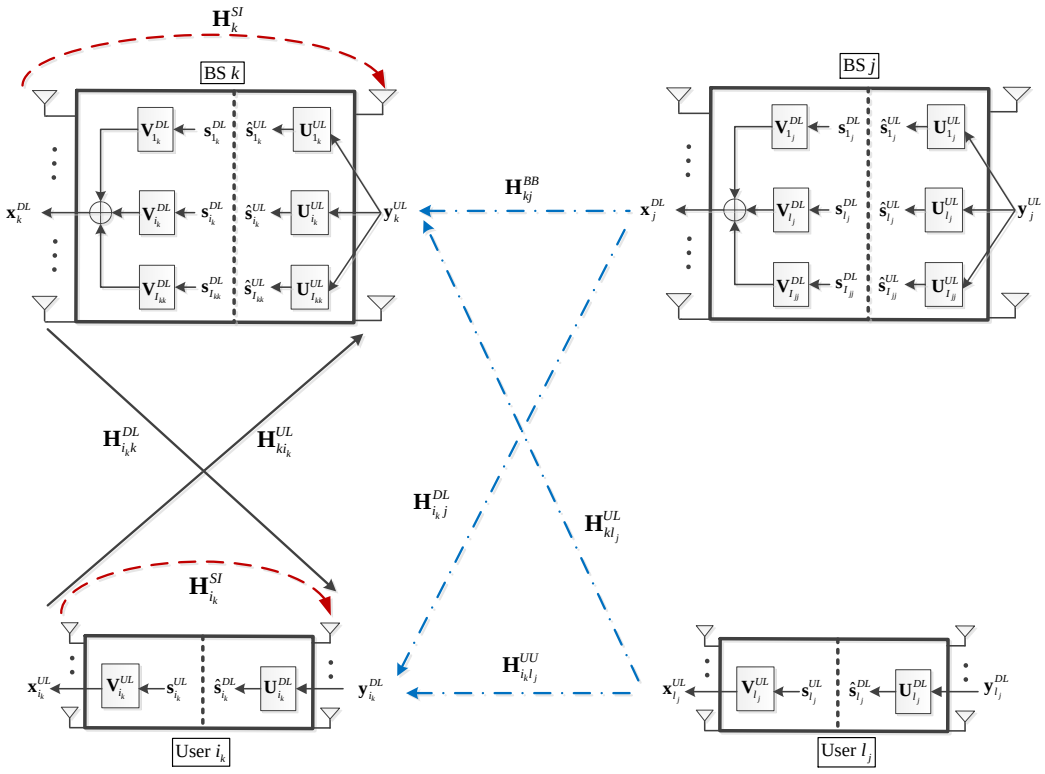

Figure 3.1: Full-duplex MIMO multi-cell system. Dashed arrows denote the self-interference and the dash-dotted arrows denote the interference between different nodes.

$k,\ k = 1, \ldots, K$ is equipped with M_k transmit and N_k receive antennas, and serves I_k users in cell k. We denote i_k to be the ith user in cell k with M_{i_k} transmit and N_{i_k} receive antennas. We define the set of BSs as $\mathcal{K} = \{1, \ldots, K\}$ and users as $\mathcal{I} = \{i_k \mid k \in \{1, 2, \ldots, K\},\ i \in \{1, 2, \ldots, I_k\}\}$. We adopt the same limited DR models at the FD transmitters and at the FD receivers as in Chapter 2. Fortunately, the system descriptions from Section 2.2 of Chapter 2 are directly applicable for this study. Hence, we do not repeat them in this section. Recall the signal received by

the BS k and that received by the user i_k can be written, respectively, as

$$\mathbf{y}_k^{\mathrm{UL}} = \sum_{j=1}^{K}\sum_{l=1}^{I_j} \mathbf{H}_{kl_j}^{\mathrm{UL}}\mathbf{x}_{l_j}^{\mathrm{UL}} + \mathbf{H}_k^{\mathrm{SI}}\left(\mathbf{x}_k^{\mathrm{DL}} + \mathbf{c}_k^{\mathrm{DL}}\right) + \sum_{j=1, j\neq k}^{K} \mathbf{H}_{kj}^{\mathrm{BB}}\mathbf{x}_j^{\mathrm{DL}} + \mathbf{e}_k^{\mathrm{UL}} + \mathbf{n}_k^{\mathrm{UL}}, \quad (3.1)$$

$$\mathbf{y}_{i_k}^{\mathrm{DL}} = \sum_{j=1}^{K} \mathbf{H}_{i_k j}^{\mathrm{DL}}\mathbf{x}_j^{\mathrm{DL}} + \mathbf{H}_{i_k}^{\mathrm{SI}}\left(\mathbf{x}_{i_k}^{\mathrm{UL}} + \mathbf{c}_{i_k}^{\mathrm{UL}}\right) + \sum_{(l,j)\neq(i,k)} \mathbf{H}_{i_k l_j}^{\mathrm{UU}}\mathbf{x}_{l_j}^{\mathrm{UL}} + \mathbf{e}_{i_k}^{\mathrm{DL}} + \mathbf{n}_{i_k}^{\mathrm{DL}}. \quad (3.2)$$

For the convenience of presentation, we will use the following notation in the rest of the this section:

$$\mathbf{H}_{i_k}^{\mathrm{X}} = \begin{cases} \mathbf{H}_{ki_k}^{\mathrm{UL}}, & \text{if X} = \mathrm{UL}, \\ \mathbf{H}_{i_k k}^{\mathrm{DL}}, & \text{if X} = \mathrm{DL}. \end{cases} \quad (3.3)$$

3.2.2 Fairness Design with Perfect CSI

3.2.2.1 Problem Formulation

The problem that maximizes the minimum SINR of users can be formulated as:

$$\max_{\mathbf{.v},\mathbf{u}} \quad \min_{\forall i_k \in \mathcal{I}, m^{\mathrm{X}} \in \mathcal{M}} \ \gamma_{i_k,m}^{\mathrm{X}}\left(\mathbf{v}, \mathbf{u}_{i_k,m}^{\mathrm{X}}\right) \quad (3.4)$$

$$\text{s.t.} \quad \sum_{m=1}^{d_{i_k}^{\mathrm{UL}}} \left(\mathbf{v}_{i_k,m}^{\mathrm{UL}}\right)^H \mathbf{v}_{i_k,m}^{\mathrm{UL}} \leq P_{i_k}, \ i_k \in \mathcal{I}, \quad (3.5)$$

$$\sum_{i=1}^{I_k}\sum_{m=1}^{d_{i_k}^{\mathrm{DL}}} \left(\mathbf{v}_{i_k,m}^{\mathrm{DL}}\right)^H \mathbf{v}_{i_k,m}^{\mathrm{DL}} \leq P_k, \ k \in \mathcal{K}, \quad (3.6)$$

where P_{i_k} in (3.5) is the transmit power constraint at the user i_k, and P_k in (3.6) is the total power constraint at the BS k. Here, the optimization variable $\mathbf{u}$ denotes the stacked vectors of all receive filters in the uplink and downlink channel. Furthermore, $\mathcal{M}$ denotes the set of all uplink and downlink data streams, i.e.,

$\mathcal{M} = \left\{m = 1, \ldots, d_{i_k}^{\mathrm{X}}, i_k \in \mathcal{I},\ \mathrm{X} = \{\mathrm{UL},\ \mathrm{DL}\}\right\}$. The problem formulation (3.4)-(3.6) has two critical shortcomings. First, it requires an iterative search for a SOCP feasibility test [107, 108], which has a high computational complexity and necessitates a centralized implementation. Second, it ignores the overall throughput of the cell for the purpose of maintaining fairness. In the following, we address both those issues through a reformulation of the original problem.

3.2.2.2 Harmonic-Sum Minimization

In order to balance both the throughput for cell-edge users and the overall throughput, we choose to maximize the harmonic-sum of the user throughput, which is the sum of reciprocals of the user SINRs [109]. The harmonic-sum has the following properties for any set of positive numbers:

$$\min\{x_1, x_2, \ldots, x_N\} \geq \frac{1}{\sum_{i=1}^{N} \frac{1}{x_i}}, \tag{3.7}$$

$$\frac{1}{N}\sum_{i=1}^{N} x_i \geq \frac{N}{\sum_{i=1}^{N} \frac{1}{x_i}}, \tag{3.8}$$

It is easy to see from (3.7) and (3.8) that maximizing the harmonic-sum will indirectly maximize the minimum value and the arithmetic average of SINRs, respectively. These properties allow the maximization of the harmonic-sum to indirectly balance the overall throughput and the user fairness.

The harmonic-sum objective function for multi-cell multistream multi-user MIMO systems can be expressed as

$$\mathrm{SINR}_{\mathrm{H}} = \frac{1}{\sum_{k=1}^{K}\sum_{i=1}^{I_k}\sum_{\mathrm{X}\in\{\mathrm{UL,DL}\}}\sum_{m=1}^{d_{i_k}^{\mathrm{X}}} \frac{1}{\gamma_{i_k,m}^{\mathrm{X}}}}. \tag{3.9}$$

Maximizing the harmonic-sum $\mathrm{SINR_H}$ is equivalent to minimizing $1/\mathrm{SINR_H}$. Therefore, using the uplink and downlink SINRs from (2.3) and (2.4) of Chapter 2, respectively, this problem can be written as

$$\min_{\mathbf{v},\mathbf{u}} \quad \sum_{k=1}^{K}\sum_{i=1}^{I_k}\sum_{\mathrm{X}\in\{\mathrm{UL,DL}\}}\sum_{m=1}^{d_{i_k}^{\mathrm{X}}} \frac{\left(\mathbf{u}_{i_k,m}^{\mathrm{X}}\right)^H \mathbf{Q}_{i_k}^{\mathrm{X}}\left(\mathbf{v}\right)\mathbf{u}_{i_k,m}^{\mathrm{X}} - \left|\left(\mathbf{u}_{i_k,m}^{\mathrm{X}}\right)^H \mathbf{H}_{i_k}^{\mathrm{X}}\mathbf{v}_{i_k,m}^{\mathrm{X}}\right|^2}{\left|\left(\mathbf{u}_{i_k,m}^{\mathrm{X}}\right)^H \mathbf{H}_{i_k}^{\mathrm{X}}\mathbf{v}_{i_k,m}^{\mathrm{X}}\right|^2} \tag{3.10}$$

$$\text{s.t.} \quad (3.5),\ (3.6), \tag{3.11}$$

where $\mathbf{Q}_{i_k}^{\mathrm{X}}\left(\mathbf{v}\right)$, $\mathrm{X}\in\{\mathrm{UL,DL}\}$, is defined in (2.3) and (2.4). The problem (3.10)-(3.11) can be equivalently rewritten as

$$\min_{\mathbf{v},\mathbf{u}} \sum_{k=1}^{K}\sum_{i=1}^{I_k}\sum_{\mathrm{X}\in\{\mathrm{UL,DL}\}}\sum_{m=1}^{d_{i_k}^{\mathrm{X}}}\Big(\left(\mathbf{u}_{i_k,m}^{\mathrm{X}}\right)^H \mathbf{Q}_{i_k}^{\mathrm{X}}(\mathbf{v})\,\mathbf{u}_{i_k,m}^{\mathrm{X}} - 1\Big) \tag{3.12}$$

$$\text{s.t.} \quad \left|\left(\mathbf{u}_{i_k,m}^{\mathrm{X}}\right)^H \mathbf{H}_{i_k}^{\mathrm{X}}\mathbf{v}_{i_k,m}^{\mathrm{X}}\right|^2 = 1,\ i_k\in\mathcal{I},\ m\in\mathcal{M}, \tag{3.13}$$

$$(3.5),\ (3.6), \tag{3.14}$$

which can be further simplified as

$$\min_{\mathbf{V},\mathbf{U}} \quad \sum_{k=1}^{K}\sum_{i=1}^{I_k}\sum_{\mathrm{X}\in\{\mathrm{UL,DL}\}} \mathrm{Tr}\left(\left(\mathbf{U}_{i_k}^{\mathrm{X}}\right)^H \mathbf{Q}_{i_k}^{\mathrm{X}}\left(\mathbf{V}\right)\mathbf{U}_{i_k}^{\mathrm{X}}\right) \tag{3.15}$$

$$\text{s.t.} \quad \left|\left(\mathbf{u}_{i_k,m}^{\mathrm{X}}\right)^H \mathbf{H}_{i_k}^{\mathrm{X}}\mathbf{v}_{i_k,m}^{\mathrm{X}}\right|^2 = 1,\ i_k\in\mathcal{I},\ m\in\mathcal{M}, \tag{3.16}$$

$$(3.5),\ (3.6), \tag{3.17}$$

where the optimization variable $\mathbf{V}\left(\mathbf{U}\right)$ denotes all transmit (receive) beamforming matrices in the uplink and downlink channels and $\mathbf{Q}_{i_k}^{\mathrm{X}}\left(\mathbf{V}\right)$ is a function of transmit beamforming matrices, $\mathbf{V}$. We also note that the phase rotation of the column vectors of the transmit beamforming matrices, $\mathbf{v}_{i_k,m}^{\mathrm{X}}$, does not affect the unit norm

constraint (3.16). Therefore, we can replace the constraint $\left|\left(\mathbf{u}_{i_k,m}^{\mathrm{X}}\right)^H \mathbf{H}_{i_k}^{\mathrm{X}} \mathbf{v}_{i_k,m}^{\mathrm{X}}\right|^2 = 1$ by $\left(\mathbf{u}_{i_k,m}^{\mathrm{X}}\right)^H \mathbf{H}_{i_k}^{\mathrm{X}} \mathbf{v}_{i_k,m}^{\mathrm{X}} = 1$. It has been shown in Appendix B.1 that this replacement does not change the objective function and other constraints.

The new optimization problem can be cast as

$$\min_{\mathbf{V},\mathbf{U}} \quad \sum_{k=1}^{K} \sum_{i=1}^{I_k} \sum_{\mathrm{X}\in\{\mathrm{UL,DL}\}} \mathrm{Tr}\left(\left(\mathbf{U}_{i_k}^{\mathrm{X}}\right)^H \mathbf{Q}_{i_k}^{\mathrm{X}}\left(\mathbf{v}\right) \mathbf{U}_{i_k}^{\mathrm{X}}\right) \tag{3.18}$$

$$\text{s.t.} \quad \left(\left(\mathbf{U}_{i_k}^{\mathrm{X}}\right)^H \mathbf{H}_{i_k}^{\mathrm{X}} \mathbf{V}_{i_k}^{\mathrm{X}}\right) \circ \mathbf{I}_{d_{i_k}^{\mathrm{X}}} = \mathbf{I}_{d_{i_k}^{\mathrm{X}}},\ i_k \in \mathcal{I},\ \forall \mathrm{X}, \tag{3.19}$$

$$\mathrm{Tr}\left(\left(\mathbf{V}_{i_k}^{\mathrm{UL}}\right)^H \mathbf{V}_{i_k}^{\mathrm{UL}}\right) \leq P_{i_k},\ i_k \in \mathcal{I}, \tag{3.20}$$

$$\sum_{i=1}^{I_k} \mathrm{Tr}\left(\left(\mathbf{V}_{i_k}^{\mathrm{DL}}\right)^H \mathbf{V}_{i_k}^{\mathrm{DL}}\right) \leq P_k,\ k \in \mathcal{K}. \tag{3.21}$$

Note that the objective function (3.18) is not jointly convex over transmit beamforming matrices in the set $\mathbf{V}$ and receive beamforming matrices in the set $\mathbf{U}$ (since they are coupled). Therefore, we cannot apply the standard convex optimization methods to obtain the optimal solution. However, as the objective function (3.18) is component-wise convex over the matrices in $\mathbf{V}$ and $\mathbf{U}$, we employ an iterative algorithm that finds the efficient solutions of $\mathbf{V}$ and $\mathbf{U}$ in an alternating fashion. Particularly, we update the transmit beamforming matrices in $\mathbf{V}$ when the receive beamforming matrices in $\mathbf{U}$ are fixed. Thereafter, we update the receive beamforming matrices in $\mathbf{U}$ using $\mathbf{V}$ obtained at the previous step. The iterations continue until convergence or a pre-defined number of iterations is reached. The Lagrangian function of the problem (3.18)-(3.21) can be written as

$$\mathcal{L}\left(\mathbf{V},\mathbf{U},\boldsymbol{\lambda},\boldsymbol{\Delta}\right) =$$
$$\sum_{k=1}^{K} \sum_{i=1}^{I_k} \sum_{\mathrm{X}\in\{\mathrm{UL,DL}\}} \mathrm{Tr}\left(\left(\mathbf{U}_{i_k}^{\mathrm{X}}\right)^H \mathbf{Q}_{i_k}^{\mathrm{X}}\left(\mathbf{v}\right) \mathbf{U}_{i_k}^{\mathrm{X}}\right) + \sum_{i_k\in\mathcal{I}} \lambda_{i_k}^{\mathrm{UL}} \left(\mathrm{Tr}\left(\left(\mathbf{V}_{i_k}^{\mathrm{UL}}\right)^H \mathbf{V}_{i_k}^{\mathrm{UL}}\right) - P_{i_k}\right) +$$

$$\sum_{k=1}^{K}\lambda_k^{\mathrm{DL}}\left(\sum_{i=1}^{I_k}\mathrm{Tr}\left(\left(\mathbf{V}_{i_k}^{\mathrm{DL}}\right)^H\mathbf{V}_{i_k}^{\mathrm{DL}}\right)-P_k\right)+\sum_{k=1}^{K}\sum_{i=1}^{I_k}\sum_{\mathrm{X}\in\{\mathrm{UL},\mathrm{DL}\}}\mathrm{Tr}\left(\boldsymbol{\Delta}_{i_k}^{\mathrm{X}}\left(\mathbf{I}_{d_{i_k}^{\mathrm{X}}}-\left(\mathbf{U}_{i_k}^{\mathrm{X}}\right)^H\mathbf{H}_{i_k}^{\mathrm{X}}\mathbf{V}_{i_k}^{\mathrm{X}}\right)\right),\tag{3.22}$$

where $\lambda_{i_k}^{\mathrm{UL}}$ and λ_k^{DL} are dual variables associated with the power constraints (3.20) and (3.21), respectively, and $\boldsymbol{\Delta}_{i_k}^{\mathrm{X}}$ is a diagonal matrix with dual variables for the equality constraint (3.19). Here, $\boldsymbol{\lambda}$ and $\boldsymbol{\Delta}$ are the set of all dual variables for the power and equality constraints, respectively.

The optimal transmit and receive beamforming matrices can be computed by taking the derivative of the Lagrangian function $\mathcal{L}\left(\mathbf{V},\mathbf{U},\boldsymbol{\lambda},\boldsymbol{\Delta}\right)$ with respect to $\mathbf{V}$ and $\mathbf{U}$, respectively. They can be expressed as

$$\mathbf{U}_{i_k}^{\mathrm{X}}=\left(\mathbf{H}_{i_k}^{\mathrm{X}}\mathbf{V}_{i_k}^{\mathrm{X}}\left(\mathbf{V}_{i_k}^{\mathrm{X}}\right)^H\left(\mathbf{H}_{i_k}^{\mathrm{X}}\right)^H+\boldsymbol{\Sigma}_{i_k}^{\mathrm{X}}\left(\mathbf{v}\right)\right)^{-1}\mathbf{H}_{i_k}^{\mathrm{X}}\mathbf{V}_{i_k}^{\mathrm{X}}\tilde{\boldsymbol{\Delta}}_{i_k}^{\mathrm{X}},\tag{3.23}$$

$$\mathbf{V}_{i_k}^{\mathrm{X}}=\left(\bar{\lambda}_{i_k}^{\mathrm{X}}\mathbf{I}_{\bar{M}_{i_k}^{\mathrm{X}}}+\mathbf{X}_{i_k}^{\mathrm{X}}\left(\mathbf{U}\right)\right)^{-1}\left(\mathbf{H}_{i_k}^{\mathrm{X}}\right)^H\mathbf{U}_{i_k}^{\mathrm{X}}\left(\boldsymbol{\Delta}_{i_k}^{\mathrm{X}}\right)^H,\tag{3.24}$$

where $\mathbf{X}_{i_k}^{\mathrm{X}}\left(\mathbf{U}\right)$ is defined in (3.25)-(3.26), $\bar{\lambda}_{i_k}^{\mathrm{X}}$ in (3.27) given at the bottom of the next page. Here, $\boldsymbol{\Delta}_{i_k}^{\mathrm{X}}$ and $\tilde{\boldsymbol{\Delta}}_{i_k}^{\mathrm{X}}$ are the diagonal matrices that scale the column vectors of the transmit and receive beamforming matrices, respectively so that equality constraint (3.19) is met. By plugging the optimal receive and transmit beamforming matrices in (3.23) and (3.24) into (3.19), respectively, the optimal scaling matrices can be computed as

$$\boldsymbol{\Delta}_{i_k}^{\mathrm{X}}=\left(\mathbf{I}_{d_{i_k}^{\mathrm{X}}}\circ\left(\left(\mathbf{U}_{i_k}^{\mathrm{X}}\right)^H\mathbf{H}_{i_k}^{\mathrm{X}}\left(\bar{\lambda}_{i_k}^{\mathrm{X}}\mathbf{I}_{\bar{M}_{i_k}^{\mathrm{X}}}+\mathrm{X}_{i_k}^{\mathrm{X}}\left(\mathbf{U}\right)\right)^{-1}\left(\mathbf{H}_{i_k}^{\mathrm{X}}\right)^H\mathbf{U}_{i_k}^{\mathrm{X}}\right)\right)^{-1},\tag{3.28}$$

$$\tilde{\boldsymbol{\Delta}}_{i_k}^{\mathrm{X}}=\left(\mathbf{I}_{d_{i_k}^{\mathrm{X}}}\circ\left(\left(\mathbf{V}_{i_k}^{\mathrm{X}}\right)^H\left(\mathbf{H}_{i_k}^{\mathrm{X}}\right)^H\left(\mathbf{H}_{i_k}^{\mathrm{X}}\mathbf{V}_{i_k}^{\mathrm{X}}\left(\mathbf{V}_{i_k}^{\mathrm{X}}\right)^H\left(\mathbf{H}_{i_k}^{\mathrm{X}}\right)^H+\boldsymbol{\Sigma}_{i_k}^{\mathrm{X}}\left(\mathbf{v}\right)\right)^{-1}\mathbf{H}_{i_k}^{\mathrm{X}}\mathbf{V}_{i_k}^{\mathrm{X}}\right)\right)^{-1}\tag{3.29}$$

The values of the Lagrange multiplier $\bar{\lambda}_{i_k}^{\mathrm{X}}$ in (3.24) are calculated numerically by

making sure that the power constraints in (3.20) and (3.21) are satisfied. If the values of the Lagrange multipliers $\bar{\lambda}_{i_k}^{\mathrm{X}}$ are negative, we assign $\bar{\lambda}_{i_k}^{\mathrm{X}}$ as zeros. The iterative alternating algorithm for solving the optimization problem (3.18)-(3.21) is given in Algorithm 2. The proof of convergence for Algorithm 2 is given in Appendix B.2.

$$\begin{aligned}
&\mathbf{X}_{i_k}^{\mathrm{UL}}(\mathbf{U}) = \\
&\sum_{j=1}^{K}\sum_{l=1}^{I_j}\left(\left(\mathbf{H}_{ji_k}^{\mathrm{UL}}\right)^H \mathbf{U}_{l_j}^{\mathrm{UL}}\left(\mathbf{U}_{l_j}^{\mathrm{UL}}\right)^H \mathbf{H}_{ji_k}^{\mathrm{UL}} + \beta\left(\mathbf{H}_{ji_k}^{\mathrm{UL}}\right)^H \mathrm{diag}\left(\mathbf{U}_{l_j}^{\mathrm{UL}}\left(\mathbf{U}_{l_j}^{\mathrm{UL}}\right)^H\right)\mathbf{H}_{ji_k}^{\mathrm{UL}}\right) \\
&+ \kappa\mathrm{diag}\left(\left(\mathbf{H}_{i_k}^{\mathrm{SI}}\right)^H \mathbf{U}_{i_k}^{\mathrm{DL}}\left(\mathbf{U}_{i_k}^{\mathrm{DL}}\right)^H \mathbf{H}_{i_k}^{\mathrm{SI}}\right) + \beta\left(\mathbf{H}_{i_k}^{\mathrm{SI}}\right)^H \mathrm{diag}\left(\mathbf{U}_{i_k}^{\mathrm{DL}}\left(\mathbf{U}_{i_k}^{\mathrm{DL}}\right)^H\right)\mathbf{H}_{i_k}^{\mathrm{SI}} \\
&+ \sum_{(l,j)\neq(i,k)}\left(\left(\mathbf{H}_{l_ji_k}^{\mathrm{UU}}\right)^H \mathbf{U}_{l_j}^{\mathrm{DL}}\left(\mathbf{U}_{l_j}^{\mathrm{DL}}\right)^H \mathbf{H}_{l_ji_k}^{\mathrm{UU}} + \beta\left(\mathbf{H}_{l_ji_k}^{\mathrm{UU}}\right)^H \mathrm{diag}\left(\mathbf{U}_{l_j}^{\mathrm{DL}}\left(\mathbf{U}_{l_j}^{\mathrm{DL}}\right)^H\right)\mathbf{H}_{l_ji_k}^{\mathrm{UU}}\right),
\end{aligned} \tag{3.25}$$

$$\begin{aligned}
&\mathbf{X}_{i_k}^{\mathrm{DL}}(\mathbf{U}) = \\
&\sum_{j=1,j\neq k}^{K}\sum_{l=1}^{I_j}\left(\left(\mathbf{H}_{jk}^{\mathrm{BB}}\right)^H \mathbf{U}_{l_j}^{\mathrm{UL}}\left(\mathbf{U}_{l_j}^{\mathrm{UL}}\right)^H \mathbf{H}_{jk}^{\mathrm{BB}} + \beta\left(\mathbf{H}_{jk}^{\mathrm{BB}}\right)^H \mathrm{diag}\left(\mathbf{U}_{l_j}^{\mathrm{UL}}\left(\mathbf{U}_{l_j}^{\mathrm{UL}}\right)^H\right)\mathbf{H}_{jk}^{\mathrm{BB}}\right) \\
&+ \sum_{l=1}^{I_k}\left(\kappa\mathrm{diag}\left(\left(\mathbf{H}_{k}^{\mathrm{SI}}\right)^H \mathbf{U}_{l_k}^{\mathrm{UL}}\left(\mathbf{U}_{l_k}^{\mathrm{UL}}\right)^H \mathbf{H}_{k}^{\mathrm{SI}}\right) + \beta\left(\mathbf{H}_{k}^{\mathrm{SI}}\right)^H \mathrm{diag}\left(\mathbf{U}_{l_k}^{\mathrm{UL}}\left(\mathbf{U}_{l_k}^{\mathrm{UL}}\right)^H\right)\mathbf{H}_{k}^{\mathrm{SI}}\right) \\
&+ \sum_{j=1}^{K}\sum_{l=1}^{I_j}\left(\left(\mathbf{H}_{l_jk}^{\mathrm{DL}}\right)^H \mathbf{U}_{l_j}^{\mathrm{DL}}\left(\mathbf{U}_{l_j}^{\mathrm{DL}}\right)^H \mathbf{H}_{l_jk}^{\mathrm{DL}} + \beta\left(\mathbf{H}_{l_jk}^{\mathrm{DL}}\right)^H \mathrm{diag}\left(\mathbf{U}_{l_j}^{\mathrm{DL}}\left(\mathbf{U}_{l_j}^{\mathrm{DL}}\right)^H\right)\mathbf{H}_{l_jk}^{\mathrm{DL}}\right).
\end{aligned} \tag{3.26}$$

$$\left(\bar{\lambda}_{i_k}^{\mathrm{X}},\ \bar{N}_{i_k}^{\mathrm{X}},\ \bar{M}_{i_k}^{\mathrm{X}}\right) = \begin{cases} (\lambda_{i_k},\ N_k,\ M_{i_k}) & \text{if X} = UL, \\ (\lambda_k, N_{i_k},\ M_k) & \text{if X} = DL. \end{cases} \tag{3.27}$$

Algorithm 2 Harmonic-Sum Maximization Algorithm.

1: Set the iteration number $n = 0$ and initialize the transmit beamforming matrices $\mathbf{V}_{i_k}^{\mathrm{X},[0]},\ i_k \in \mathcal{I},\ \mathrm{X} \in \{\mathrm{UL},\mathrm{DL}\}$.
2: Compute the receive beamforming matrices $\mathbf{U}_{i_k}^{\mathrm{X},[n]}$ from (3.23) and (3.29).
3: **repeat**
4: $n \leftarrow n + 1$.
5: Configure $\bar{\lambda}_{i_k}^{\mathrm{X}}$ with an initial value.
6: **for** $l = 1, \ldots$ **do**
7: Update the transmit beamforming matrices $\mathbf{V}_{i_k}^{\mathrm{X},[n]},\ \forall\,(i,k,\mathrm{X})$ using (3.24) and (3.28).
8: Update $\bar{\lambda}_{i_k}^{\mathrm{X}}$ numerically using bisection search.
9: **end for**
10: Compute the receive matrices $\mathbf{U}_{i_k}^{\mathrm{X},[n]},\ \forall\,(i,k,\mathrm{X})$ from (3.23) and (3.29).
11: **until** convergence of the objective function in (3.18), or a predefined number of iterations is reached.

The proposed algorithm can be computed in a distributed manner because the computation of transmit beamforming matrix of one user in (3.24) does not require information about transmit beamforming matrices of other users. Therefore, the transmit beamforming matrices can be computed for each user in parallel as long as the receive beamforming matrices and CSI are shared among BSs. However, Max-Min SINR algorithm [107] requires computation of all transmit beamforming matrices of all users without parallelism [110].

3.2.2.3 Complexity Analysis

Assuming the same number of transmit antennas (M), receive antennas (N) and same number of data streams (d) at each node, in this section, we will compare the computational complexity of the proposed algorithm with those of the weighted-sum-rate [84, 111] and Max-Min SINR [107] algorithms, which also employ an alternating iterative algorithm.

The Max-Min SINR algorithm requires iterative searches for the highest minimum SINR value using the bisection algorithm, where each search requires to solve an

Table 3.1: Comparison of Computational Complexity

Proposed Algorithm	Weighted-Sum-Rate	Max-Min SINR
$\|\mathcal{I}\| N(Nd + NM + M^2)$ $+ M^3 + Nd^2 + MNd + d^3 + d^2M$	$\|\mathcal{I}\| N(d^2 + Nd + NM + M^2)$ $+ M^3 + MNd + d^3 + d^2M$	$M^2d^3 \|\mathcal{I}\|^3$

SOCP problem. This can be solved using an iterative interior point method requiring $\mathcal{O}\left(M^2d^3 \left|\mathcal{I}\right|^3\right)$ calculations per iteration of the interior point method. The complexity of the weighted-sum-rate algorithm is analyzed in [84]. We summarize the complexity of these algorithms in Table 3.1. Given that the number of users, $|\mathcal{I}|$, is expected to be much greater than the number of transmit antennas M, receive antennas N or the number of data streams per user, d, it can be easily seen from Table 3.1 that overall computational complexity of Max-Min SINR algorithm is much higher than the complexity of the proposed algorithm.

3.2.3 Fairness Design with Imperfect CSI

In this section, we will study the fairness problem under imperfect CSI scenario. We characterize the imperfect CSI using the norm-bounded deterministic (or worst-case) model, where the instantaneous channel lies in a known set of possible values [96–98]. In particular, it is expressed as

$$\mathbf{H} \in \mathcal{H} = \left\{ \tilde{\mathbf{H}} + \mathbf{\Lambda} : \|\mathbf{\Lambda}\|_F \leq \epsilon \right\}, \tag{3.30}$$

where $\tilde{\mathbf{H}}$, $\mathbf{\Lambda}$, and ϵ denote the nominal value of the CSI, the channel error matrix, and the uncertainty bound, respectively. Here, $\mathbf{H}$ represents all the channels in the FD multi-cell system.

With the imperfect CSI, the max-min optimization problem can be written as[3]

$$\max_{\cdot,\mathbf{v},\mathbf{u}} \min_{\forall i_k\in\mathcal{I},m^X\in\mathcal{M}} \min_{\|\mathbf{\Lambda}\|_F\leq\epsilon} \quad \gamma^{\mathrm{X}}_{i_k,m}\left(\mathbf{v},\mathbf{u}^{\mathrm{X}}_{i_k,m}\right) \tag{3.31}$$

$$\text{s.t.} \quad \sum_{m=1}^{d^{\mathrm{UL}}_{i_k}} \left(\mathbf{v}^{\mathrm{UL}}_{i_k,m}\right)^H \mathbf{v}^{\mathrm{UL}}_{i_k,m} \leq P_{i_k},\ i_k\in\mathcal{I}, \tag{3.32}$$

$$\sum_{i=1}^{I_k}\sum_{m=1}^{d^{\mathrm{DL}}_{i_k}} \left(\mathbf{v}^{\mathrm{DL}}_{i_k,m}\right)^H \mathbf{v}^{\mathrm{DL}}_{i_k,m} \leq P_k,\ k\in\mathcal{K}. \tag{3.33}$$

To simplify the presentation, we will use the result in [112, Lemma 1], which has also been used in [45, Appendix A], [102] to express $\min_{\|\mathbf{\Lambda}\|_F\leq\epsilon}\ \gamma^{\mathrm{X}}_{i_k,m}$ as

$$\begin{aligned}\tilde{\gamma}^{\mathrm{X}}_{i_k,m}\left(\mathbf{v},\mathbf{u}^{\mathrm{X}}_{i_k,m}\right) &\triangleq \min_{\|\mathbf{\Lambda}\|_F\leq\epsilon}\ \gamma^{\mathrm{X}}_{i_k,m}\left(\mathbf{v},\mathbf{u}^{\mathrm{X}}_{i_k,m}\right)\\ &= \frac{\left(\mathbf{u}^{\mathrm{X}}_{i_k,m}\right)^H \mathbf{E}^{\mathrm{X}}_{i_k,m}\left(\mathbf{v}\right)\mathbf{u}^{\mathrm{X}}_{i_k,m}}{\left(\mathbf{u}^{\mathrm{X}}_{i_k,m}\right)^H \mathbf{F}^{\mathrm{X}}_{i_k,m}\left(\mathbf{v}\right)\mathbf{u}^{\mathrm{X}}_{i_k,m}},\end{aligned} \tag{3.34}$$

where $\mathbf{E}^{\mathrm{X}}_{i_k,m}$ and $\mathbf{F}^{\mathrm{X}}_{i_k,m}$ are defined as

$$\mathbf{E}^{\mathrm{X}}_{i_k,m}\left(\mathbf{v}\right) = \tilde{\mathbf{H}}^{\mathrm{X}}_{i_k}\mathbf{v}^{\mathrm{X}}_{i_k,m}\left(\tilde{\mathbf{H}}^{\mathrm{X}}_{i_k}\mathbf{v}^{\mathrm{X}}_{i_k,m}\right)^H - \epsilon^2\left\|\mathbf{v}^{\mathrm{X}}_{i_k,m}\right\|^2\mathbf{I}_{\bar{N}^{\mathrm{X}}_{i_k}}, \tag{3.35}$$

$$\begin{aligned}\mathbf{F}^{\mathrm{X}}_{i_k,m}\left(\mathbf{v}\right) = \tilde{\mathbf{\Sigma}}^{\mathrm{X}}_{i_k}\left(\mathbf{v}\right) &+ \tilde{\mathbf{H}}^{\mathrm{X}}_{i_k}\sum_{l=1}^{d^{\mathrm{X}}_{i_k}}\mathbf{v}^{\mathrm{X}}_{i_k,l}\left(\mathbf{v}^{\mathrm{X}}_{i_k,l}\right)^H\left(\tilde{\mathbf{H}}^{\mathrm{X}}_{i_k}\right)^H - \tilde{\mathbf{H}}^{\mathrm{X}}_{i_k}\mathbf{v}^{\mathrm{X}}_{i_k,m}\left(\tilde{\mathbf{H}}^{\mathrm{X}}_{i_k}\mathbf{v}^{\mathrm{X}}_{i_k,m}\right)^H\\ &- \epsilon^2\left\|\mathbf{v}^{\mathrm{X}}_{i_k,m}\right\|^2\mathbf{I}_{\bar{N}^{\mathrm{X}}_{i_k}} + \epsilon^2\Theta^{\mathrm{X}}_{i_k}\mathbf{I}_{\bar{N}^{\mathrm{X}}_{i_k}}.\end{aligned} \tag{3.36}$$

Here, $\tilde{\mathbf{\Sigma}}^{\mathrm{X}}_{i_k}\left(\mathbf{v}\right)$ is obtained by replacing the channel matrices $\mathbf{H}$ in $\mathbf{\Sigma}^{\mathrm{X}}_{i_k}\left(\mathbf{v}\right)$ given in (2.5)

[3]Note that under perfect CSI case, solving harmonic-sum problem instead of max-min problem results in a distributed and a low complexity algorithm. On the other hand, for the imperfect CSI case, the solution of both max-min and harmonic sum problems are centralized, which requires the use of SDR technique, and thus harmonic-sum metric does not have much improvement over max-min metric in terms of complexity when there is a channel uncertainty. Therefore, in this section, we will only focus on the max-min problem.

and (2.6) with the estimated ones $\tilde{\mathbf{H}}$, and $\Theta_{i_k}^{\mathrm{X}}$ is expressed as

$$\Theta_{i_k}^{\mathrm{UL}} = \sum_{j=1}^{K}\sum_{l=1}^{I_j}(1+\beta)\left\|\mathbf{V}_{l_j}^{\mathrm{UL}}\right\|_F^2 + \sum_{l=1}^{I_k}(\kappa+\beta)\left\|\mathbf{V}_{l_k}^{\mathrm{DL}}\right\|_F^2 + \sum_{j=1,j\neq k}^{K}\sum_{l=1}^{I_j}(1+\beta)\left\|\mathbf{V}_{l_j}^{\mathrm{DL}}\right\|_F^2, \tag{3.37}$$

$$\Theta_{i_k}^{\mathrm{DL}} = \sum_{j=1}^{K}\sum_{l=1}^{I_j}(1+\beta)\left\|\mathbf{V}_{l_j}^{\mathrm{DL}}\right\|_F^2 + (\kappa+\beta)\left\|\mathbf{V}_{i_k}^{\mathrm{UL}}\right\|_F^2 + \sum_{(l,j)\neq(i,k)}(1+\beta)\left\|\mathbf{V}_{l_j}^{\mathrm{UL}}\right\|_F^2. \tag{3.38}$$

Using the simplified SINR definition in (3.34) and epigraph form with the slack variable γ, the problem (3.31)-(3.33) can be rewritten as

$$\min_{\mathbf{v},\mathbf{u},\gamma} \quad -\gamma \tag{3.39}$$

$$\text{s.t.} \quad \sum_{m=1}^{d_{i_k}^{\mathrm{UL}}}\left(\mathbf{v}_{i_k,m}^{\mathrm{UL}}\right)^H\mathbf{v}_{i_k,m}^{\mathrm{UL}} \leq P_{i_k},\ i_k\in\mathcal{I}, \tag{3.40}$$

$$\sum_{i=1}^{I_k}\sum_{m=1}^{d_{i_k}^{\mathrm{DL}}}\left(\mathbf{v}_{i_k,m}^{\mathrm{DL}}\right)^H\mathbf{v}_{i_k,m}^{\mathrm{DL}} \leq P_k,\ k\in\mathcal{K}, \tag{3.41}$$

$$\tilde{\gamma}_{i_k,m}^{\mathrm{X}}\left(\mathbf{v},\mathbf{u}_{i_k,m}^{\mathrm{X}}\right) \geq \gamma,\ i_k\in\mathcal{I},\ m\in\mathcal{M}. \tag{3.42}$$

Because of the minimum SINR constraints in (3.42), the optimization problem (3.39)-(3.42) is non-convex. Thus we iteratively compute the transmit and receive beamforming matrices to monotonically improve the minimum SINR.

3.2.3.1 Receive Filter Design

The receive beamforming matrices optimization problem to maximize the minimum SINR among all users' data streams under fixed transmit beamforming matrices can be solved independently, since the SINR terms in (2.3) and (2.4) depend on a single

stream receive filter. Therefore, the optimal receiver beamforming matrices can be computed by solving the following problem:

$$\max_{\cdot, \mathbf{u}^{\mathrm{X}}_{i_k,m}} \quad \tilde{\gamma}^{\mathrm{X}}_{i_k,m}\left(\mathbf{v}, \mathbf{u}^{\mathrm{X}}_{i_k,m}\right). \tag{3.43}$$

Using [101, 113], and as derived in [45, Appendix B], the optimal solution of (3.43) can be given as

$$\mathbf{u}^{\mathrm{X}}_{i_k,m} = \frac{\left(\mathbf{F}^{\mathrm{X}}_{i_k,m}(\mathbf{v})\right)^{-1/2} \mathbf{w}^{\mathrm{X}}_{i_k,m}}{\left\| \left(\mathbf{F}^{\mathrm{X}}_{i_k,m}(\mathbf{v})\right)^{-1/2} \mathbf{w}^{\mathrm{X}}_{i_k,m} \right\|}, \tag{3.44}$$

where $\mathbf{w}^{\mathrm{X}}_{i_k,m}$ is the principle eigenvector of $\left(\mathbf{F}^{\mathrm{X}}_{i_k,m}(\mathbf{v})\right)^{-1/2} \mathbf{E}^{\mathrm{X}}_{i_k,m}(\mathbf{v}) \left(\mathbf{F}^{\mathrm{X}}_{i_k,m}(\mathbf{v})\right)^{-1/2}$, and $\mathbf{E}^{\mathrm{X}}_{i_k,m}(\mathbf{v})$ and $\mathbf{F}^{\mathrm{X}}_{i_k,m}(\mathbf{v})$ are defined in (3.35) and (3.36), respectively.

3.2.3.2 Precoder Design

To solve the transmit beamforming matrices design problem under fixed receive beamforming matrices, we apply the inverse relationship between max-min fairness and power minimization problems proposed for broadcast and multicast channels in [45], [106, Theorem 3], and [114, Claim 3], respectively. Denoting $\tilde{P} = \{P_{i_k},\ i_k \in \mathcal{I},\ P_k,\ k \in \mathcal{K}\}$, and $\rho_{i_k} = P_{i_k}/\tilde{P},\ i_k \in \mathcal{I}$ and $\rho_k = P_k/\tilde{P},\ k \in \mathcal{K}$, the problem (3.39)-(3.42) can be rewritten as

$$\mathcal{P}\left(\tilde{\mathcal{P}}\right) = \min_{\mathbf{v},\mathbf{u},\gamma} \quad -\gamma \tag{3.45}$$

$$\text{s.t.} \quad \sum_{m=1}^{d^{\mathrm{UL}}_{i_k}} \left(\mathbf{v}^{\mathrm{UL}}_{i_k,m}\right)^H \mathbf{v}^{\mathrm{UL}}_{i_k,m} \leq \rho_{i_k}\tilde{P},\ i_k \in \mathcal{I}, \tag{3.46}$$

$$\sum_{i=1}^{I_k} \sum_{m=1}^{d^{\mathrm{DL}}_{i_k}} \left(\mathbf{v}^{\mathrm{DL}}_{i_k,m}\right)^H \mathbf{v}^{\mathrm{DL}}_{i_k,m} \leq \rho_k \tilde{P}, k \in \mathcal{K}, \tag{3.47}$$

$$\tilde{\gamma}^{\mathrm{X}}_{i_k,m}\left(\mathbf{v},\mathbf{u}^{\mathrm{X}}_{i_k,m}\right)\geq\gamma, i_k\in\mathcal{I}, m\in\mathcal{M}. \tag{3.48}$$

Now consider the power minimization problem below:

$$\begin{aligned}
\mathcal{Q}(\gamma)=\min_{\mathbf{v},\mathbf{u},\tau}\quad & \tau && (3.49)\\
\text{s.t.}\quad & \sum_{m=1}^{d^{\mathrm{UL}}_{i_k}}\left(\mathbf{v}^{\mathrm{UL}}_{i_k,m}\right)^H\mathbf{v}^{\mathrm{UL}}_{i_k,m}\leq\rho_{i_k}\tau,\ i_k\in\mathcal{I}, && (3.50)\\
& \sum_{i=1}^{I_k}\sum_{m=1}^{d^{\mathrm{DL}}_{i_k}}\left(\mathbf{v}^{\mathrm{DL}}_{i_k,m}\right)^H\mathbf{v}^{\mathrm{DL}}_{i_k,m}\leq\rho_k\tau, k\in\mathcal{K}, && (3.51)\\
& \tilde{\gamma}^{\mathrm{X}}_{i_k,m}\left(\mathbf{v},\mathbf{u}^{\mathrm{X}}_{i_k,m}\right)\geq\gamma,\ i_k\in\mathcal{I},\ m\in\mathcal{M}. && (3.52)
\end{aligned}$$

Using a minimum SINR constraint γ^* in (3.52), assume that the optimal solution of the problem $\mathcal{Q}(\gamma^*)$ in (3.49)-(3.52) is $\mathbf{v}^*,\mathbf{u}^*,\tau^*$. It was shown in [106, Theorem 3] that $\mathbf{v}^*,\mathbf{u}^*,\gamma^*$ is the optimal solution of the problem $\mathcal{P}(\tau^*)$ in (3.45)-(3.48), and thus we can solve the problem $\mathcal{Q}(\gamma)$ to solve the problem $\mathcal{P}\left(\tilde{\mathcal{P}}\right)$, and vice versa. Under the fixed receiver beamforming matrices, the problem $\mathcal{Q}(\gamma)$ is a quadratically constrained quadratic program (QCQP), which can be solved through SDR techniques [45]. Let $\tilde{\mathbf{V}}^{\mathrm{X}}_{i_k,m}=\mathbf{v}^{\mathrm{X}}_{i_k,m}\left(\mathbf{v}^{\mathrm{X}}_{i_k,m}\right)^H$, then the transmit beamforming matrices design problem can be written as

$$\begin{aligned}
\min_{\tilde{\mathbf{V}},\tau}\quad & \tau && (3.53)\\
\text{s.t.}\quad & \sum_{m=1}^{d^{\mathrm{UL}}_{i_k}}\mathrm{Tr}\left\{\tilde{\mathbf{V}}^{\mathrm{UL}}_{i_k,m}\right\}\leq\rho_{i_k}\tau,\ i_k\in\mathcal{I}, && (3.54)\\
& \sum_{i=1}^{I_k}\sum_{m=1}^{d^{\mathrm{DL}}_{i_k}}\mathrm{Tr}\left\{\tilde{\mathbf{V}}^{\mathrm{DL}}_{i_k,m}\right\}\leq\rho_k\tau,\ k\in\mathcal{K}, && (3.55)\\
& \tilde{\gamma}^{\mathrm{X}}_{i_k,m}\left(\tilde{\mathbf{V}},\mathbf{u}^{\mathrm{X}}_{i_k,m}\right)\geq\gamma,\ i_k\in\mathcal{I},\ m\in\mathcal{M}, && (3.56)
\end{aligned}$$

$$\tilde{\mathbf{V}}^{\mathrm{X}}_{i_k,m} \succeq \mathbf{0},\ i_k \in \mathcal{I},\ m \in \mathcal{M}, \tag{3.57}$$

$$\mathrm{rank}\left(\tilde{\mathbf{V}}^{\mathrm{X}}_{i_k,m}\right) = 1,\ i_k \in \mathcal{I},\ m \in \mathcal{M}, \tag{3.58}$$

where $\tilde{\mathbf{V}}$ denotes all matrices $\tilde{\mathbf{V}}^{\mathrm{X}}_{i_k,m},\ i_k \in \mathcal{I},\ m \in \mathcal{M}$, and $\tilde{\gamma}^{\mathrm{X}}_{i_k,m}\left(\tilde{\mathbf{V}}, \mathbf{u}^{\mathrm{X}}_{i_k,m}\right)$ is obtained by replacing $\mathbf{v}^{\mathrm{X}}_{i_k,m}\left(\mathbf{v}^{\mathrm{X}}_{i_k,m}\right)^H$ in (2.3) and (2.4) with $\tilde{\mathbf{V}}^{\mathrm{X}}_{i_k,m}$. The problem (3.53)-(3.58) is still non-convex because of the rank constraint in (3.58). By dropping this constraint, the problem (3.53)-(3.58) can be solved through semidefinite programming (SDP) techniques. If the optimal solution $\mathbf{V}^{\mathrm{X}}_{i_k,m}$ has rank 1, then it is also an optimal solution for (3.49)-(3.52), and the optimal $\mathbf{v}^{\mathrm{X}}_{i_k,m}$ can be obtained through rank-one decomposition. Otherwise, one can apply Gaussian randomization [42] to obtain the approximate solution of the beamforming vectors. The steps of the proposed robust algorithm are given in Algorithm 3. Since each step of the Algorithm 3 increases the minimum SINR, Algorithm 3 converges, as it has been shown in [45].

Algorithm 3 Robust Fairness Algorithm.

1: Initialize the transmit beamforming vectors $\mathbf{v}^{\mathrm{X}}_{i_k,m},\ i_k \in \mathcal{I},\ m \in \mathcal{M}$ to ensure the power constraints are satisfied.
2: **repeat**
3: Compute the receive beamforming vectors $\mathbf{u}^{\mathrm{X}}_{i_k,m},\ i_k \in \mathcal{I},\ m \in \mathcal{M}$ from (3.44).
4: Update the target minimum SINR from (3.34).

$$\gamma^* = \min_{i_k \in \mathcal{I},\ m \in \mathcal{M}} \quad \tilde{\gamma}^{\mathrm{X}}_{i_k,m}. \tag{3.59}$$

5: Compute the transmit beamforming vectors $\mathbf{v}^{\mathrm{X}}_{i_k,m},\ i_k \in \mathcal{I},\ m \in \mathcal{M}$ by solving $\mathcal{Q}(\gamma^*)$ through (3.53)-(3.58).
6: Scale the transmit beamforming vectors $\mathbf{v}^{\mathrm{X}}_{i_k,m},\ i_k \in \mathcal{I},\ m \in \mathcal{M}$ to ensure the power constraints are satisfied.
7: Update the target minimum SINR

$$\gamma^* = \min_{i_k \in \mathcal{I},\ m \in \mathcal{M}} \quad \tilde{\gamma}^{\mathrm{X}}_{i_k,m}. \tag{3.60}$$

8: **until** convergence of the minimum SINR, γ^*.

3.2.4 Numerical Results and Discussions

In this section, we numerically investigate the proposed algorithms for an FD multi-cell multi-user MIMO system. As in Section 2.5 of Chapter 2, we choose the simulation parameters from the 3GPP LTE specifications [103]. Therefore, the same simulation settings in Section 2.5 are applicable that also includes Table 2.2 of Chapter 2, unless stated otherwise. The maximum transmit power for each BS and mobile user is set to 24 dBm and 23 dBm, respectively. We average the results over 1000 independent channel realizations. Similar to the previous chapter, the rate is calculated as the spectral efficiency via $\log_2(1+\Gamma^X_{i_k,m}),,\ i_k \in \mathcal{I},\ m \in \mathcal{M},\ X \in \{\mathrm{UL},\mathrm{DL}\}$.

3.2.4.1 Perfect CSI Results

The proposed fairness design presented in Section 3.2.2 is based on an iterative update of the design parameters. The iterative nature of the algorithm is to ensure that a local optimal solution is obtained. Hence, it is of interest to observe the convergence behavior of this algorithm. Fig. 3.2 shows the convergence of the objective function in (3.18) for both FD and HD operations. As expected, the strictly non-increasing behavior of the optimization objective is observed as the number of iterations increases. Moreover, we observe that HD setup converges with relatively fewer iterations with the penalty of worse performance. This is because the FD design needs to consider additional interference terms in the design process, which may contribute to the slower convergence of the algorithm.

Fig. 3.3 provides a comparison of the sum rates achieved by FD and HD systems. The HD transmission design is a special case of our system model, which can be obtained by ignoring the additional interference for the UL and DL transmissions. Also, we assume that each BS in HD operation serves the same number of downlink

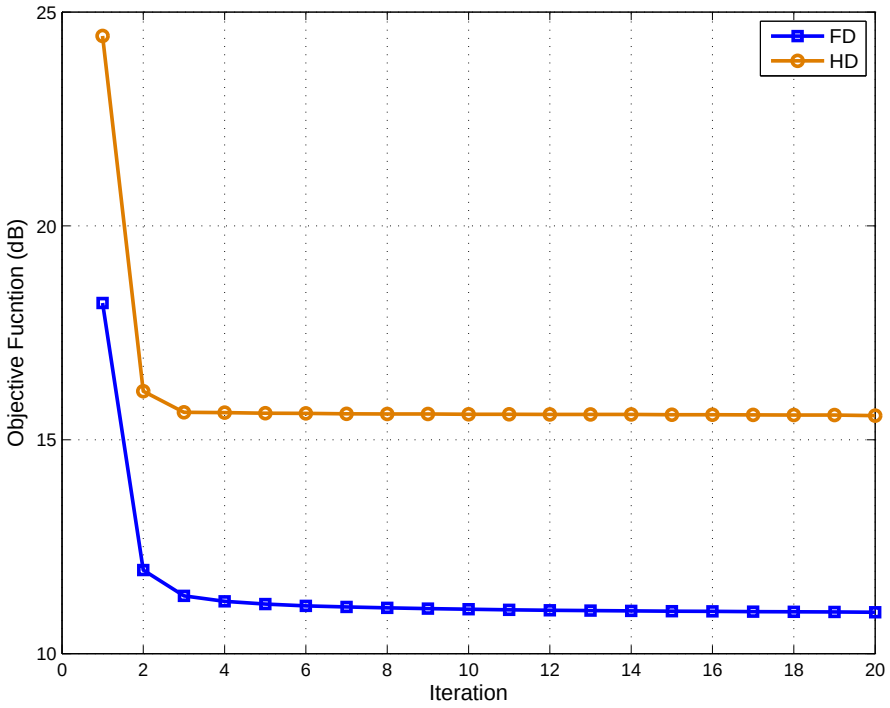

Figure 3.2: Convergence of the objective function in (3.18) for perfect CSI design with $\kappa = \beta = -120$ dB.

and uplink users to guarantee fairness among them as in the FD system. As we see from Fig. 3.3, both FD and HD transmissions achieve the same rates at around $\kappa = \beta \approx -92$ dB. This is to say, FD outperforms HD transmission when $\kappa = \beta < -92$ dB, which has been achieved by recent advanced self-interference cancellation techniques reported in [25]. We also note that the spectral efficiency gain for FD over HD transmission varies with different κ and β values. This is due to the fact that the higher transmitter (receiver) distortion, represented by κ (β) corresponds to larger residual self-interference. Therefore, with smaller values of κ (β), we obtain a higher spectral efficiency gain. In particular, going from $\kappa = \beta = -100$ dB to $\kappa = \beta = -120$ dB, the spectral efficiency gain over HD operation improves from 25%

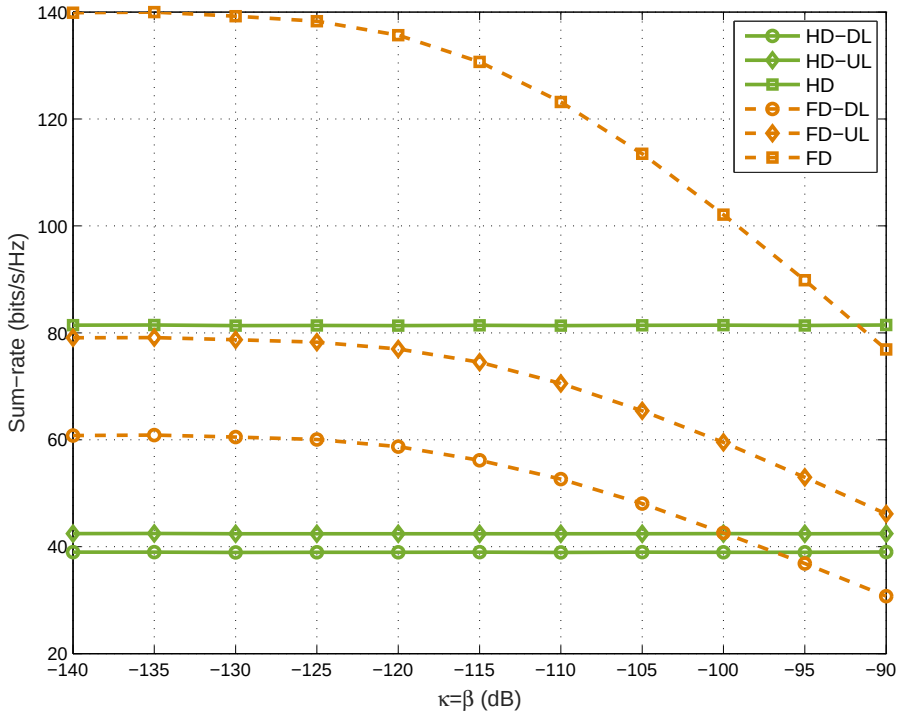

Figure 3.3: Total sum-rates achieved for FD and HD setups with perfect CSI.

to 65%, respectively.

In order to understand the impact of inter-cell interference, we study the system sum-rate with respect to distance between BSs. Unlike the results presented above, in this case we keep the positions of users fixed with respect to its BS location. We note that when we increase the distance between the BSs, however, the inter-user distance among the users in different small-cells are also increased. Therefore, it essentially captures both impacts of inter-cell and inter-user interference. As we see from Fig. 3.4, as the distance between the BSs increases, the inter-cell as well as inter-user interference decreases, which leads to an increase in total sum-rates and improves the spectral efficiency gains over the HD transmission, irrespective of transceiver distortions. In particular, with an increase of BS distance from 40 m to 100 m, the

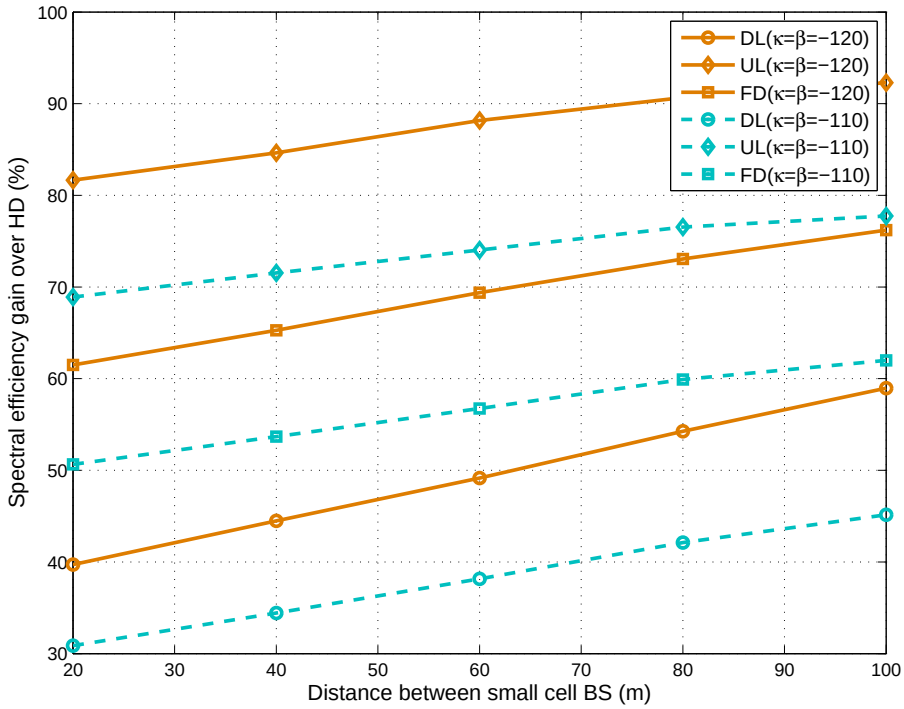

Figure 3.4: Total sum-rates achieved for FD and HD setups with perfect CSI and varying distance between BSs. The parameters representing transceiver distortion are chosen as $\kappa = \beta = -110$ dB and $\kappa = \beta = -120$ dB

spectral efficiency gain over HD setup increases from from 65% to 76%, respectively. The relatively small increase in spectral efficiency over HD setup indicates that the system performance is largely dominated by residual self-interference inherent to FD system. We also note that as the FD setup experiences less transceiver distortion, it provides higher spectral efficiency gain over HD setup. This is apparent from the superior spectral efficiency gain obtained for $\kappa = \beta = -120$ dB over that of $\kappa = \beta = -110$ dB.

Fig. 3.5 shows the Cumulative Distribution Function (CDF) of three algorithms, where we compare the proposed algorithm with WMMSE and Max-Min SINR fairness algorithms. The individual user rate along the x-axis of this figure denotes the

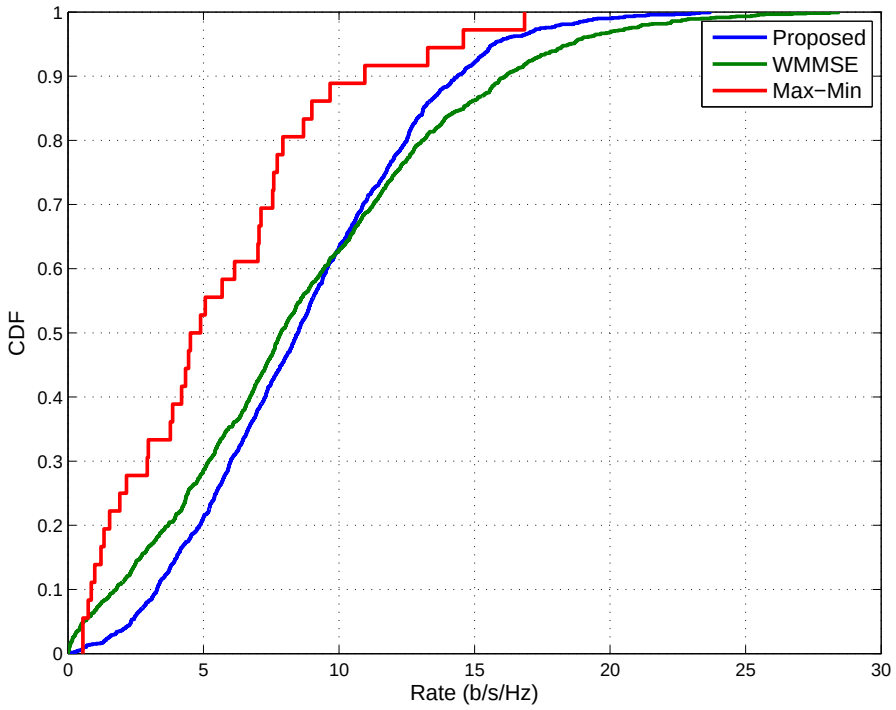

Figure 3.5: Comparison of CDFs of individual user rate among the proposed, Max-Min and sum-rate maximizing WMMSE designs with $\kappa = \beta = -80$ dB

total rate obtained by each user in the uplink and downlink transmissions. It can be observed from this result that the Max-Min fairness algorithm provides the highest fairness to the users at the lower individual rate, i.e., below 1 b/s/Hz, since it maximizes the minimum SINR. Compared to WMMSE and proposed algorithms, the users are less likely to be served by the Max-Min SINR design when the data rate increases, e.g., beyond 2 b/s/Hz. In contrast, it is more likely that a user with higher individual rate will be served by WMMSE design since it maximizes the total throughput. Nonetheless, compared to the WMMSE design, a user is more likely to be served by the proposed design if it experiences a rate, for instance below 9 b/s/Hz. Furthermore, we note that the LTE user throughput requirement is specified at two points:

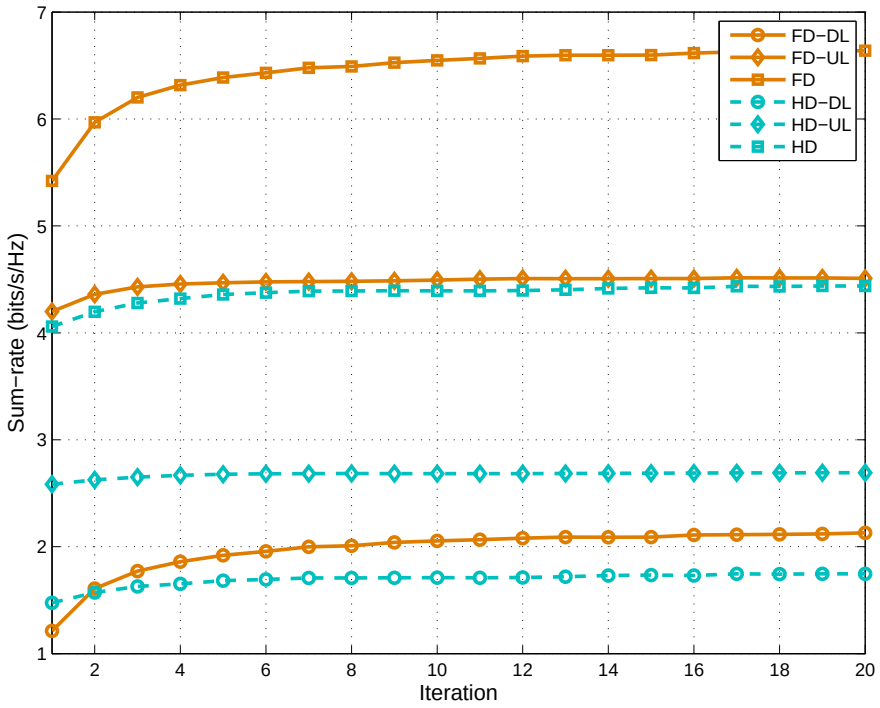

Figure 3.6: Convergence of minimum SINR i.e., improved associated rate in the presence of imperfect CSI with $s = 0.02$ and $\kappa = \beta = -120$ dB.

at the average and at the fifth-percentile of the user distribution (where 95 percent of the users have better performance) [115]. The fifth-percentile users correspond to ones operating on the cell edge [116]. It can be observed from this figure that the proposed algorithm almost surely provides a better fifth-percentile user throughput when compared to the WMMSE design, and also against the Max-Min SINR fairness algorithm when the individual rate is above 1 b/s/Hz.

3.2.4.2 Imperfect CSI Results

After observing the gains offered by FD transmission over HD setup with perfect CSI, in this section we show the performance with imperfect CSI. As discussed in Section

3.2.3, we consider the norm-bounded CSI uncertainty to obtain worst-case fairness among mobile users. This is to say, knowing the boundary of the uncertainty region denoted by ϵ, we provide the worst-case transceiver design to obtain fairness among mobile users.

We first study the convergence behavior of the proposed algorithm with imperfect CSI, as presented in Section 3.2.3. Fig. 3.6 shows the convergence of the proposed algorithm for both FD and HD setups over multiple design parameters. The result is obtained by averaging the convergence behavior of the network, over several channel realizations. As expected, we observe strictly non-decreasing behavior of the optimization objective, i.e., improved minimum SINR in terms of associated rate, as the number of iterations increase. Furthermore, as in the case of perfect CSI, it is observed that HD setup converges with relatively fewer optimization iterations compared to its FD counterpart.

In Fig. 3.7, we present the sum-rate performances for both FD and HD setups against the measure of CSI uncertainty, s. As we see from this figure, as the boundary of the CSI uncertainty, i.e., s increases, the sum-rate decreases for both FD and HD systems. It is perceivable, since larger s means higher CSI uncertainty, hence lower rate. Furthermore, we observe that for increasing CSI uncertainty, the performance of FD setup falls more rapidly than its HD counterpart. For example, for the same decrease in CSI quality from $s = 0$ to $s = 0.2$, the sum-rate difference between FD and HD setups goes from 28.5 b/s/Hz to 5 b/s/Hz. This is due to the fact that the FD system involves a larger number of channels, i.e., self-interference and inter-user interference channels; and thus increased CSI uncertainty with its transmission, which degrades its performance more than that of the HD transmission. Hence, the performance of FD system is more susceptible to an increasing s in comparison to a

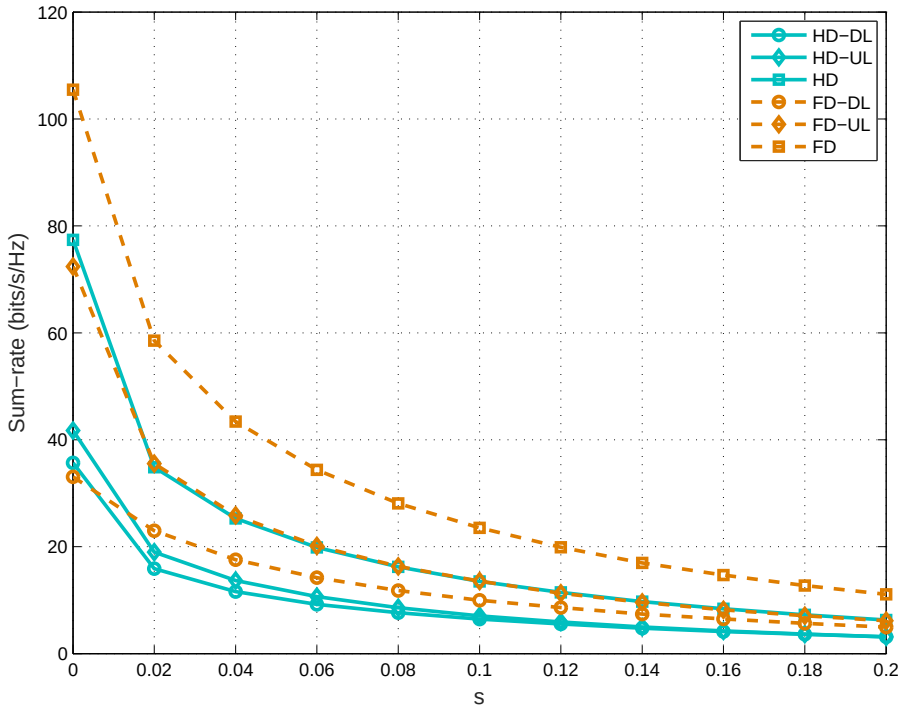

Figure 3.7: Total sum-rates achieved for FD and HD setups with varying CSI uncertainties and $\kappa = \beta = -120$ dB.

HD setup.

Next we compare the performance of robust and non-robust FD setups with various design parameters. The objective of this result is to show the performance gain that can be harnessed through a robust design in the presence of CSI uncertainty. To this end, we make the following observations from Fig. 3.8. We observe that with small CSI uncertainty i.e., $s = 0.1$, as the κ and β increase, the sum-rate decreases sharply. This is to say, in this regime the transceiver distortion is a more limiting factor on the sum-rate performance than the CSI uncertainty. On the other hand, with larger s, i.e., $s = 0.2$, the rate of decrease of total sum-rate with increasing κ and β is relatively smaller, i.e., the sum-rate curves flatten out for the FD setup.

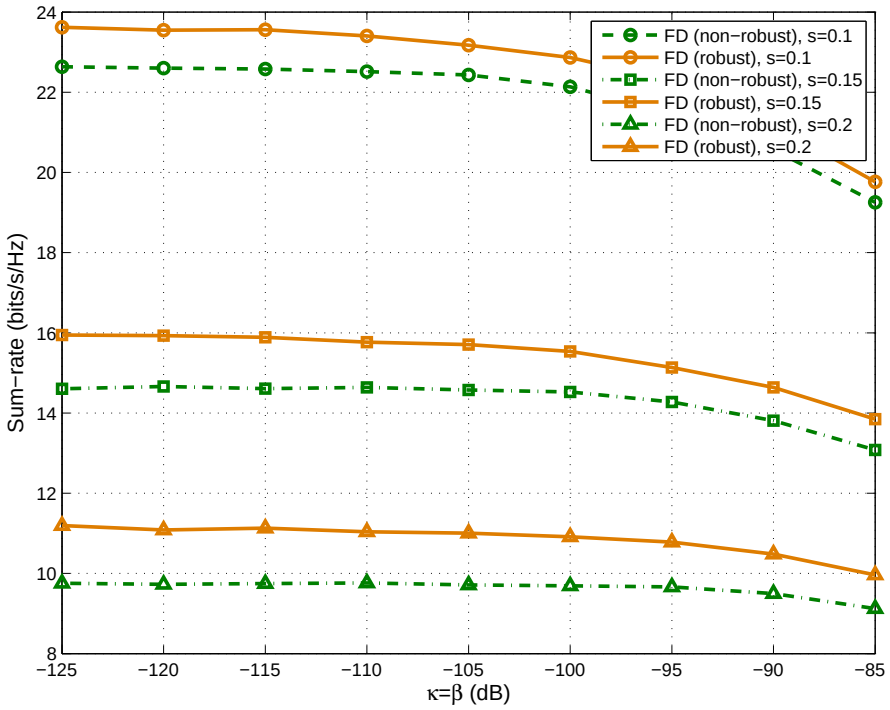

Figure 3.8: Total sum-rates achieved for robust and non-robust FD setups with varying CSI uncertainties and transceiver distortions.

This indicates that the CSI uncertainty is a more limiting factor on the sum-rate performance than the transceiver distortion. In addition, we observe that with lower κ and β, the difference between robust and non-robust design is noticeable. However, with increasing κ and β, the difference in performance becomes smaller as the system performance is dominated by transceiver distortion rather than CSI uncertainty in this region. Finally, we observe that as the CSI uncertainty increases, the difference between the sum-rate performance of the robust and non-robust designs also increases.

3.3 Fairness in D2D Communications

In this section, we turn our focus on another interference-limited communication system, namely D2D communications. Different from the FD communication which is also an interference-limited communication system, in this case, however, the system performance is limited by the inter-user interference, as in wireless interference networks.

The seeming spectrum scarcity and ever growing demands for new wireless services have encouraged the concept of opportunistic spectrum access through cognitive radios so as to better utilize the available wireless spectrum [117]. In this communication scenario, unlicensed Secondary Users (SUs) are allowed to dynamically access the spectrum of the Primary User (PU) provided that they do not degrade the performance of the latter [118]. For example, in an underlay cognitive concept, the SUs are only allowed to transmit if the resulting interference to the PU's receiver does not exceed a certain threshold value (set by macrocells or the regulatory body). By treating macrocells as PUs and D2D users as SUs, the concept of (in-band) underlay D2D transmission is deemed to be a suitable technology in cellular networks [119]-[120]. To that end, controlling the interference power to the macrocell users is key to the successful coexistence.

The emergence of IA has shown that the sum-rate of the wireless interference networks can scale linearly with the number of users in the network at high SINR. In the specific context of IA for D2D communications, recently there have been a few studies reported, such as [121–124]. In [121], the authors have considered cellular communications with underlay D2D transmissions and have derived the total Degrees of Freedom (DoF) achievable for the network. The authors in [122] have considered IA for D2D communications, where several grouping mechanisms for D2D

users are considered. An opportunistic IA scheme has been proposed in [123], where the underlaying D2D users are selected only if they meet a certain scheduling metric. The study in [124] investigates IA schemes for D2D communications, where multiple D2D transmitters communicate to a single D2D receiver, as in a local area network system. However, none of these studies have taken into account SINR fairness among the D2D users. In addition, the IA techniques face the practical challenge of obtaining the CSI at the transmitter [125,126]. In the context of MIMO interference networks, the technique of IA has been studied with the assumption that CSI is estimated through channel estimation at the transmitter side [125], or it has been obtained via quantized feedback from the receiver [126]. To account for this practical design aspect, we also consider CSI uncertainty in our design, along with SINR fairness for D2D communications.

To the best of our knowledge, this thesis reports the first study that considers the transceiver optimization considering SINR fairness among the D2D users in the context of IA. We assume that users involved in the D2D communications coexist in an underlay fashion with the macrocell (i.e., PU) and form groups possibly based on positions or specific services required by D2D users, as suggested in [122]. To this end, we aim at designing precoders and receiver filters so as to maximize the minimum SINR for D2D users in the presence of CSI uncertainty. Due to the non-convexity of the optimization problem, similar to the previous study for fairness in FD communications, we follow an alternating minimization algorithm that involves the SDR technique. It is observed that at low SNR and high CSI error with relaxed interference power constraint, the D2D users perform very close to that of the users in the non-cognitive system, but performance degrades considerably with stringent interference power constraint.

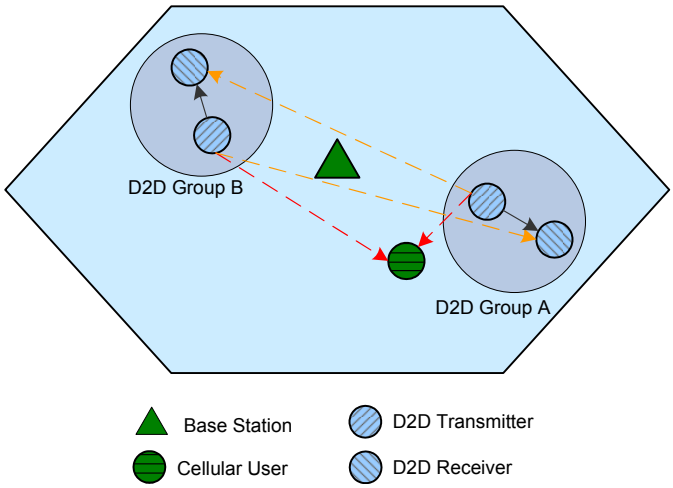

Figure 3.9: An illustration of underlay D2D communications in a cellular network. Solid and dashed lines indicate desired signals and interference, respectively.

3.3.1 System Model

Let us consider a cellular network, composed of one primary-user pair (one BS and one cellular user) denoted as user pair 0 and C D2D groups operating in underlay cognitive transmission mode, as shown in Fig. 3.9 for $C = 2$. Each D2D group c is composed of K secondary-user (D2D user) pairs. A D2D link in each group makes use of N_T transmit and N_R receive antennas. Also, each D2D user i in group c, encodes its messages, $s^c_{m,i}$, onto $d^c_i \leq \min(N_T, N_R)$ independent data streams sent along the beamforming vectors $v^c_{m,i}$, where $m = 1, \ldots, d^c_i$ such that $\mathbb{E}[s^c_i (s^c_i)^H] = \mathbf{I}_{d^c_i}$ i.e., data streams are independent and have unit power. In D2D group c, the data streams are observed at user j after passing through the channel, $H^c_{i,j}$. Furthermore, we assume that the primary-link uses N^{pu}_T and N^{pu}_R antennas at the transmitter and receiver, respectively, to transmit $d^{pu} \leq \min(N^{pu}_T, N^{pu}_R)$ independent parallel data streams.

3.3.1.1 Precoding at the D2D Transmitter

Let us consider $V_i^c = [v_{1,i}^c, \ldots, v_{d_i^c,i}^c] \in \mathbb{C}^{N_T \times d_i^c}$ as the precoding matrix of user i in D2D group c. The resultant precoded signal, S_i^c, can be represented as

$$S_i^c = \sum_{m=1}^{d_i^c} v_{m,i}^c s_{m,i}^c = V_i^c s_i^c, \tag{3.61}$$

where $s_i^c \in \mathbb{C}^{d_i^c \times 1}$ is transmitted symbol vector at user i in D2D group c. Note that each data stream, $s_{m,i}^c$, i.e., the m-th stream of user i in D2D group c is sent along the beamforming vector, $v_{m,i}^c$. The maximum transmission power, P_i^c, for user i in D2D group c, i.e., total power constraint is then given by, $\sum_{m=1}^{d_i^c} (v_{m,i}^c)^H v_{m,i}^c = \|V_i^c\|_F^2 \leq P_i^c$.

3.3.1.2 Channel Uncertainty

We assume that the D2D link between transmitting user i and receiving user j in group c can be expressed as [96–98]

$$H_{i,j}^c = \hat{H}_{i,j}^c + \Delta_{i,j}^c, \tag{3.62}$$

where $\hat{H}_{i,j}^c$ is the channel estimate available at the transmitter i and $\Delta_{i,j}^c$ is the corresponding CSI error matrix. For the latter, we consider a norm-bounded model in order to obtain a worst-case robust design where the CSI uncertainty is assumed to be lying in a spherical region within a radius, $\epsilon_{i,j}^c$, as

$$\mathcal{R} \triangleq \left\{\Delta_{i,j}^c : \|\Delta_{i,j}^c\|_F \leq \epsilon_{i,j}^c\right\} = \left\{\Delta_{i,j}^c : \mathrm{Tr}(\Delta_{i,j}^c (\Delta_{i,j}^c)^H) \leq {\epsilon_{i,j}^c}^2\right\}. \tag{3.63}$$

This model is applicable where the CSI is obtained via feedback from the receiver (e.g., in FDD) or estimated at the transmitter through pilot signals (e.g., in TDD)

[35].

3.3.1.3 Interference Suppression at the D2D Receiver

The signal received at user i in D2D group c, is given by

$$y_i^c = H_{i,i}^c V_i^c s_i^c + \sum_{j=1, j\neq i}^{K} H_{j,i}^c V_j^c s_j + \sum_{c'=1, c'\neq c}^{C} \sum_{j=1}^{K} H_{j,i}^{c'} V_j^{c'} s_j^{c'} + z_i^c, \tag{3.64}$$

where $H_{i,i}^c \in \mathbb{C}^{N_R \times N_T}$ is the channel matrix and $z_i^c \in \mathbb{C}^{N_R \times 1}$ is the effective AWGN vector at user i of c-th D2D group with distribution, $\mathcal{CN}(\mathbf{0}_{N_R}, \sigma_i^2 \mathbf{I}_{N_R})$. The first term in the above expression is the intended signal for user i in D2D group c, the second term refers to the interference from other users in D2D group c, and the third term refers to the interference from users in the neighboring D2D groups. Note that we assume the inter-cell interference that results from the neighboring macrocells is mitigated through macrocell coordination and therefore neglected in our analysis. We further assume that interference from cellular users to receiving users in the D2D groups is negligible. This assumption is not specifically restrictive since we assume that D2D group will be formed by nearby users. Using (3.62), the received signal can be decomposed as

$$\begin{aligned} y_i^c =& (\hat{H}_{i,i}^c + \Delta_{i,i}^c) V_i^c s_i^c + \sum_{j=1, j\neq i}^{K} (\hat{H}_{j,i}^c + \Delta_{j,i}^c) V_j^c s_j^c + \sum_{c'=1, c'\neq c}^{C} \sum_{j=1}^{K} (\hat{H}_{j,i}^{c'} + \Delta_{j,i}^{c'}) V_j^{c'} s_j^{c'} + z_i^c \\ =& \sum_{c=1}^{C} \sum_{j=1}^{K} \hat{H}_{j,i}^c V_j^c s_j^c + \sum_{c=1}^{C} \sum_{j=1}^{K} \Delta_{j,i}^c V_j^c s_j^c + z_i^c. \end{aligned} \tag{3.65}$$

As with precoders, the transmitting D2D user also designs the receive filter, $U_i^c = [u_{1,i}^c, \ldots, u_{d_i^c,i}^c]$ based on available channel estimate $\hat{H}_{i,i}^c$. Projecting the received signal

onto the columns of U_i^c, on a per-stream basis it can be written as

$$(u_{m,i}^c)^H y_i^c = (u_{m,i}^c)^H \left(\sum_{c=1}^{C} \sum_{j=1}^{K} \sum_{l=1}^{d_j^c} \hat{H}_{j,i}^c v_{l,j}^c s_{l,j}^c \right) + (u_{m,i}^c)^H \left(\sum_{c=1}^{C} \sum_{j=1}^{K} \sum_{l=1}^{d_j^c} \Delta_{j,i}^c v_{l,j}^c s_{l,j}^c \right) + (u_{m,i}^c)^H z_i^c, \tag{3.66}$$

where $v_{l,j}^c$ is the precoder for l-th stream of user j in D2D group c. Therefore, the SINR of the m-th stream for user i in c-th D2D group, $\gamma_{m,i}^c$, is given by

$$\gamma_{m,i}^c(u_{m,i}^c, \mathbb{V}, \Lambda) = \frac{\|(u_{m,i}^c)^H (\hat{H}_{i,i}^c + \Delta_{i,i}^c) v_{m,i}^c\|_2^2}{I_{m,i}^c + I_{\Delta_{m,i}^c} + \|u_{m,i}^c\|_2^2 \sigma_{i,c}^2}, \tag{3.67}$$

where $I_{m,i}^c = \sum_{(l,j,c') \neq (m,i,c)} \|(u_{m,i}^c)^H \hat{H}_{j,i}^{c'} v_{l,j}^{c'}\|_2^2$ accounts for the inter-stream, inter-user and inter-cell interferences from the neighboring D2D groups, $I_{\Delta_{m,i}^c} = \sum_{(l,j,c') \neq (m,i,c)} \|(u_{m,i}^c)^H \Delta_{j,i}^{c'} v_{l,j}^{c'}\|_2^2$ is the residue interference due to the channel uncertainty at the m-th stream of user i in D2D group c, $\mathbb{V}$ and Λ denote the sets of $\{v_{m,i}^c, \forall m, i, c\}$ and $\{\Delta_{i,j}^c, \forall i, j, c\}$, respectively.

3.3.2 Problem Formulation

Considering that the system performance is often limited by the worst stream, our objective is to find the precoders and receive filters that maximize the minimum SINR over all streams across all users of underlaying D2D groups in the cellular network. As for the interference power constraint, we follow a conservative approach where each D2D user is aware of a preset interference power constraint (set by the BS) that is tolerable by the cellular user.

3.3.2.1 Overview of the Optimization Problem

Maximizing the minimum SINR of the data streams considering the bounded channel uncertainty as well as an interference power constraint (that is tolerable by the macro-cell user) is an NP-hard problem. Following [45], [106, Theorem 3], and [114, Claim 3], we consider the corresponding inverse problem, i.e., jointly minimizing the transmit power subject to a minimum SINR constraint. The inverse optimization problem can be formulated as

$$\min_{\alpha_c, U_i^c, V_i^c} \quad \alpha_c \tag{3.68a}$$

$$\text{subject to} \quad \text{Tr}(\Delta_{i,j}^c {\Delta_{i,j}^c}^H) \leq {\epsilon_{i,j}^c}^2, \forall i, j, c \tag{3.68b}$$

$$\max \|(U_0)^H H_{i,0}^c V_i^c\|_F^2 \leq P_{th}^c, \ \|\Delta_{i,0}^c\|_F \leq \epsilon_{i,0}^c, \forall i, c \tag{3.68c}$$

$$\gamma_{m,i}^c(u_{m,i}^c, \mathbb{V}, \Lambda) \geq \gamma_{th}^c, \forall m, i, c \tag{3.68d}$$

$$\|V_i^c\|_F^2 \leq \alpha_c \mu_i^c, \forall i, c \tag{3.68e}$$

where U_0 is the receive filter for the cellular user (denoted as user 0), $H_{i,0}^c$ is the channel matrix between user i in D2D group c to the cellular user, P_{th}^c is the preset interference power constraint that is tolerable by the cellular user, γ_{th}^c is a certain minimum SINR threshold, $\mu_i^c = \frac{P_i^c}{\min(P_1^c, \ldots, P_K^c)}$ and α_c is an optimization variable to ensure that D2D user i is transmitting at a reduced power of $\alpha_c \mu_i^c \leq P_i$. In order to simplify the above optimization problem, we can follow approaches in [45, 102, 112] so as to exploit the bound on the channel uncertainty and derive the worst-case SINR expression as shown in (3.69), in the next page. Inequality a follows from the lower and upper bound properties of triangle inequality applied at the numerator and denominator of (3.67), respectively. Inequality b follows from the properties that $\text{Tr}(A_1 B_1) = \text{Tr}(B_1 A_1)$ for any $A_1 \in \mathbb{C}^{M \times N}$, $B_1 \in \mathbb{C}^{N \times M}$ and $\text{Tr}(A_2 B_2) \leq \text{Tr}(A_2)\text{Tr}(B_2)$ for any positive

definite matrices, $A_2, B_2 \in \mathbb{C}^{N\times N}$ [101]. Considering this worst-case SINR, the above optimization problem can be written as

$$\min_{\alpha_c, U_i^c, V_i^c} \quad \alpha_c \tag{3.70a}$$

$$\text{subject to max } \|(U_0)^H H_{i,0}^c V_i^c\|_F^2 \leq P_{th}^c, \|\Delta_{i,0}^c\|_F \leq \epsilon_{i,0}^c, \forall i, c \tag{3.70b}$$

$$\hat{\gamma}_{m,i}^c(u_{m,i}^c, \mathbb{V}) \geq \gamma_{th}^c, \forall i, m, c \tag{3.70c}$$

$$\|V_i^c\|_F^2 \leq \alpha_c \mu_i^c, \forall i, c \tag{3.70d}$$

Also, similar bounding can be applied to the interference power constraint involving channel uncertainty to the cellular user. Using the property of triangle inequality, the interference power constraint can be decomposed as

$$\begin{aligned} \max \quad & \|U_0^H H_{i,0}^c V_i^c\|_F^2, \quad \|\Delta_{i,0}^c\|_F \leq \epsilon_{i,0}^c \\ & \leq \|U_0^H \hat{H}_{i,0}^c V_i^c\|_F^2 + {\epsilon_{i,0}^c}^2 \sum_{m=1}^{d_i^c} \sum_{r=1}^{d^{pu}} \|u_{r,0}\|^2 \|v_{m,i}^c\|^2, \forall i, c \end{aligned} \tag{3.71}$$

$$\begin{aligned} & \inf_{\Delta_{i,j}^c} \quad \gamma_{m,i}^c(u_{m,i}^c, \mathbb{V}, \Lambda) \\ & = \frac{\|(u_{m,i}^c)^H (\hat{H}_{i,i}^c + \Delta_{i,i}^c) v_{m,i}^c\|^2}{\sum_{(l,j,c')\neq(m,i,c)} \|(u_{m,i}^c)^H (\hat{H}_{j,i}^{c'} + \Delta_{j,i}^{c'}) v_{l,j}^{c'}\|^2 + \|(u_{m,i}^c)\|^2 \sigma_{i,c}^2} \\ & \overset{a}{\geq} \frac{\|(u_{m,i}^c)^H \hat{H}_{i,i}^c v_{m,i}^c\|^2 - \|(u_{m,i}^c)^H \Delta_{i,i}^c v_{m,i}^c\|^2}{\sum_{l,j,c} \|(u_{m,i}^c)^H \hat{H}_{j,i}^c v_{l,j}^c\|^2 + \sum_{l,j,c} \|(u_{m,i}^c)^H \Delta_{j,i}^c v_{l,j}^c\|^2 - \|(u_{m,i}^c)^H \hat{H}_{i,i}^c v_{m,i}^c\|^2} \\ & \qquad\qquad - \|(u_{m,i}^c)^H \Delta_{i,i}^c v_{m,i}^c\|^2 + \|(u_{m,i}^c)^H\|^2 \sigma_{i,c}^2 \\ & \overset{b}{\geq} \frac{\|(u_{m,i}^c)^H \hat{H}_{i,i}^c v_{m,i}^c\|^2 - {\epsilon_{i,i}^c}^2 \|(u_i^c)\|^2 \|v_{m,i}^c\|^2}{\sum_{(l,j,c')\neq(m,i,c)} \|(u_{m,i}^c)^H \hat{H}_{j,i}^{c'} v_{l,j}^{c'}\|^2 + \|(u_{m,i}^c)^H\|^2 \sum_{(l,j,c')\neq(m,i,c)} {\epsilon_{j,i}^{c'}}^2 \|{v^{c'}}_{l,j}\|^2} \\ & \qquad\qquad + \|(u_{m,i}^c)^H\|^2 \sigma_{i,c}^2 \\ & \triangleq \hat{\gamma}_{m,i}^c(u_{m,i}^c, \mathbb{V}). \end{aligned} \tag{3.69}$$

where $u_{r,0}$ denotes the receive filter of r-th stream for the cellular user. Therefore, the overall optimization problem can be reformulated as

$$\min_{\alpha_c, U_i^c, V_i^c} \quad \alpha_c \tag{3.72a}$$

$$\text{subject to} \quad \|U_0^H \hat{H}_{i,0}^c V_i^c\|_F^2 +$$

$$\epsilon_{i,0}^{c\,2} \sum_{m=1}^{d_i^c} \sum_{r=1}^{d^{pu}} \|u_{r,0}\|^2 \|v_{m,i}^c\|^2 \leq P_{th}^c, \forall i, c \tag{3.72b}$$

$$\hat{\gamma}_{m,i}^c(u_{m,i}^c, \mathbb{V}) \geq \gamma_{th}^c, \forall m, i, c \tag{3.72c}$$

$$||V_i^c||_F^2 \leq \alpha_c \mu_i^c, \forall i, c \tag{3.72d}$$

The SINR constraint in the above optimization problem is jointly non-convex in the optimization variables U_i^c and V_i^c. Therefore, we follow an alternating minimization approach to solve this problem, as in the previous section. In particular, we optimize the receive filters with fixed precoders and then minimum SINR over all streams across all users in any given D2D group is obtained and the target SINR is updated as well. After that, the precoders are optimized with fixed receive filters. Then the minimum SINR is determined with up-scaled transmit power and target SINR is updated accordingly. This process continues until the minimum SINR converges. Each of these subproblems is discussed below.

3.3.3 Receive Filter Design

For the fixed precoders, the worst-case SINR depends on the receive filters. Therefore, the optimization of the receive filters can be formulated as an unconstrained

subproblem

$$\text{max.} \quad \hat{\gamma}^c_{m,i}(u^c_{m,i}, \mathbb{V}), \forall m, i, c \tag{3.73}$$

Following [101, 113], and as derived in [45, Appendix B], the optimal solution, $(u^c_{m,i})$, of the above unconstrained optimization problem can be derived as

$$u^c_{m,i} = \frac{\{\Psi^c_{m,i}\}^{-\frac{1}{2}} w^c_{m,i}}{||\{\Psi^c_{m,i}\}^{-\frac{1}{2}} w^c_{m,i}||}, \tag{3.74}$$

where $w^c_{m,i}$ is the principal eigenvector of $(\Psi^c_{m,i})^{-\frac{1}{2}} \Phi^c_{m,i} (\Psi^c_{m,i})^{-\frac{1}{2}}$, and

$$\hat{\gamma}^c_{m,i}(u^c_{m,i}, \mathbb{V}) = \frac{(u^c_{m,i})^H \Phi^c_{m,i} u^c_{m,i}}{(u^c_{m,i})^H \Psi^c_{m,i} u^c_{m,i}},$$

where

$$\begin{aligned}\Psi^c_{m,i} = &\sum_{l,j,c} \hat{H}^c_{j,i} v^c_{l,j} (v^c_{l,j})^H (\hat{H}^c_{j,i})^H + \sum_{l,j,c} {\epsilon^c_{j,i}}^2 ||v^c_{l,j}||^2 I_{M_r} \\ &- \hat{H}^c_{i,i} v^c_{m,i} (v^c_{m,i})^H (\hat{H}^c_{i,i})^H - {\epsilon^c_{i,i}}^2 ||v^c_{m,i}||^2 I_{M_r} + \sigma^2_{i,c} I_{M_r},\end{aligned}$$

and

$$\Phi^c_{m,i} = \hat{H}^c_{i,i} v^c_{m,i} (v^c_{m,i})^H (\hat{H}^c_{i,i})^H - {\epsilon^c_{i,i}}^2 ||v^c_{m,i}||^2 I_{M_r}.$$

3.3.4 Precoder Design

As we have studied in the case of FD communications in Section 3.2.3.2, the problem of precoder design with QoS constraint is NP-hard in general [45,106,114]. Therefore, we apply the SDR technique to solve this problem, as in the previous section [45].

Let us define the precoder of the m-th stream for user i in D2D group c as $V_{m,i}^c = (v_{m,i}^c)(v_{m,i}^c)^H$, a semidefinite matrix. Following this definition, the first term on the right hand side of (3.71) can be expanded as below

$$\begin{aligned}
&\|U_0^H \hat{H}_{i,0}^c V_{i,c}\|_F^2 = \|[U_0^H \hat{H}_{i,0}^c v_{1,i}^c, U_0^H \hat{H}_{i,0}^c v_{2,i}^c, \ldots, U_0^H \hat{H}_{i,0}^c v_{d_i^c,i}^c]\|_F^2 \\
&= \mathrm{Tr}[(\hat{H}_{i,0}^c)^H U_0 U_0^H \hat{H}_{i,0}^c V_{1,i}^c] + \ldots + \mathrm{Tr}[(\hat{H}_{i,0}^c)^H U_0 U_0^H \hat{H}_{i,0}^c V_{d_i^c,i}^c] \\
&\leq \sum_{m=1}^{d_i^c} P_{th}^{\hat{H}_{m,i}^c}, \qquad (3.75)
\end{aligned}$$

where $P_{th}^{\hat{H}_{m,i}^c}$ is the interference power due to the transmission of the m-th stream from user i in D2D group c that is related to the estimated channel. We define $a_{m,i}^c \triangleq \mathrm{vec}(U_0^H \hat{H}_{i,0}^c V_{m,i}^c)$ such that $\|a_{m,i}^c\|^2 \leq P_{th}^{\hat{H}_{m,i}^c}$. Using the Schur complement [101], each of the terms in the above equation can be written into a positive semidefinite form as

$$\Theta_{th}^{\hat{H}_{m,i}^c} = \begin{bmatrix} P_{th}^{\hat{H}_{m,i}^c} & (a_{m,i}^c)^H \\ a_{m,i}^c & I \end{bmatrix} \succeq 0. \qquad (3.76)$$

Similar steps can be followed for the remaining streams of user i in D2D group c as well. On the other hand, each of the components of the second term on the right hand side of (3.71) can be written as, $\mathrm{Tr}[V_{m,i}^c] \leq \frac{P_{th}^{\Delta_{m,i}^c}}{{\epsilon_{i,0}^c}^2 \sum_{r=1}^{d^{pu}} \|u_{r,0}\|^2}$, such that ${\epsilon_{i,0}^c}^2 \sum_{m=1}^{d_i^c} \sum_{r=1}^{d^{pu}} \|u_{r,0}\|^2 \mathrm{Tr}[V_{m,i}^c] \leq \sum_{m=1}^{d_i^c} P_{th}^{\Delta_{m,i}^c}$, where $P_{th}^{\Delta_{m,i}^c}$ is the interference power component due to the transmission of the m-th stream from user i in D2D group c that is related to the channel uncertainty. Note that with fixed receive filters and positive semidefinite $V_{m,i}^c$, the SINR in (3.69) can be written as, $\tilde{\gamma}_{m,i}^c$, which is given in the following page (3.77), where $\mathbb{V}_{sd}$ denotes the set of semidefinite precoders, $\{(V_{m,i}^c), \forall m, i, c\}$. Therefore, SINR constraints in the above optimization problem now becomes convex inequalities. Hence, the problem of optimizing the precoders

with fixed receive filters and interference power constraint can be reformulated as

$$\min_{\alpha_c, V^c_{m,i}} \quad \alpha_c \tag{3.78a}$$

$$\text{subject to} \quad \sum_{m=1}^{d_i^c} P_{th}^{\hat{H}^c_{m,i}} + \sum_{m=1}^{d_i^c} P_{th}^{\Delta^c_{m,i}} \leq P^c_{th}, \forall i, c \tag{3.78b}$$

$$\Theta_{th}^{\hat{H}^c_{m,i}} \succeq 0, \forall m, i, c \tag{3.78c}$$

$$\mathrm{Tr}[V^c_{m,i}] \leq \frac{P_{th}^{\Delta^c_{m,i}}}{{\epsilon^c_{i,0}}^2 \sum_{r=1}^{d^{pu}} \|u_{r,0}\|^2}, \forall m, i, c \tag{3.78d}$$

$$\tilde{\gamma}^c_{m,i}(u^c_{m,i}, \mathbb{V}_{sd}) \geq \hat{\gamma}^c_{th}, \forall m, i, c \tag{3.78e}$$

$$\sum_{m=1}^{d_i^c} \mathrm{Tr}[V^c_{m,i}] \leq \alpha_c \mu^c_i, \forall i, c \tag{3.78f}$$

$$V^c_{m,i} \succeq 0, \forall m, i, c \tag{3.78g}$$

$$\mathrm{rank}(V^c_{m,i}) = 1, \forall m, i, c. \tag{3.78h}$$

Note that the optimal α_c^* that is obtained from this minimum power precoder design problem will return the minimum SINR threshold for the original max-min fair SINR problem. The last two constraints in the above optimization problem ensue from the definition of $V^c_{m,i}$ i.e., positive semidefiniteness of $V^c_{m,i}$. However, the problem is still non-convex due to rank-1 constraint. Therefore, we relax the problem by dropping the above rank-1 constraint, and in turn, the problem becomes a semidefinite problem that can be efficiently solved using available optimization

$$\begin{aligned}
&\tilde{\gamma}^c_{m,i}(u^c_{m,i}, \mathbb{V}) \\
&= \frac{\mathrm{Tr}((\hat{H}^c_{i,i})^H u^c_{m,i}(u^c_{m,i})^H \hat{H}^c_{i,i} V^c_{m,i}) - {\epsilon^c_{i,i}}^2 \|(u^c_{m,i})\|^2 \mathrm{Tr}(V^c_{m,i})}{\sum_{(l,j,c') \neq (m,i,c)} \mathrm{Tr}((\hat{H}^{c'}_{j,i})^H u^c_{m,i}(u^c_{m,i})^H \hat{H}^{c'}_{j,i} V^{c'}_{l,j}) + \|(u^c_{m,i})\|^2 \sum_{(l,j,c') \neq (m,i,c)} {\epsilon^{c'}_{j,i}}^2 \mathrm{Tr}(V^{c'}_{m,i}) + \|(u^c_{m,i})\|^2 \sigma^2_{i,c}} \\
&\triangleq \tilde{\gamma}^c_{m,i}(u^c_{m,i}, \mathbb{V}_{sd}).
\end{aligned} \tag{3.77}$$

toolboxes.

3.3.5 Numerical Results and Discussions

In this section, we illustrate the worst-case data rate performance of the D2D users in a cellular network using numerical simulations. The simulations are performed in an underlay D2D-enabled cellular network, where there is one primary-user pair and two D2D groups ($C = 2$) that coexist with the PU. Each D2D group is composed of $K = 2$ secondary-user pairs, where each D2D transmitter and receiver are equipped with two and three antennas, respectively. We also assume that primary-user link makes use of three antennas both at the transmitter and receiver. We further consider that both PU and SUs send one independent data stream. The channel model used in the simulation is a quasi-static Rayleigh flat fading channel, which is obtained by generating independent and identically distributed (i.i.d) Gaussian random variables with zero mean and unit variance. Furthermore, we assume that CSI uncertainty bounds are equal, i.e., $\epsilon_{i,j} = \epsilon, \forall i, j$. We also assume that users in the D2D groups have the same total transmit power i.e., $P_1^c = P_2^c$, which gives $\mu_i^c = 1, \forall i, c$.

As a benchmark, we have simulated a robust non-cognitive IA system (without the macrocell) to compare the worst-case data rate that is achievable from a D2D enabled cellular interference network in the presence of channel uncertainty and an interference power constraint from the BS. For the sake of simplicity, we neglected the path-loss in our simulation. Fig. 3.10 shows the comparison of the worst-case data rate over all streams across all users in a D2D group underlaying in the cellular network with that of the users in an IA system without the primary network (non-cognitive system). As it is seen from the figure, the users in the D2D group generally perform worse relative to the users in the non-cognitive system since the former needs

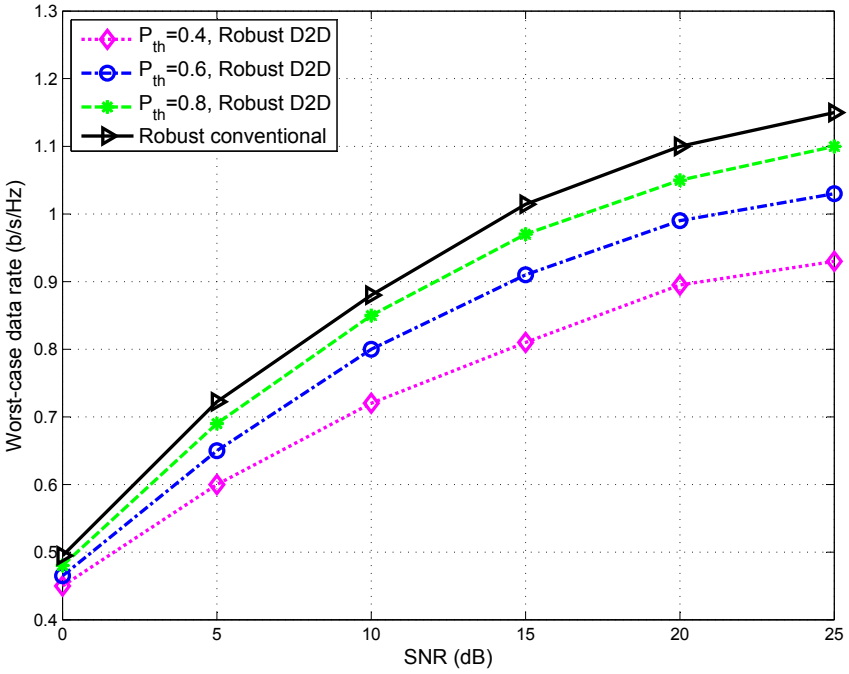

Figure 3.10: Worst-case stream data rate with SNR for D2D users in a cellular interference network, $C = K = 2$, $N_T = 2$, $N_R = N_T^{pu} = N_R^{pu} = 3$, $d_1^c = d_2^c = d^{pu} = 1$, $\epsilon = 0.15$.

to satisfy an additional interference power constraint. In addition, it is observed that as the interference power constraint becomes stringent, the worst-case stream data rate of the users in the D2D group degrades. That is to say, the worst-case stream data rate of the users in the D2D group approach that of the users in the non-cognitive system when the interference power constraint is relaxed. However, at low SNR with relaxed interference power constraint, e.g., at SNR=0 dB with $P_{th} = 0.8$, the worst-case stream data rate of the users in the D2D group is very close to that of the users in the non-cognitive system since this relaxed interference power constraint at low SNR has minimal impact on the optimization of precoders and receive filters.

Fig. 3.11 shows the worst-case stream data rate with CSI error at an SNR of

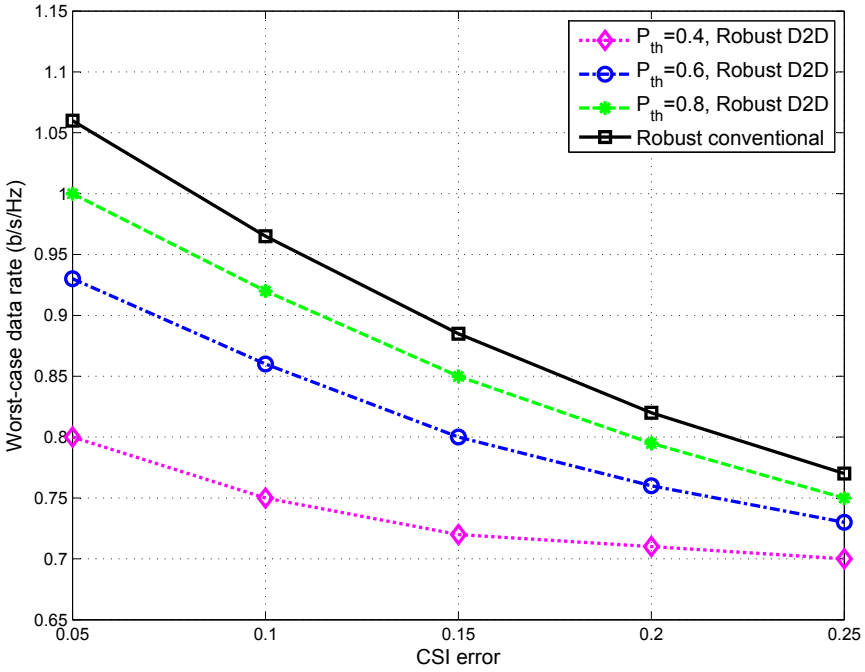

Figure 3.11: Worst-case stream data rate with CSI error (ϵ) for D2D users in a cellular interference network, $C = K = 2$, $N_T = 2$, $N_R = N_T^{pu} = N_R^{pu} = 3$, $d_1^c = d_2^c = d^{pu} = 1$.

10 dB. As expected, as the CSI error increases i.e., the radius of the uncertainty region increases, the worst-case stream data rate of the users in the D2D group degrades. Furthermore, the D2D users perform worse than that of the users in the non-cognitive system due to an additional interference power constraint set by the macrocell BS or the primary network. However, as seen from this figure, with relaxed interference power constraint, the performance gap of the worst-case stream data rate between the users involved in the D2D communication and that of the users in the non-cognitive system becomes narrower in the high CSI error regime. The reason being at the high CSI error with relaxed interference power constraint, the CSI error becomes the performance bottleneck.

3.4 Conclusions

In this chapter, we have studied the design of precoders and receive filters for the fairness problems in FD and D2D communications. In the first part of this chapter, we have studied the transmit and receive beamforming designs in order to address the fairness problem in FD MIMO multi-cell systems under the assumption of limited-DR. In particular, we consider design approaches with both perfect and imperfect CSI. Since the globally optimal solution is difficult to obtain due to the non-convex nature of the problems, we resort to alternating minimization to obtain locally optimal solutions. The optimization objective is found to be converging in a few iterations. The simulation results suggest that the FD transmission provides better sum-rate performance when compared to that of HD transmission with low to moderate transceiver distortion. Furthermore, we notice that the spectral efficiency gain of the FD transmission increases with increasing distance between the small-cell BSs due to reduced inter-cell interference. In comparison to the widely studied WMMSE and Max-Min SINR algorithms, our results reveal that the proposed algorithm offers a better fairness among the cell-edge users. In dealing with practical design issues, our study demonstrates that the proposed robust design similarly provides improved sum-rate performance when compared to HD transmission in the presence of bounded CSI uncertainty. In comparison to a non-robust design, the results demonstrates that a higher sum-rate is achievable with the aid of a robust design in the presence of CSI uncertainty.

In the second part of this chapter, we have studied the same problem of robust fairness transceiver design for D2D-enabled cellular network. For this research problem, our objective was to maximize the minimum SINRs of the D2D users. In order to protect the PU (i.e., macrocell users) from the cognitive transmission of the users

involved in the D2D communications, there is an interference power constraint which is taken into account, in addition to the CSI uncertainty. Due to the non-convexity of the optimization problem, we have followed an iterative alternative minimization algorithm that involves the SDR technique. In order to evaluate the performance of the proposed transceiver, we have compared the worst-case stream data rate of users involved in the D2D communications with that of users in an IA system without the primary network (non-cognitive case). It is observed that at low SNR with relaxed interference power constraint, the worst-case stream data rate of the users involved in the D2D communications is very close to that of the users in the non-cognitive system. However, the performance degrades considerably with stringent interference power constraint. Further, in line with our expectation, the worst-case stream data rate of the D2D users degrades as the CSI error increases, while the performance gap becomes narrower at high CSI error with relaxed interference power constraint.

Chapter 4

Interference Alignment for Power Line Communications

4.1 Introduction

In Chapters 2 and 3, we investigated interference mitigations techniques for interference-limited systems, such as FD and D2D communication systems. In this chapter, we focus on another interference-limited system, namely PLC where the system performance is limited by the inter-user interference, as presented in Chapter 1. With the exploitation of existing large power grid infrastructures, data transmission over the power grid, i.e., PLC is a cost-efficient solution for providing communication services, such as local area networking [14]. Besides the phase-neutral (P-N) port, which can enable Single-Input Single-Output (SISO) PLC technology, many countries deploy multiconductor cables, e.g., an additional earth (E) wire, that creates more feeding and receiving possibilities. Therefore, it becomes possible to transmit and receive data over multiple conductors and opens a way to perform spatial processing via well-established MIMO technology [127].

The multiple simultaneous pair-wise communications in power line networks closely resemble signal transmission over an interference channel in wireless networks, where all users share the common communication medium (cf. Fig. 1.2). Furthermore, each feeding port may also intend to send signals to each of the receiving ports in

the network, as in wireless X-network (cf. Fig. 1.3).

As presented in Chapter 1, the IA is an optimal multiplexing gain transmission strategy. The benefit of achieving the maximum multiplexing gain makes IA an attractive spectral efficient transmission technique for PLC networks. The key idea of the IA is to jointly design the precoders and receive filters such that each receive filter creates both signal and interference subspaces, while each transmitter precodes its signals in a way to make sure that for any given receiver, the signals from undesired transmitters fall into the interference subspace of that receiver [32].

Although IA has been extensively studied in the context of wireless networks, only recently has it been studied in the context of PLC networks, as part of contributions of this thesis. To present a thorough treatment, in this chapter, we start by examining the feasibility of IA in the context of MIMO PLC interference networks. In particular, we investigate practicality of the Min-IL and Max-SINR algorithms to PLC networks that were originally proposed to achieve IA in the context of MIMO wireless interference networks [128]. Assuming AWGN, our initial results show that IA is equally applicable in the context of MIMO PLC interference networks and the sum-rate can be significantly improved through the exploitation of the Max-SINR algorithm. It is found that at high SNR, the performance gain in terms of sum-rate over orthogonal transmissions is around 30% for a 3-user 2×2 MIMO PLC network. Furthermore, we compare the performance of a MIMO PLC interference network with that of a MIMO wireless interference network having equivalent link qualities of the former. Our results suggest that MIMO PLC offers a lower sum-rate than the equivalent MIMO wireless network.

Since noise in PLC is dominated by disturbances induced into the grid from attached appliances and equipments, it is generally spectrally and spatially not white.

This has been substantiated in various measurement campaigns for MIMO PLC in indoor environments [129–132]. While spectral dependencies are of somewhat secondary importance for the operation of linear IA over spatial MIMO channel, the spatial correlation is directly relevant for the IA filter design and performance. Concerning this, we investigate the impact of spatial noise correlation on the performance of linear IA for MIMO PLC. We exploit the practical noise data collected by the special task force 410 of the European Telecommunications Standards Institute (ETSI) during a measurement campaign in several homes throughout Europe [131,132]. The availability of the measured noise data allows us to evaluate the IA performance with practical levels of spatial noise correlation in real MIMO PLC networks. Since the previous results reveal that the Max-SINR based IA design provides a better sum-rate performance than the Min-IL based design and also has the ability to take into account the noise statistics [128], we only consider the former for this particular analysis. Our specific objectives are twofold. First, we examine the impact of spatially correlated noise on performance when the Max-SINR is designed assuming independent noise across different ports, which could be considered as a mismatched design. This is to say, we investigate the benefits of incorporating noise correlation into the IA design. Second, we show that assuming spatially independent noise at different PLC receiver ports underestimates achievable rates. Overall, our results highlight that proper exploitation of practical noise correlation levels in PLC leads to further gains in sum-rate for transmission with IA. More specifically, with a proper IA design that accounts for practical noise correlation levels, a rate gain as high as 34% over a mismatched IA design is obtained for the considered PLC setup.

The IA techniques generally require the availability of the CSI at the transmitter. The BIA scheme is an exception in that it works without having the CSI at the

transmitter [133, 134]. Rather, the technique requires that the channel seen by each receiving port changes following a specific pattern. Even though the load modulation changes the channel transfer characteristics over time slots, we show that it is ineffective for the purpose of the blind IA in PLC X-network. Hence, we propose a transmission scheme that offers the desired channel variation and can achieve the maximum multiplexing gain with the proposed scheme for PLC X-networks.

The rest of the chapter is organized as follows. Section 4.2 discusses the IA for the MIMO PLC interference network with different IA techniques assuming both AWGN and MIMO PLC measured noise. In Section 4.3, we present the BIA for PLC X-networks, where we investigate different network scenarios for the feasibility of this IA scheme. We summarize this chapter in Section 4.4.

4.2 IA for MIMO PLC Interference Networks

In this section, we investigate the technique of IA for MIMO PLC interference networks. In the first part of this section, we concentrate on the IA design assuming AWGN, while we present results with the practical measured noise in the second part of this section.

4.2.1 System Model

Let us consider a K-user MIMO PLC network, composed of K transmitter-receiver (Tx-Rx) pairs as shown in Fig. 4.1 for $K = 3$. Similar to wireless interference networks, we assume that all transmitters communicate simultaneously to its intended receiver on a pair basis, thereby creating interference-limited communication scenario for the PLC network. The underlying PLC network consists of 3-conductor cables. i.e., P, E, and N. Due to Kirchhoff's circuit law, with 3 conductors it is only possible

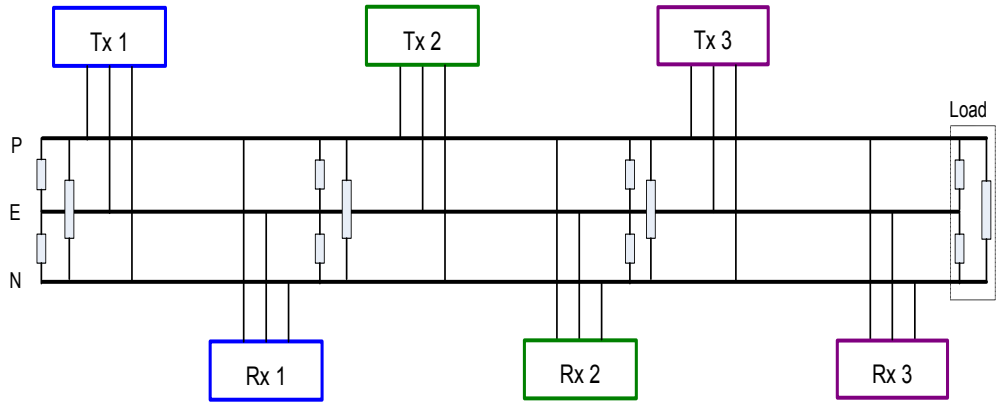

Figure 4.1: Illustration of a 3-conductor cables MIMO PLC interference network with 3 Tx-Rx pairs (setup-I).

to feed 2 transmit signals simultaneously over three possible ports, i.e., P–N, P–E or N–E ports. While on the receiving end all 3 ports are available, we restrict our attention to a symmetric case of equal number of feeding and receiving ports. Another variation of this network setup can be obtained by merely interchanging the positions of the corresponding Tx-Rx pairs as shown in Fig. 4.2. Additionally, more conductors can be used to create more feeding and receiving possibilities. In principle, with α conductors $\alpha - 1$ communication channels are available between any given Tx-Rx pair.

We assume that each Tx-Rx pair makes use of N_{t} and N_{r} ports at the transmitting and receiving end, respectively. Each transmitter, i, encodes its messages, s_i^m, onto $d_i \leq \min(N_{\mathrm{t}}, N_{\mathrm{r}})$ independent parallel data streams sent along the beamforming vectors, v_i^m. Note that each data stream is sent along the beamforming vector, v_i^m, with a power, ρ_i^m, for the m-th stream of i-th transmitter such that $\sum_{m=1}^{d_i} \rho_i^m \leq P_i$, where P_i is the maximum power of transmitter i.

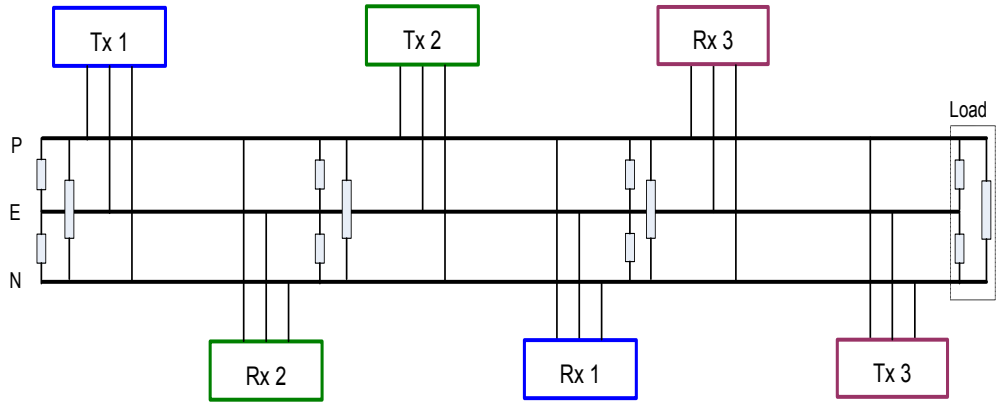

Figure 4.2: Illustration of a 3-conductor cables MIMO PLC interference network with 3 Tx-Rx pairs, a variation of setup-I (setup-II).

4.2.2 Precoding at the PLC Transmitter

For this study, we assume that perfect CSI is available at the transmitters. This can be assumed for broadband PLC, where transmitter side CSI is also used for bit-loading. Let us denote $V_i = [v_i^1, v_i^2, \ldots, v_i^{d_i}]$ as the $\mathbb{C}^{N_t \times d_i}$ precoding matrix which is designed based on the available channel estimate at PLC transmitter i. The precoded signal, S_i, at transmitter i can be represented as

$$\begin{aligned} S_i &= \sum_{m=1}^{d_i} v_i^m s_i^m \\ &= V_i s_i. \end{aligned} \tag{4.1}$$

4.2.3 Interference Suppression at the PLC Receiver

The received signal at the corresponding PLC receiver i is given by

$$y_i = H_{i,i} V_i s_i + \sum_{j=1, j\neq i}^{K} H_{i,j} V_j s_j + w_i, \tag{4.2}$$

where $H_{i,i} \in \mathbb{C}^{N_\mathrm{r} \times N_\mathrm{t}}$ is the channel matrix between Tx-Rx pair i and $w_i \in \mathbb{C}^{N_\mathrm{r} \times 1}$ is the effective noise vector at PLC receiver i with distribution $\mathcal{CN}(\mathbf{0}_{N_\mathrm{r}}, \sigma_i^2 \mathbf{I}_{N_\mathrm{r}})$. Although we assume AWGN for this initial study, later in this chapter we extend our results for PLC-specific measured noise. We also assume the application of multicarrier modulation, such as Orthogonal Frequency Division Multiplexing (OFDM), bearing in mind the broadband PLC systems. It allows us to decompose frequency-selective PLC channel into a number of parallel subchannels i.e., $H_{i,j}, \forall i, j$, as in subcarriers of an OFDM system. It is worthwhile to mention that compared to the wireless channel which is often modeled with the assumption of independent fading coefficients in the channel matrix H, the MIMO PLC channel shows a rather high spatial correlation [135, 136].

As with the precoder, transmitter also designs the filter $U_i = [u_i^1, u_i^2, \ldots, u_i^{d_i}] \in \mathbb{C}^{N_\mathrm{r} \times d_i}$, for receiver i, based on the perfect CSI available at its end. After projecting the received signal onto the columns of U_i, per-stream components of the received signal at each subcarrier can be written as

$$(u_i^m)^H y_i = (u_i^m)^H H_{i,i} v_i^m s_i^m + (u_i^m)^H \sum_{(j,l) \neq (i,m)} H_{i,j} v_j^l s_j^l + (u_i^m)^H w_i, \tag{4.3}$$

For brevity, the signal transmission model presented above does not show any subcarrier index. Instead it is presented for an arbitrary subcarrier keeping in mind that real system would perform signal processing per subcarrier basis. Following (4.3), the SINR for the m-th stream of i-th user, γ_i^m is given by

$$\gamma_i^m = \frac{\rho_i^m \| (u_i^m)^H H_{i,i} v_i^m \|_2^2}{(u_i^m)^H \Upsilon_i^m (u_i^m)}, \tag{4.4}$$

and the corresponding interference plus noise covariance matrix, Υ_i^m is given by

$$\Upsilon_i^m = \sum_{(j,l)\neq(i,m)} \rho_j^l H_{i,j} v_j^l (v_j^l)^H (H_{i,j})^H + \sigma_i^2 \mathbf{I}_{N_\mathrm{r}}. \tag{4.5}$$

If the interference resulting from the simultaneous transmissions of all PLC transmitters are aligned into the null space of U_i at PLC receiver i, the following conditions have to be satisfied for perfect IA [128],

$$U_i^H H_{i,j} V_j = 0, \forall j \neq i \tag{4.6}$$

$$\mathrm{rank}(U_i^H H_{i,i} V_i) = d_i, \forall i, \tag{4.7}$$

That is, the desired signals are received through a $d_i \times d_i$ full rank channel matrix while the interference is completely eliminated at receiver i.

4.2.4 IA Algorithms

In this section, we present a brief background on two popular IA algorithms, namely Min-IL and Max-SINR, that were proposed in the context of MIMO wireless interference networks [128]. These iterative algorithms were devised based on the assumption that communication channel is reciprocal. We can assume that the PLC channel transfer function is also reciprocal as suggested in [136], so these algorithms are directly applicable for MIMO PLC systems as well.

4.2.4.1 Min-IL based IA

The Min-IL algorithm is designed to iteratively minimize the leakage interference power at each receiver in order to find the optimum precoders and receive filters. In particular, the goal is to progressively achieve IA by reducing leakage interference

at each receiver. The quality of alignment is measured by the power of the leakage interference at each receiver, i.e., the interference power that remains in the received signal after the receive filter is applied. To this end, IA is said to be feasible if the leakage interference converges to zero. The total interference leakage power at receiver i due to transmissions of all undesired transmitters j ($j \neq i$) is given by

$$\Theta_i = \mathrm{Tr}(U_i^H \Phi_i U_i), \tag{4.8}$$

And the interference covariance matrix, Φ_i is given as

$$\Phi_i = \sum_{j=1, j\neq i}^{K} \sum_{l=1}^{d_j} \rho_j^l H_{i,j} v_j^l (v_j^l)^H H_{i,j}^H. \tag{4.9}$$

The optimum receive filter, $(U_i)_{\mathrm{opt}}$ for receiver i in the original network is then calculated by solving

$$(U_i)_{\mathrm{opt}} = \arg\min_{U_i} \Theta_i. \tag{4.10}$$

As suggested in [128], the solution to the above problem is the eigenvectors corresponding to d_i smallest eigenvalues of the interference covariance matrix Φ_i. Then the transmit precoding matrix in the reciprocal network would be the receive filter in the original network as derived above. Further, in the reciprocal network, receive filter $(\overleftarrow{U}_j)_{\mathrm{opt}}$, for receiver j is obtained by,

$$(\overleftarrow{U}_j)_{\mathrm{opt}} = (V_j)_{\mathrm{opt}} = \arg\min_{\overleftarrow{U}_j} \overleftarrow{\Theta}_j, \tag{4.11}$$

where $\overleftarrow{\Theta}_j$ is the total interference leakage at receiver j in the reciprocal network.

Similarly, $(\overleftarrow{U}_j)_{\text{opt}}$ is obtained by taking eigenvectors corresponding to d_j smallest eigenvalues of the interference covariance matrix, $\overleftarrow{\Phi}_j$ which can be obtained as

$$\overleftarrow{\Phi}_j = \sum_{i=1, i\neq j}^{K} \sum_{m=1}^{d_i} \overleftarrow{\rho}_i^m \overleftarrow{H}_{j,i} \overleftarrow{v}_i^m (\overleftarrow{v}_i^m)^H \overleftarrow{H}_{j,i}^H. \tag{4.12}$$

The receive filters in the reciprocal network are then used as precoding matrices in the original network. The iteration continues until the algorithm converges.

4.2.4.2 Feasibility of IA

In order to determine the feasibility of the IA for a given number of data streams transmitted, we calculate the interference leakage in the desired signal space. If d_i denotes the number of streams transmitted from user i, it is necessary to meet the following condition in order to achieve perfect IA,

$$\sum_{m=1}^{d_i} \Lambda_m[\Phi_i] = 0, \tag{4.13}$$

where $\Lambda_m[B]$ denotes the m-th smallest eigenvalue of matrix B. Note that $\sum_{m=1}^{d_i} \Lambda_m[\Phi_i]$ basically indicates total interference power in the desired signal space. Furthermore, the fraction of interference power in the desired signal space is given by

$$\theta_i = \frac{\sum_{m=1}^{d_i} \Lambda_m[\Phi_i]}{\text{Tr}(\Phi_i)}. \tag{4.14}$$

When IA is feasible, the fraction of interference leakage in the desired signal space will be zero.

4.2.4.3 Max-SINR based IA

The Min-IL algorithm discussed above only seeks to achieve perfect IA. However, it makes no effort in maximizing the desired signal power. To be precise, Min-IL algorithm does not consider the direct links $H_{i,i}, \forall i$ in its design at all. Keeping this drawback in mind, Max-SINR algorithm was proposed to maximize SINR at the receivers, instead of only minimizing the leakage interference. To this end, the receive filters are chosen such that the SINR of stream m for user i is maximized as below

$$(u_i^m)_{\text{opt}} = \arg\max_{u_i^m} \gamma_i^m. \tag{4.15}$$

The unit vector that maximizes γ_i^m is given by

$$(u_i^m)_{\text{opt}} = \frac{(\Upsilon_i^m)^{-1} H_{i,i} v_i^m}{\|(\Upsilon_i^m)^{-1} H_{i,i} v_i^m\|}. \tag{4.16}$$

As in the case of Min-IL algorithm, we can exploit channel reciprocity in order to calculate the precoder matrices. One can refer to [128] for the convergence behavior of these two algorithms.

4.2.5 Numerical Results with AWGN

In this section, we illustrate the performance of IA in the context of MIMO PLC interference networks assuming AWGN, where all Tx-Rx pairs communicate simultaneously over the same MIMO PLC channel. We consider the broadband PLC frequency band and calculate the channel frequency response between different Tx-Rx pairs at a frequency separation of 24.4 kHz [51]. This imitates the use of multicarrier modulation such as OFDM for broadband PLC systems. The computation of channel frequency response is based on MTL theory which was reported in [137].

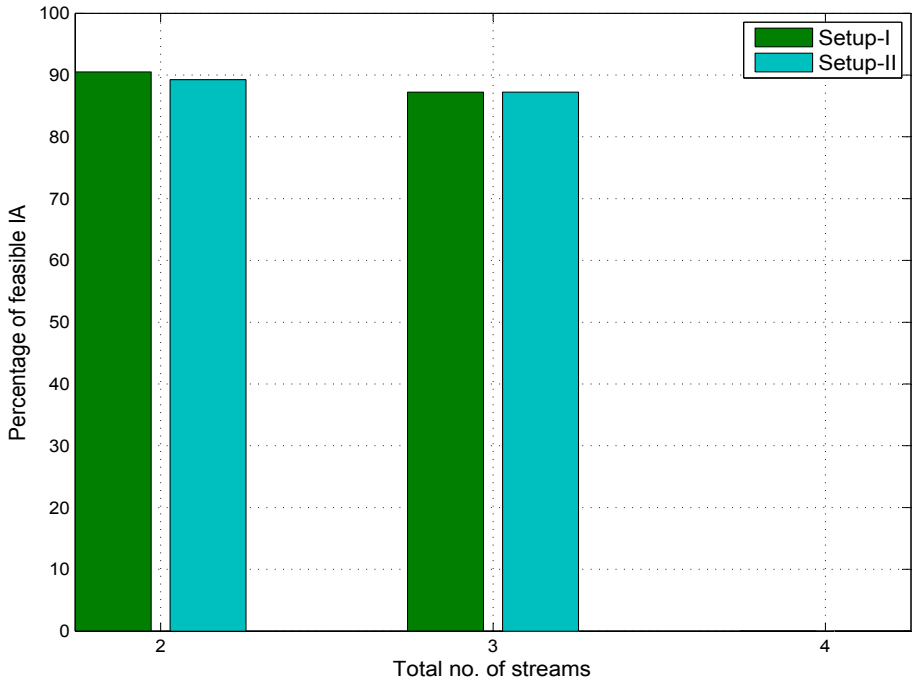

Figure 4.3: Percentage of feasible IA for $K = 3$ with 3-conductor cables i.e., $N_{\mathrm{t}} = N_{\mathrm{r}} = 2$ as shown in Fig. 4.1 (setup-I) and Fig. 4.2 (setup-II).

At first, we consider 3-conductor cables PLC networks with 3 Tx-RX pairs. Two such setups are shown in Fig. 4.1 (setup-I) and Fig. 4.2 (setup-II), where $K = 3$ and $N_{\mathrm{t}} = N_{\mathrm{r}} = 2$. Fig. 4.2 is a variation of Fig. 4.1 that is obtained by interchanging Tx-Rx pairs. Next, we consider another PLC network for $K = 3$ but with 4-conductor cables. To this end, we obtain a 3×3 MIMO PLC channel between any given Tx-Rx pair, where Tx-Rx pairs are positioned as in Fig. 4.1 and Fig. 4.2 for setups III and IV, respectively. A channel emulator for such PLC networks with branches and multiple-conductor cables is available in [138]. In order to evaluate the feasibility of IA, we consider different numbers of streams transmitted over the PLC network and then calculate the leakage interference power in the desired signal space as in (4.14). When IA is feasible, the fraction of interference leakage power in the desired

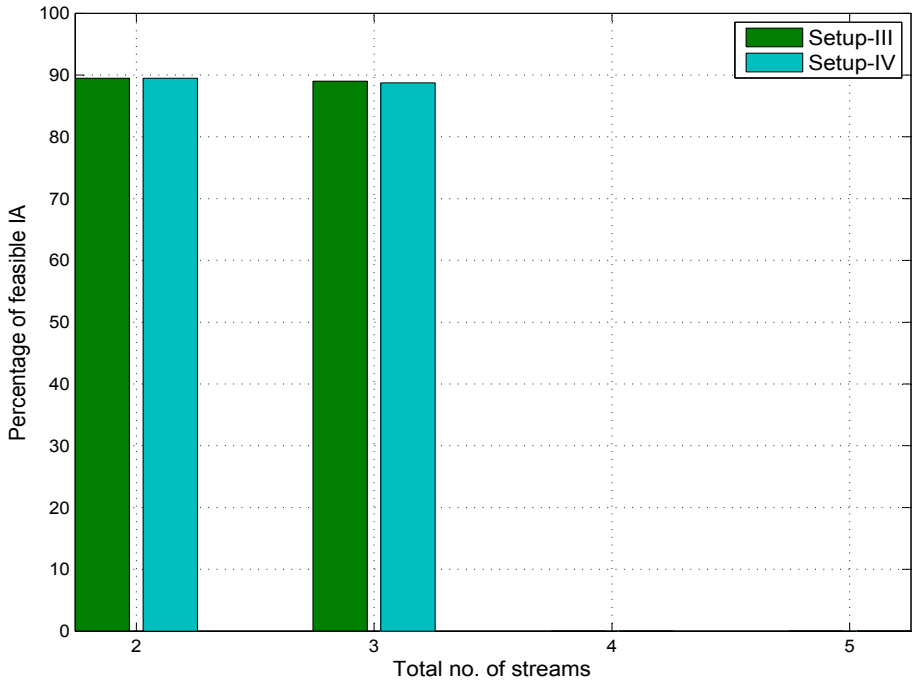

Figure 4.4: Percentage of feasible IA for $K = 3$ with 4-conductor cables i.e., $N_{\mathrm{t}} = N_{\mathrm{r}} = 3$. Tx-Rx pairs are positioned as in Fig. 4.1 and and Fig. 4.2 for setups III and IV, respectively.

signal space will be zero. We further assume that transmitters are provided with same power, i.e., $P_1 = P_2 = P_3$ as well as the streams are allocated equal power i.e., $\rho_i^m = \rho_j^l, \forall i, j, l, m$. Also, noise is kept fixed with variance, $\sigma_i^2 = 1, \forall i$. For each network realization, distance between any given Tx-Rx pair and load resistance are generated independently and randomly from uniform distributions on the intervals $[5, 15]$ m and $[5, 50]$ Ω, respectively. We generate 1000 such network realizations.

Fig. 4.3 shows the percentage of feasible IA (in terms of interference leakage power in the desired signal space calculated within nemerical errors) for MIMO PLC networks shown in Fig. 4.1 and Fig. 4.2. In particular, for these setups we consider three instances, where $\sum_{i=1}^{K} d_i = 2, 3, 4$ streams are transmitted over the networks in

Figs. 4.1 and 4.2. Note that for $K = 3$ with $N_{\mathrm{t}} = N_{\mathrm{r}} = 2$, the number of interference-free streams or DoF for each user is upper bounded by $d_i = \frac{N_{\mathrm{t}}+N_{\mathrm{r}}}{K+1} = 1, \forall i$ [32]. Therefore, the maximum achievable DoFs for both of these networks are the same, i.e, $\sum_{i=1}^{K} d_i = \frac{KN_{\mathrm{t}}}{2} = 3$. We observe from Fig. 4.3 that when $\sum_{i=1}^{K} d_i = 2, 3$ streams are transmitted over the setups in Fig. 4.1 and Fig. 4.2, IA is feasible in most of the realizations. That is to say, interference leakage power in the desired signal space is zero, and therefore feasible for these DoF allocations which is in line with MIMO wireless interference networks. On the other hand, transmitting more than 3 streams i.e., $\sum_{i=1}^{K} d_i = 4$ streams, yields interference leakage to the desired signal space, therefore IA is infeasible for this DoF allocation. It is important to note that when the interference leakage in the desired signal space is not zero for some of the realizations as it is seen from Fig. 4.3 while $\sum_{i=1}^{K} d_i = 2, 3$ are transmitted, it does not necessarily mean that IA is infeasible for these DoF allocations. That is because the iterative Min-IL algorithm may not converge to the global minimum, yielding non-zero interference leakage in the desired signal space.

Fig. 4.4 shows the percentage of feasible IA for a PLC network with 4-conductor cables, i.e., $N_{\mathrm{t}} = N_{\mathrm{r}} = 3$ and $K = 3$, for setups III and IV as discussed in the beginning of this section. The maximum achievable DoFs for these networks are upper bounded as $\sum_{i=1}^{K} d_i = \frac{KN_{\mathrm{t}}}{2} = 4.5$. To determine the feasibility of IA, we transmit $\sum_{i=1}^{K} d_i = 2, 3, 4, 5$ streams over these PLC networks. Similar to the previous figure, when $\sum_{i=1}^{K} d_i = 2, 3$ streams are transmitted over these setups, in most of the realizations the percentage of interference leakage in the desired signal space is zero, and therefore feasible for these DoF allocations. Although the total number of DoFs for these setups are upper bound by 4.5, transmitting $\sum_{i=1}^{K} d_i = 4$ streams over these networks are infeasible since the total DoF allocation in this case is also

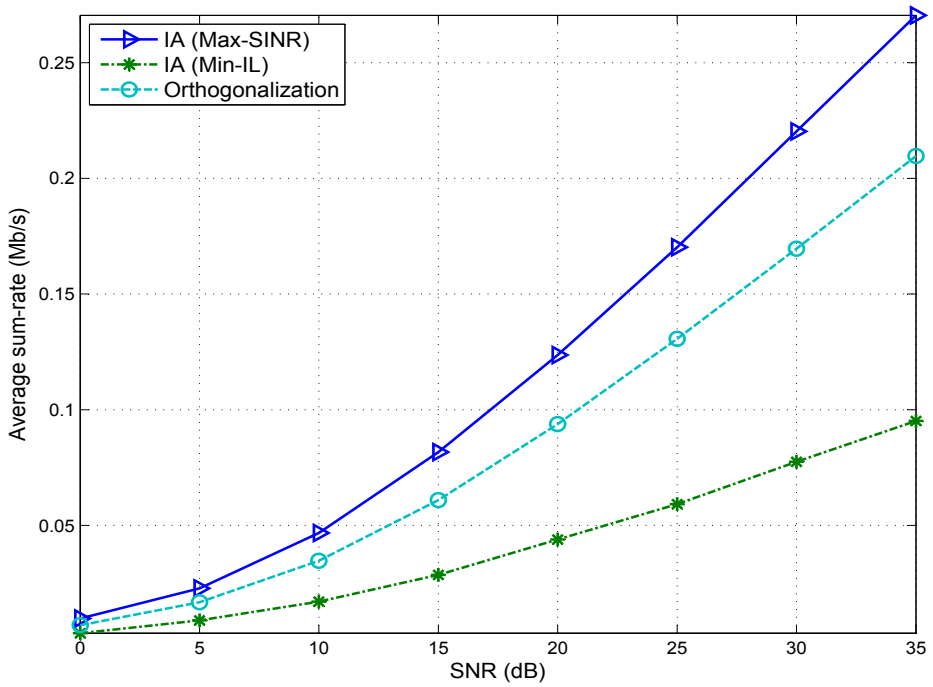

Figure 4.5: Comparison of average sum-rates of IA and orthogonal transmissions for MIMO PLC network in Fig. 4.1.

limited by DoF upper bound of an individual user. As an example, a choice of $d_1 = 2, d_2 = d_3 = 1$ would be infeasible since user 1 violates the upper bound for its DoF allocation. In the same context, $d_1 = d_2 = 2, d_3 = 0$ would be infeasible. Lastly, a total DoF allocation of 5 streams is clearly infeasible, which is also confirmed by the simulation results as shown in Fig. 4.4. Therefore, these results further validate the feasibility of IA for PLC interference networks.

4.2.5.1 Comparison with Orthogonal Transmission

In this section, we compare the sum-rate performances of IA algorithms with transmission techniques that are based on channel orthogonalization, such as Time Division Multiple Access (TDMA). With orthogonal transmission, it is only possible

to transmit 2 streams simultaneously at a given time-frequency resource over 2 antennas. To this end, we compute the singular value decomposition of MIMO PLC channel and then 2 data streams are transmitted on the eigenmodes of the channel. To be fair with IA based precoding, orthogonal transmissions are provided with 3 times transmission power i.e., $P_{\text{o}} = 3P_i, \forall i$ for $K = 3$ at a given time/frequency slot.

Fig. 4.5 compares the sum-rates for the Max-SINR, Min-IL and orthogonal transmissions for the network setup in Fig. 4.1. As it is observed, the Max-SINR based IA provides a higher sum-rate than the Min-IL algorithm based IA design. This is inline with the MIMO wireless networks as the Max-SINR algorithm considers direct links $H_{i,i}, \forall i$ in the design of precoders and receive filters in an effort to maximize the SINRs of direct links, thus provides higher sum-rate. Furthermore, the Max-SINR based IA outperforms channel orthogonalization technique, which is also in line with our expectation since channel orthogonalization only allows simultaneous transmission of 2 data streams whereas the Max-SINR based IA allows simultaneous transmission of 3 streams. To be precise, the sum-rate gain at high SNR for Max-SINR based IA over orthogonal transmission is around 30% for this network setup. In contrast to the wireless communications, we see that the Min-IL algorithm performs worse than orthogonal transmission. This may be attributed to the fact that MIMO PLC channel exhibits a high level of spatial correlation, resulting a lower SINR for the direct links $H_{i,i}, \forall i$.

4.2.5.2 Comparison with Wireless Communication

In this section, we provide a comparison between sum-rate performances of the MIMO PLC interference network and that of a MIMO wireless interference network with equivalent link qualities for IA transmission. In particular, we consider the setup in

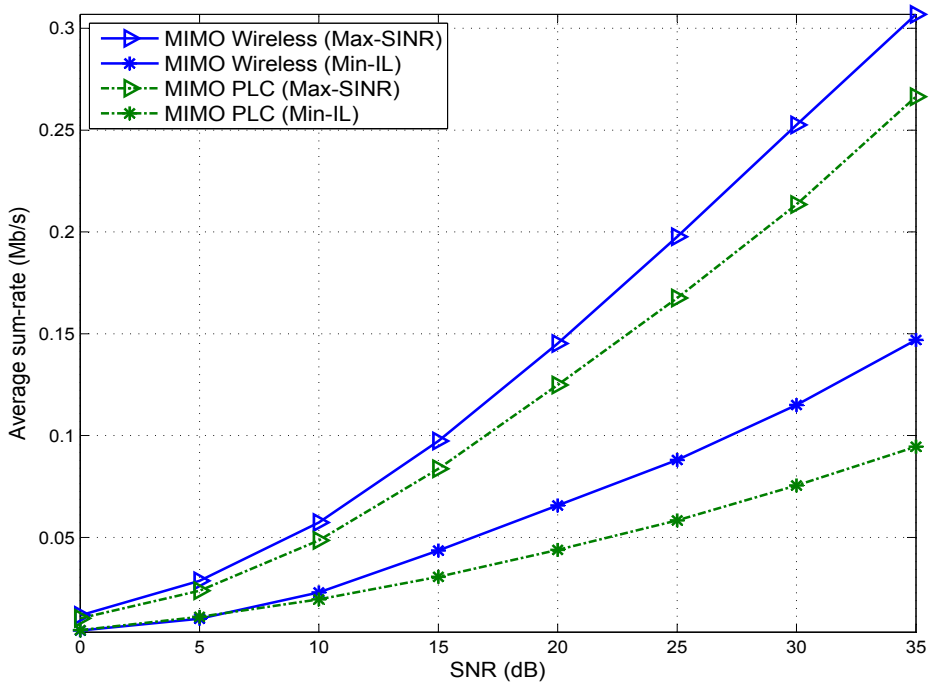

Figure 4.6: Comparison of average sum-rates with IA algorithms for the MIMO PLC network in Fig. 4.1 and a wireless interference network with equivalent link qualities.

Fig. 4.1 and compute the average power gains of the channel given as below

$$\beta_{i,j} = \frac{1}{N_{\text{sim}} \times N_{\text{sub}}} \sum_{q=1}^{N_{\text{sim}}} \sum_{f=1}^{N_{\text{sub}}} |H_{i,j}^{q,f}|^2, \tag{4.17}$$

where $H_{i,j}^{q,r}$ is the (i,j) elements in channel H for the q-th network realization and f frequency value, N_{sim} and N_{sub} are the number of network realizations and frequencies considered in the simulation. We then use these average power gains, $\beta_{i,j}$, as the second order moments of Rayleigh distributions to generate the channel gains of the corresponding wireless MIMO links. This way we can compare the sum-rate for the MIMO PLC interference network with a similar MIMO wireless interference network having complex Gaussian channel coefficients with the same average gains for all

direct and cross-channel coefficients.

Fig. 4.6 compares the sum-rates for Max-SINR and Min-IL algorithms in the context of MIMO PLC setup in Fig. 4.1 and an equivalent wireless interference network, for which channel gains are obtained as discussed above. It is observed form this result that the IA algorithms for MIMO PLC interference network provide lower sum-rates than that can be obtained from the equivalent MIMO wireless interference network, although we use the same IA algorithms for both communication scenarios. We note that this is due to the fact that MIMO PLC channel exhibits relatively higher spatial correlation than the wireless channel, which causes the degradation in the sum-rate performance [136].

4.2.6 Numerical Results with Practical Measured Noise

In this section, we present our results with practical measure MIMO PLC noise. To this end, we restrict our analysis to Max-SINR based IA since it provides a better sum-rate performance than the Min-IL based design and also has the ability to take into account the noise statistics. Different from previous section, we now assume that the noise w_i is Gaussian distributed with the covariance matrix Ψ_i,

$$\Psi_i = \begin{bmatrix} \psi_{ii} & \psi_{ij} \\ \psi_{ji} & \psi_{jj} \end{bmatrix}, \tag{4.18}$$

whose off-diagonal elements are non-zero for spatially correlated receiving ports [129]–[132].

To quantify the performance of the Max-SINR based IA design in the presence of spatially correlated noise, we simulate an interference-limited MIMO PLC network as it is illustrated in Fig. 4.1. For this simulation, we set the distance between

each Tx-Rx pair at 100 and 200 meters to simulate two different network scenarios, i.e., network scenarios 1 and 2, respectively. The shorter distance between the Tx-RX pairs may replicate a power line wiring in a house, while the larger distance replicates the same in a large office. In both network scenarios, PLC transmitters and receivers are terminated with load resistances chosen from the range between 10Ω to 50Ω. We consider the same frequency band from 2 to 30 MHz and calculate the channel frequency responses between different Tx-Rx pairs at a frequency separation of 24.4 kHz. This imitates the use of OFDM for broadband PLC systems as in the previous section. For the PLC MIMO transmission, we consider two configurations: transmission using the P-E/N-E and the P-N/N-E ports, respectively. The total transmit Power Spectral Density (PSD) over both ports is set to -55 dBm/Hz, which is a commonly applied spectral mask for broadband PLC systems [127].

The additive noise is taken from measured noise traces made available to us and reported in [131, 132]. Since the measurement probe applied a star-style receiver [131, 132] while we consider a delta-type receiver (see Fig. 4.2, cf. [127, Ch. 1]), we take the difference of time domain measured noise between ports P, E, and N, to obtain equivalent noise in delta-type receiver configuration. We denote such possible modes as P-N, P-E, and N-E. We then obtain the noise covariance matrix of the noise through the use of Welch's spectral estimation technique. We assume that each transmitter sends a single data stream, i.e., $d_i = 1$, $\forall i$, and that $P_i = P$, $\forall i$, according to the above-mentioned PSD limit.

We now investigate the rate performances for two IA designs: one that incorporates the noise correlation in (4.18), i.e., a proper design and one that assumes uncorrelated noise in the IA filter computation (4.16), thus rendering a mismatched design. The latter can be considered as a benchmark design, for the case that an esti-

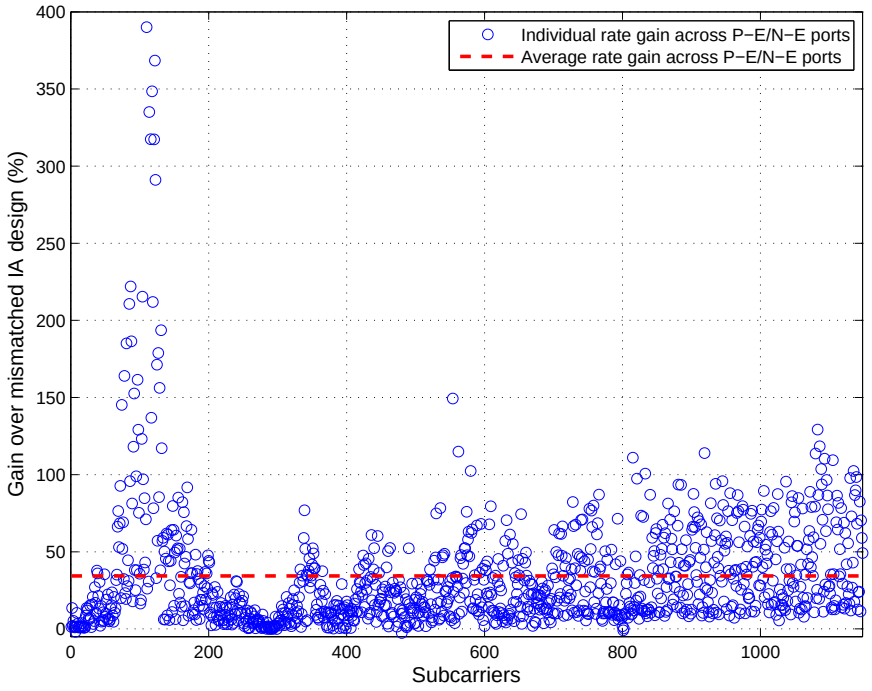

Figure 4.7: Subcarrier rate gain for a matched IA design with correlated noise over a mismatched IA design (i.e., that ignores spatial noise correlation during IA filter computation) for OL 3 of the dataset 1 across P-E/N-E ports in the network scenario 2.

mation of the noise correlation is not attempted. We first evaluate the performances of these designs for a noise dataset collected in Valencia, Spain (henceforth, denoted as dataset 1) at three different outlets (OLs) in the frequency range $2-30$ MHz [131,132]. While receiving ports may have roughly similar noise PSDs, the spatial correlations across these ports can be substantially different. For example, the average noise PSDs of the P-E and N-E receiving ports at OL 3 are about -67 dBm/Hz, while the spatial correlations across P-E/N-E and P-N/N-E receiving ports are 0.56 and 0.28, respectively.

Figs. 4.7 and 4.8 illustrate the rate gains of the matched (proper) IA design over the mismatched one as a function of the subcarrier index using the measured noise at

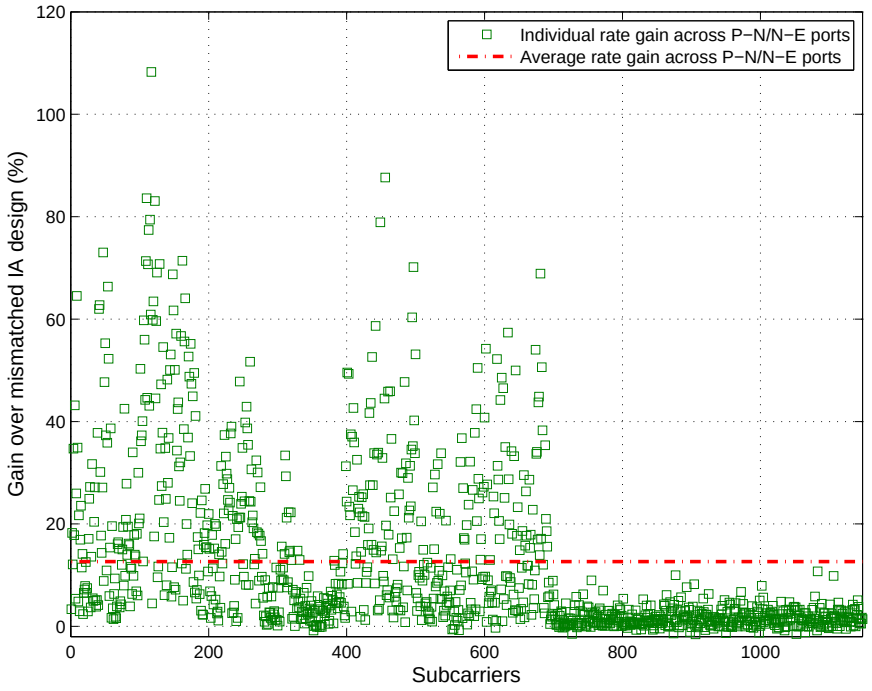

Figure 4.8: Subcarrier rate gain for a matched IA design with correlated noise over a mismatched IA design across P-N/N-E ports with the same network configuration as in Fig. 4.7.

OL 3 and network scenario 2 across P-E/N-E and P-N/N-E ports, respectively. We notice that considering actual noise correlation in the IA design leads to significant improvements in the rate performances. For example, the improvement for transmission over P-E/N-E ports, as shown in Fig. 4.7, can be as high as 390% for individual subcarriers and it is 34% on average. Comparing Figs. 4.7 and 4.8, we also observe that the (average) sum-rate gain is substantially larger for the port configuration with the large noise correlation. This is not only due to a more pronounced receiver mismatch but also due to fact that noise correlation generally improves the achievable rate. Finally, we note that for few subcarriers the rate gain is negative, i.e., the mismatched IA design assuming uncorrelated noise performs better than the matched design. We attribute this to the fact that the Max-SINR algorithm may be stuck in

Table 4.1: Rate gain of the matched over the mismatched IA design for different noise data sets and PLC MIMO configurations.

		Network Scenario 1		Network Scenario 2	
Noise Datasets	Outlets	Avg. Gain (P-E/N-E)	Avg. Gain (P-N/N-E)	Avg. Gain (P-E/N-E)	Avg. Gain (P-N/N-E)
1	1	16.92%	10.90%	28.17%	16.48%
	2	14.88%	5.23%	31.19%	8.96%
	3	16.80%	8.05%	34.38%	12.66%
2	1	6.64%	5.49%	19.17%	15.78%
	2	11.93%	6.22%	30.33%	15.75%

a local optimum as convergence to the global optimum point is not guaranteed due to the non-convex nature of the optimization problem [128].

Table 4.1 summarizes the rate gain results for noise data collected at the OLs for two different locations. Here, we also provide the results for a noise dataset from Paiporta, Spain (henceforth, denoted as dataset 2) at two different OLs. The noise in this location has a relatively lower average PSD than that of the dataset 1 (e.g., at OL 2, the average noise PSDs of P-E and N-E receiving ports are about -75 dBm/Hz). Hence, the signal to noise ratio (SNR) is relatively higher than for the dataset 1. While the average correlation coefficient across P-E/N-E ports at this OL is 0.53 and thus similar to that in OL 3 of the dataset 1, the average correlation coefficient across the P-N/N-E ports is significantly higher at 0.37.

We observe that notable rate gains are achieved for all test cases. Although, they are relatively lower for the higher SNR case, e.g., network scenario 1 vs. network scenario 2 due to short transmission distances for the former, and OL 3 of the dataset 1 vs. OL 1 of the dataset 2 due to lower noise PSD for the latter. Owing to the higher correlation across P-N/N-E ports for the dataset 2, however, the rate gains for these ports are comparable in the network scenario 2 despite having lower noise PSD. A similar explanation holds across P-E/N-E ports, e.g., for OL 2 of the dataset 2 when compared with OL 1 of the dataset 1 in the network scenario 2.

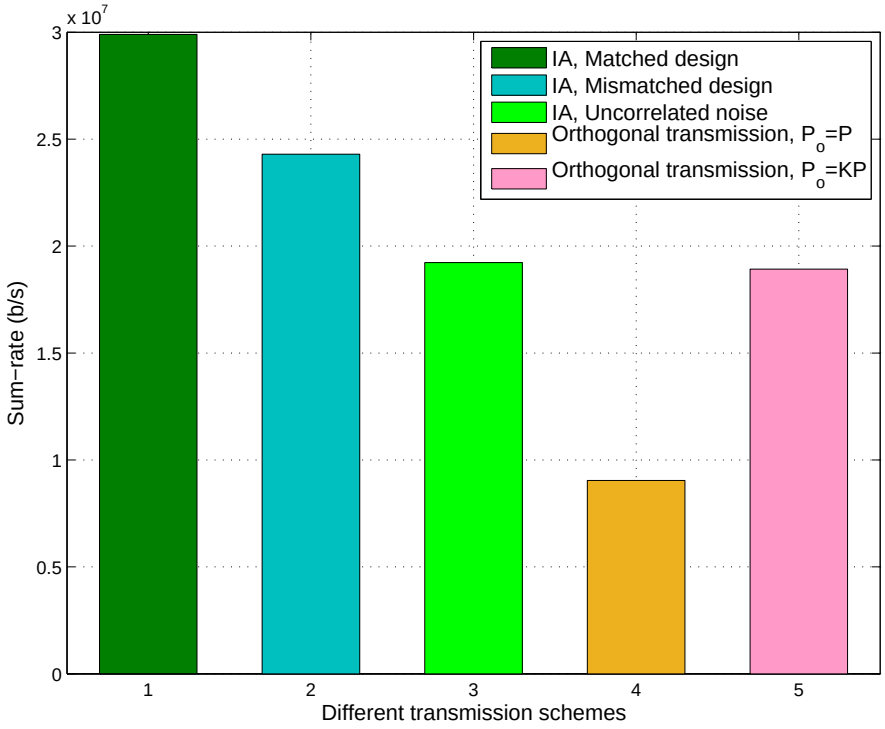

Figure 4.9: Comparison of sum-rate performances among different IA designs and orthogonal transmissions for OL 3 across P-E/N-E ports of the dataset 1 in the network scenario 2.

We finally compare the system sum-rate performances for the network scenario 2 considering correlated noise from the dataset 1 at OL 3 for (1) a matched and (2) a mismatched IA design, as well as (3) an IA design assuming uncorrelated noise with the same noise PSDs at the individual ports, i.e., the case that spatial noise correlation is absent. Fig. 4.9 shows the corresponding system sum-rate results. As a baseline, we also provide the results with conventional orthogonal transmission, such as time division multiple access. While in one instance, labelled as case (4), we assume a transmit power, $P_{\mathrm{o}} = P_i = P, \forall i$, for orthogonal transmission, we also simulate the case (5) where $P_{\mathrm{o}} = KP$, i.e., the system transmit power is identical to that in IA where all K users transmit simultaneously, as in previous section. Comparing

cases (1) and (3) we observe that a channel with noise correlation is supporting a notably increased rate and that the matched IA design is able to reap those rate gains. Furthermore, comparing cases (1) to both (4) and (5), we conclude that the Max-SINR based IA design outperforms conventional channel orthogonalization technique in terms of system sum-rate, even if the latter was allowed to transmit with a much higher per-user transmit power.

4.3 BIA for PLC X-Networks

In this section, we turn our focus on the PLC X-network, and specifically investigate the BIA for these networks. In the first part of this section, we show that the seemingly simple realization of the channel variation through impedance modulation, which has been inspired by the known fact that load changes affect PLC channel frequency responses, is not effective for the purpose of BIA for the PLC X-network. We then propose a transmission scheme through which one can realize the BIA for the PLC X-network.

4.3.1 Blind Interference Alignment

Fig. 4.10 shows a simplified version of Fig. 1.3 in Chapter 1 for the X-channel scenario, in which two senders transmit messages to two users [133]. The X-channel is a 4-node network where two nodes n_i, $i \in \{1, 2\}$, intend to communicate data u_{ij} to two different nodes n_j, $j \in \{3, 4\}$. It is shown in [133] that the maximum multiplexing gain of this channel can be achieved without CSI at the transmitters as follows.

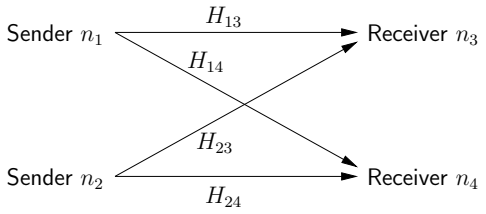

Figure 4.10: A simple transmission scenario of an X-channel setting (cf. Fig. 1.3).

Nodes n_1 and n_2 transmit

$$\boldsymbol{x}_1 = \begin{bmatrix} u_{13} + u_{14} \\ u_{13} + u_{14} \\ 0 \end{bmatrix} \tag{4.19}$$

and

$$\boldsymbol{x}_2 = \begin{bmatrix} u_{23} + u_{24} \\ 0 \\ u_{23} + u_{24} \end{bmatrix}, \tag{4.20}$$

respectively, in three successive time slots. We also assume that channel frequency-selectivity is dealt with through the use of multicarrier modulation, such as OFDM. We therefore do not indicate this notation in the following. Denoting the channel gains from node n_i to node n_j in time slot k by $H_{ij}(k)$, node n_j receives

$$\boldsymbol{y}_j = \begin{bmatrix} H_{1j}(1) \\ H_{1j}(2) \\ H_{1j}(3) \end{bmatrix} \circ \boldsymbol{x_1} + \begin{bmatrix} H_{2j}(1) \\ H_{2j}(2) \\ H_{2j}(3) \end{bmatrix} \circ \boldsymbol{x_2} + \boldsymbol{w}. \tag{4.21}$$

Defining $\boldsymbol{H}_j(k) = [H_{1j}(k)\, H_{2j}(k)]$, $\boldsymbol{u}_j = [u_{1j}\, u_{2j}]^T$ and $\mathbf{0} = [0\ 0]$, the received

signal at node n_3 can be rewritten as

$$\boldsymbol{y}_3 = \underbrace{\begin{bmatrix} \boldsymbol{H}_3(1) \\ \boldsymbol{H}_3(2) \\ \boldsymbol{0} \end{bmatrix}}_{\boldsymbol{M}_1} \boldsymbol{u}_3 + \underbrace{\begin{bmatrix} \boldsymbol{H}_3(1) \\ \boldsymbol{0} \\ \boldsymbol{H}_3(3) \end{bmatrix}}_{\boldsymbol{M}_2} \boldsymbol{u}_4 + \boldsymbol{w} \, . \tag{4.22}$$

For node n_3 to recover $\boldsymbol{u}_3$ from $\boldsymbol{y}_3$ without interference from the signal intended for node n_4, the trick of interference alignment is to ensure that

$$\begin{aligned} \boldsymbol{H}_3(1) &\neq \kappa \boldsymbol{H}_3(2) \\ \boldsymbol{H}_3(1) &= \boldsymbol{H}_3(3) \end{aligned} \tag{4.23}$$

for any constant κ. Then, matrices $\boldsymbol{M}_1$ and $\boldsymbol{M}_2$ in (4.22) have ranks 2 and 1, respectively, so that interference can completely be cancelled at node n_3 without cancelling the desired signal $\boldsymbol{u}_3$. The conditions in (4.23) can be accomplished blindly, i.e., without CSI at the transmitters. Rewriting Eq. (4.21) for node n_4, we find that the same interference cancellation can be achieved by enforcing $\boldsymbol{H}_4(1) \neq \kappa \boldsymbol{H}_4(3)$ and $\boldsymbol{H}_4(1) = \boldsymbol{H}_4(2)$. Since four data symbols are transmitted in three time slots, a multiplexing gain of $4/3$ is achieved, which is the maximum possible for this network [133].

4.3.2 Feasibility of the BIA Through Impedance Modulation

In this section, we make an attempt to achieve the BIA through impedance modulation, which would make it applicable to two-conductor e.g., SISO PLC networks. As presented in the previous section, the BIA scheme requires certain desired patterns

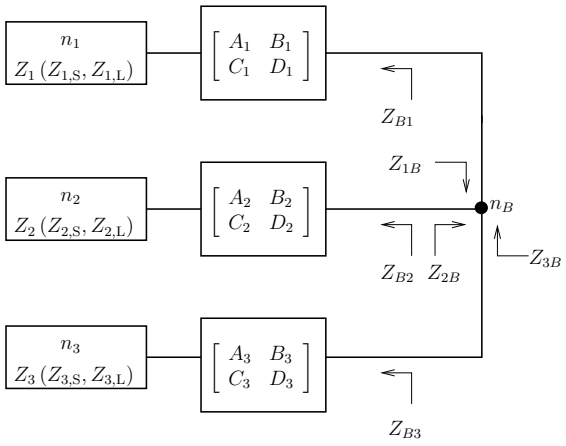

Figure 4.11: PLC network with three communication nodes.

of channel variations over time slots so as to facilitate the interference cancellation at a given receiver port. A seemingly possible way to achieve these channel variations is by modulating the input impedance of the PLC receiver modem. Accordingly, we start by considering a two-conductor PLC setup so that the network components between the three PLC devices, labeled as n_1, n_2, and n_3 in Fig. 4.11, and node n_B are represented through ABCD transmission line parameters. The corresponding ABCD-matrices $\begin{bmatrix} A_i & B_i \\ C_i & D_i \end{bmatrix}$ (see Appendix C.1 for details) relate the appropriately oriented voltages and currents at node n_i and node n_B with each other [139]. We note that they capture the aggregate effects of transmission lines, branches, loads etc. including those components that are physically behind nodes n_i from node n_B's perspective. For the following discussion it is irrelevant that the ABCD parameters are frequency-dependent, and we therefore do not indicate this dependency in our notations.

The benefit of the abstract model in Fig. 4.11 is that it fully captures the interdependencies of signals communicated between the PLC devices. First, as mentioned above, all signals have to travel through node n_B, which therefore is also referred

to as a keyhole [140]. Therefore, signals that are transmitted between, for example, node n_1 and nodes n_2 and n_3 have part of their transmission path in common, namely from node n_1 to node n_B in this case. Secondly, changes of transmission line parameters in one segment of the network, for example in the segment between nodes n_B and n_3, have an effect on the signal propagation in other segments of the network, for example in the segments between nodes n_1 and n_B and between n_2 and n_B. These features of multi-node transmission in PLC networks are different from wireless communication and have deep implications as we present below.

We now express the various relevant channel frequency responses and impedances for the network in Fig. 4.11. To this end, we denote the source impedance when PLC device i is transmitting as $Z_{i,\mathrm{S}}$, $Z_{i,\mathrm{L}}$ is the load impedance when PLC device i is receiving, and when we do not need to specify whether a PLC device is transmitting or receiving, we refer to its impedance as Z_i, $i = 1, 2, 3$. Furthermore, we denote the impedance seen into/from node n_B from/to node n_i as Z_{iB} and Z_{Bi}, respectively. Then, from (C.3) (derived in Appendix C.1) it follows that

$$Z_{Bi} = \frac{D_i Z_i + B_i}{C_i Z_i + A_i} \,, \tag{4.24}$$

and

$$Z_{iB} = Z_{Bj} \| Z_{Bk} = \frac{1}{1/Z_{Bj} + 1/Z_{Bk}} \,, \tag{4.25}$$

where $j \neq k,\ j \neq i,\ i, j, k \in \{1, 2, 3\}$. Using (C.1) and (C.3), the voltage channel frequency response from node n_i to n_B and from node n_B and to n_i can be expressed as

$$H_{iB} \triangleq \frac{V_B}{V_{i,\mathrm{S}}} = \frac{Z_{iB}}{(A_i + C_i Z_{i,\mathrm{S}}) Z_{iB} + B_i + D_i Z_{i,\mathrm{S}}} \tag{4.26}$$

and

$$H_{Bi} \triangleq \frac{V_{i,\mathrm{L}}}{V_B} = \frac{Z_{i,\mathrm{L}}}{D_i Z_{i,\mathrm{L}} + B_i} \ , \tag{4.27}$$

respectively, where $V_{i,\mathrm{S}}$ is the voltage of the source before its internal impedance $Z_{i,\mathrm{S}}$, $V_{i,\mathrm{L}}$ is the voltage at load impedance $Z_{i,\mathrm{L}}$, and V_B is the voltage at node n_B.

Using (4.26) and (4.27), the channel frequency responses between the three nodes n_1, n_2, and n_3 can be written as

$$H_{12} = H_{1B} H_{B2}, \tag{4.28}$$

$$H_{13} = H_{1B} H_{B3}, \tag{4.29}$$

$$H_{23} = H_{2B} H_{B3}. \tag{4.30}$$

Now, we utilize these insights from the network model in Fig. 4.11. We note that for the case of BIA in wireless communications [133], the requirement (4.23) has been met through staggered antenna switching at the receiving nodes. That is, a first receiver antenna configuration is chosen during slots $k = 1$ and $k = 3$, and a second antenna configuration is applied during $k = 2$. In the case of PLC networks, a receiver modem connected to two conductors can change its input impedance. Since the frequency response to a device is dependent on this impedance, see e.g. expression (4.27), the BIA scheme as described above seems to be directly applicable, without the need for an additional infrastructure, i.e., extra receiving ports.

Let us consider nodes n_1 and n_2 in Fig. 4.11 as the two transmitters and node n_3 as one of the receivers. Then, we can write the channel vector from n_1 and n_2 to n_3 as

$$\boldsymbol{H}_3(k) = [H_{13}(k) \ \ H_{23}(k)] \tag{4.31}$$

$$= [H_{1B}(k)H_{B3}(k) \;\; H_{2B}(k)H_{B3}(k)] \,, \tag{4.32}$$

where time variation with k is accomplished through modifying $Z_{3,\mathrm{L}}$ at node n_3. We note that $Z_{3,\mathrm{L}}$ directly affects $H_{B3}(k)$ via (4.27), but also $H_{1B}(k)$ and $H_{2B}(k)$ through the dependency chain:

$$Z_{3,\mathrm{L}} \overset{\text{Eq.(4.24)}}{\longrightarrow} Z_{B3} \overset{\text{Eq.(4.25)}}{\longrightarrow} (Z_{1B}, Z_{2B}) \overset{\text{Eq.(4.26)}}{\longrightarrow} (H_{1B}(k), H_{2B}(k)) \,.$$

On the other hand, we can rearrange (4.31) into

$$\boldsymbol{H}_3(k) = H_{23}(k)[H_{13}(k)/H_{23}(k) \;\; 1] \,. \tag{4.33}$$

In Appendix C.2, we show that the *ratio* $H_{13}(k)/H_{23}(k)$ is independent of Z_{B3}. Hence, $H_{13}(k)/H_{23}(k) = H_{13}/H_{23} \triangleq c$ independent of k, and thus (see (4.22))

$$\boldsymbol{M}_1 = \begin{bmatrix} \boldsymbol{H}_3(1) \\ \boldsymbol{H}_3(2) \\ \mathbf{0} \end{bmatrix} \tag{4.34}$$

$$= \begin{bmatrix} c \cdot H_{23}(1) & H_{23}(1) \\ c \cdot H_{23}(2) & H_{23}(2) \\ 0 & 0 \end{bmatrix} \,. \tag{4.35}$$

The rank of matrix $\boldsymbol{M}_1$ is one, regardless of how $H_{23}(k)$ is changed due to reconfiguration at node n_3. Hence, spatial multiplexing is not achieved.

We thus have shown that the BIA through receiver reconfiguration, a seemingly attractive scheme for PLC networks, is not possible in principle due to the properties of the transmission-line signal propagation.

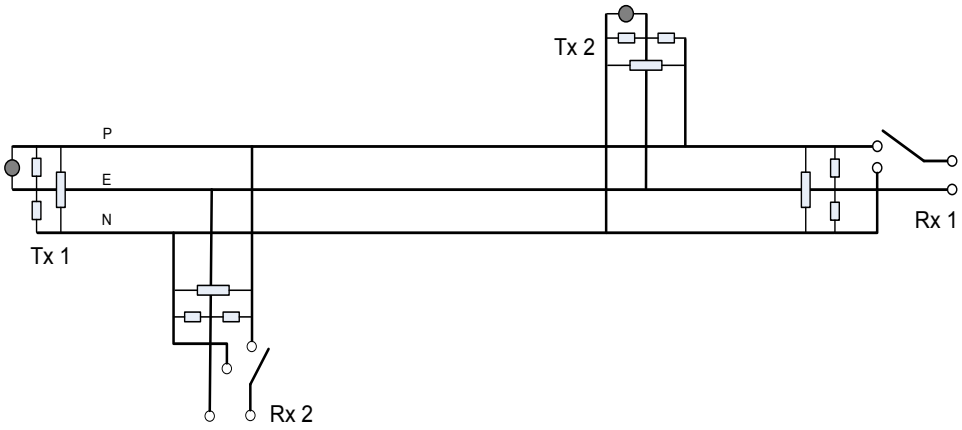

Figure 4.12: An illustration of the transmission scheme for the achievability of blind IA for the PLC X-network using multiple receiving ports.

4.3.3 Achievability of the BIA for PLC X-Networks

It is apparent from the above analysis that the ability to control the channel response to a desired receiving port while keeping channel responses to other receiver ports unchanged at the same time is a daunting task. In this section, we show that this can be achieved via a concept similar to antenna-staggering in the case of wireless communications. However, this requires multiple receiving ports, i.e., a multi-conductor structure as in MIMO or Single-Input Multi-Output (SIMO) PLC networks.

To prove this concept, we focus on a MIMO PLC X-network with switches at the receiving end to alternate between the receiving ports, as it is illustrated in Fig. 4.12. The switching between the receiver ports essentially serves the same purpose of antenna switching in wireless communications [133]. Since switching at a given receiving port has negligible impact on the channel response to the other receiving port due to the attached impedance in parallel as shown in Fig. 4.12, it can produce desired channel patterns for the realization of the blind IA.

In order to simulate the blind IA, we consider a MIMO PLC X-network configuration with two transmitters and two receivers, as it is illustrated in Fig. 4.12. Note

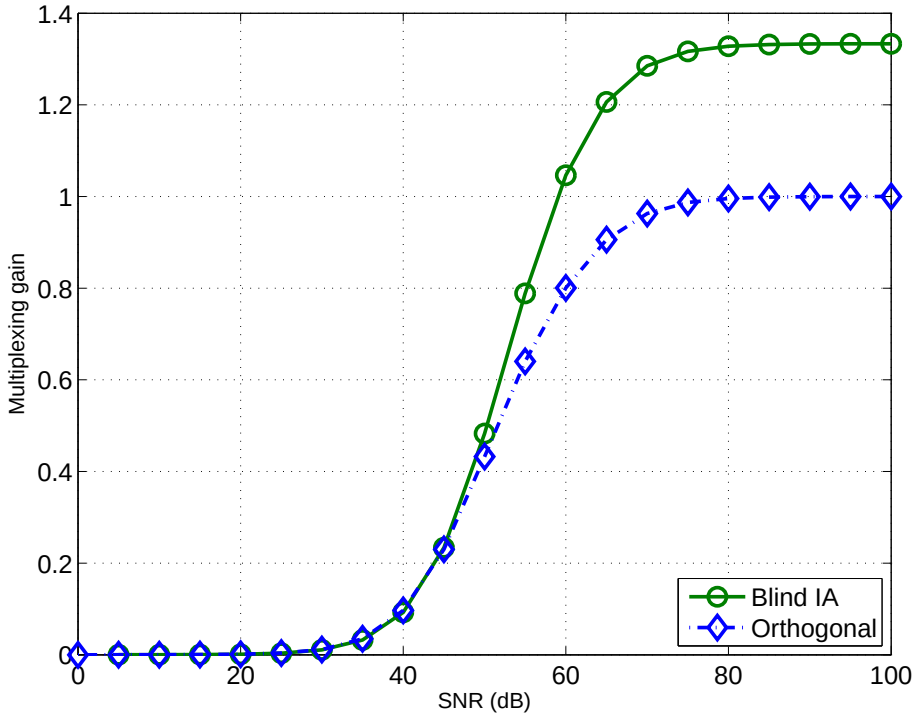

Figure 4.13: A comparison of multiplexing gains for the proposed BIA and an orthogonal transmission.

that we are not specifically restricted to a MIMO configuration, since a SIMO configuration also offers multiple receiving ports. We assume a distance of 20 m between the nodes, i.e., between Tx1 and Rx2, Rx2 and Tx2, Tx2 to Rx1. The positions of transmitters and receivers are not limited to this configuration as one can obtain a different configuration by placing the transmitters and the receivers at different locations. The PLC transmitters and receivers are terminated with load resistances chosen from the range between 25 Ω to 100 Ω. We choose the frequency band from 2 to 30 MHz with a frequency separation of 24.4 kHz for the OFDM system. As in the previous cases, the computation of channel frequency response is based on MTL theory [137], via a simulator reported in [138]. We further assume that both transmitters are provided with same power, i.e., $P_1 = P_2$ and noise is kept fixed with

variance equal to one. This permits the use of transmission power as the transmitter side SNR. We note that each transmitter sends a single data stream intended for each of the receivers in the PLC X-network.

To show the effectiveness of the proposed technique, we compute the multiplexing gain, which can be obtained by calculating the slope of total sum-rate curve [32], and plot with respect to the transmitter side SNR. The results in Fig. 4.13 suggest that multiplexing gains of 4/3 and 1 can be achieved with BIA and an orthogonal transmissions, respectively. Since an orthogonal transmission uses channel orthogonalization, the maximum multiplexing gain for this scheme is 1. We also note that for the considered PLC X-network configuration in Fig. 4.12, the maximum multiplexing gain that is achievable is 4/3, as we show in Section 4.3.1 [133]. This confirms the achievability of the BIA with the proposed multiconductor transmission scheme.

4.4 Conclusions

In this chapter, we have addressed the IA design for PLC networks. As this is the first study considering IA for PLC networks, we have confirmed the feasibility of IA by investigating different PLC network setups. It was found that the feasibility conditions for IA that exist in the context of MIMO wireless interference networks also hold for MIMO PLC interference network. For a 3-user 2×2 MIMO PLC network, our results show that at high SNR, the Max-SINR based IA provides a significant performance gain of around 30% over the orthogonal transmission techniques. Furthermore, we compared the sum-rate performance of a MIMO PLC interference network with that of a MIMO wireless interference network having equivalent link qualities. It was observed that IA in the context of MIMO PLC provides lower sum-rate than its wireless counterpart. It can be attributed to the fact that MIMO PLC channel exhibits rela-

tively higher spatial correlation than the MIMO wireless channel, which degrades the sum-rate. Moreover, we have evaluated the system sum-rate in the presence of the spatially correlated measured MIMO PLC noise. In the process, we have learnt that the spatial correlation actually helps to improve the system sum-rate, which justifies its inclusion in the system design. Finally, we have considered the BIA for PLC X-networks. It is shown that even though the load modulation changes the channel responses over time slots, it is ineffective for the purpose of the blind IA in PLC X-network. We then propose a multiconductor network configuration with multiple receiving ports, essentially to serve the same purpose of antenna switching in wireless communications. The transmission scheme is shown to achieve the maximum multiplexing gain with BIA for the PLC X-network.

Chapter 5

Summary and Directions for Future Works

5.1 Summary of Contributions

The research works presented in this thesis are focused on providing solutions for interference-limited communication systems, such as FD, D2D, and power line communications. In the specific context of FD communications, we proposed robust, power-efficient, and fair transceiver designs for multi-cell MIMO FD communication systems. The concept of fair transceiver design is also studied in the context of underlay D2D networks. As a solution to mitigate interference in PLC networks, we investigated different IA techniques in the context of PLC interference and X-networks.

In Chapter 2, we proposed a power-efficient design for multi-cell MIMO FD communications. To this end, the original non-convex and NP-hard problem is posed as a DCP and efficiently solved via SCA. In addition to assuming the availability of perfect CSI, we considered both stochastic and bounded uncertainty in our designs. The results quantified potential power savings, with respect to an HD setup and a non-robust design, under a wide range of design parameters.

Another design objective that has been investigated in Chapter 3 is the fairness problem in both FD and D2D communications. The sum-rate maximization approach

only aims at optimizing the total network throughput, leaving users at the cell-edge or the ones experiencing poor channel conditions unserved. Therefore, we proposed a transceiver design that guarantees performance fairness among the users. In addition to perfect CSI design, we considered imperfect CSI design by way of norm-bounded uncertainty to provide worst-case design formulation. The non-convex precoder optimization problem is solved via a low-complexity iterative algorithm. The results confirm a considerable improvement in fairness performance among the FD and D2D users.

In Chapter 4, we studied IA techniques for rate improvement in PLC networks. Recognizing that multiple simultaneous connections in PLC lead to an interference-limited communication as in the wireless networks, we studied the applicability of IA in the context of both PLC interference and X-networks. Initially, we focused on studying the feasibility and evaluated the system sum-rate performance with the IA transmission assuming AWGN for MIMO PLC networks. As an extension of this work, we utilized measured noise from real MIMO PLC networks to evaluate the system performance. In particular, we investigated the impact of spatially correlated noise with Max-SINR algorithm which takes into account noise statistics. Our results quantified improved sum-rate performance with spatially correlated noise, suggesting that the noise correlation must be taken into account in the system design. Finally, we investigated the feasibility and achievability of the BIA for PLC X-networks. In particular, we explored network scenarios where the BIA is not achievable through the impedance modulation. Therefore, we proposed a transmission scheme that facilitates the implementation of the BIA for the PLC X-network. The results confirm that the optimal multiplexing gain can be obtained with the proposed transmission scheme for the PLC X-network.

5.2 Directions for Future Works

The complicated interference scenarios in FD, D2D and power line communications present numerous challenging research problems. Some interesting avenues for future research are summarized below.

5.2.1 Decentralized Algorithms for FD Communication Systems

The algorithms presented in Chapter 2 for the sum-power minimization in multi-cell MIMO FD communications rely on processing at the Remote Centralized Processor (RCP) unit. The RCP facilitates the computation and distribution of the precoders and the receiver filters among the BSs and users. Therefore, the implementation of the algorithm is limited by the backhaul capacity and computational power of the RCP. Furthermore, it necessitates the symbol level synchronization due to joint processing of the transmitted signals. In an effort to mitigate these implementation issues, an important future direction for this work would be investigating decentralized algorithms. A decentralized algorithm would allow the implementation with limited backhaul capacity, less computation power, and flexible system requirements (e.g., strict carrier phase synchronization would no longer be needed at the BSs) [141].

The decentralized algorithm can be enabled by controlling the inter-cell interference, while designing the precoders and receiver filters with minimal cooperation at the BSs and the mobile users. Since the design problems for precoders are inherently coupled among the BSs, one way to decouple the precoder design problem is to exploit primal decomposition method so that each BS can independently design the precoders for its own users [71].

Although the beamformer design with perfect CSI in Chapter 3 can be imple-

mented in a distributed fashion, the robust fairness design relies on the centralized processing. Therefore, a decentralized algorithm under constrained feedback capacity is also an interesting research problem for this design objective.

5.2.2 Robust Multi-cell D2D Communications

In Section 3.3 of the Chapter 3, we assumed that the inter-cell interference that results from transmissions of users in the neighboring macrocells is mitigated through macrocell coordination, and is therefore neglected in our analysis. As a next step, one can consider such interference from neighboring macrocells as a colored noise in the received signal, as shown on the right side of Fig. 5.1. This will allow us to analyze the impact of such interference on the performance of D2D users. Furthermore, in our previous analysis we assumed that the interference from cellular users to the D2D receivers are negligible. Although this is a valid assumption when the D2D users are located at a distance from the cellular users so that the interference can be neglected, a more inclusive communication scenario can be considered by assuming that there are cellular users nearby that interfere the D2D reception in the uplink transmission.

Another related future work for this topic would be considering the total interference power constraint from a given D2D group, rather than the individual interference power constraint from each D2D user. This assumption is less restrictive on the transmission power of D2D users, and hence it may improve the overall performance of D2D communications.

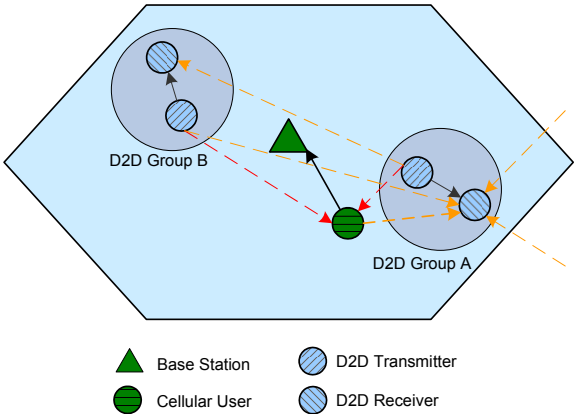

Figure 5.1: An illustration of an underlay D2D communication in a cellular network with resulting interference from cellular users and neighboring macrocells. Solid and dashed lines indicate desired signals and interference, respectively.

5.2.3 Feedback Reduction for IA in PLC Networks

One important characteristics of the PLC channel is that it is often correlated in the time domain. As we discussed in Chapter 4, the implementation of the IA technique requires the availability of the CSI at the transmitter. In practice, the reduction of the CSI feedback is a key design aspect for practical implementation of IA algorithms. Therefore, a relevant future research direction for this work is to exploit the time correlation of the PLC channel in order to reduce the amount of the CSI feedback. There are a few studies in the context of wireless networks, which may be readily applicable in the context of PLC networks as well [142, 143].

5.3 Concluding Remarks

The performance benefits and implementation challenges of the IA techniques and the FD communications have rekindled the interest in developing novel physical layer solutions. Along these research directions, the contributions from this thesis provide a stepping stone to mitigate different instances of interference so as to improve the

system performances in both wireless and wireline communication systems. Together with practical design aspects, such as CSI uncertainty, we have explored power-efficient and fair resource allocation techniques for the system design at the physical layer of the interference-limited communication systems. These are timely contributions to advance the next generation communication technologies in order to support a variety of communication needs and services.

Bibliography

[1] S. Haykin and M. Moher, *Communication Systems*, 5th ed. UK: John Wiley & Sons Ltd, Mar. 2009.

[2] R. H. Etkin, D. N. C. Tse, and H. Wang, "Gaussian interference channel capacity to within one bit," *IEEE Trans. Inf. Theory*, vol. 54, no. 12, pp. 5534–5562, Dec. 2008.

[3] M. Duarte and A. Sabharwal, "Full-duplex wireless communications using off-the-shelf radios: Feasibility and first results," in *Proc. Asilomar Conf. Signals, Systems, Comput.*, pp. 1558–1562, Nov. 2010.

[4] J. I. Choi, M. Jain, K. Srinivasan, P. Levis, and S. Katti, "Achieving single channel, full duplex wireless communication," in *Proc. ACM Int. Conf. Mobile Comput. Net. (MOBICOM)*, pp. 1–12, Sept. 2010.

[5] A. Sabharwal, P. Schniter, D. Guo, D. W. Bliss, S. Rangarajan, and R. Wichman, "In-band full-duplex wireless: Challenges and opportunities," *IEEE J. Sel. Areas Commun.*, vol. 32, no. 9, pp. 1637–1652, Sept. 2014.

[6] Z. Zhang, X. Chai, K. Long, A. V. Vasilakos, and L. Hanzo, "Full duplex techniques for 5G networks: Self-interference cancellation, protocol design, and relay selection," *IEEE Commun. Mag.*, vol. 53, no. 5, pp. 128–137, May 2015.

[7] W. Choi, H. Lim, and A. Sabharwal, "Power-controlled medium access control protocol for full-duplex WiFi networks," *IEEE Trans. Wireless Commun.*, vol. 14, no. 7, pp. 3601–3613, July 2015.

[8] S. Kam, D. Kim, H. Lee, and D. Hong, "Bidirectional full-duplex systems in a multispectrum environment," *IEEE Trans. Veh. Technol.*, vol. 64, no. 8, pp. 3812–3817, Aug. 2015.

[9] A. Asadi, Q. Wang, and V. Mancuso, "A survey on device-to-device communication in cellular networks," *IEEE Commun. Surveys Tut.*, vol. 16, no. 4, 2014.

[10] S. Mumtaz and J. Rodriguez, Eds. *Smart Device to Smart Device Communication*, Germany: Springer, 2014.

[11] X. Lin, J. Andrews, and A. Ghosh, "Spectrum sharing for device-to-device communication in cellular networks," *IEEE Trans. Wireless Commun.*, vol. 13, no. 12, pp. 6727–6740, Dec. 2014.

[12] M. Noura and R. Nordin, "A survey on interference management for device-to-device (D2D) communication and its challenges in 5G networks," *J. Net. Comput. Applications*, vol. 71, pp. 130–150, Aug. 2016.

[13] L. Lampe, A. Tonello, and T. Swart, Eds., *Power Line Communications: Principles, Standards and Applications from Multimedia to Smart Grid*, 2nd ed. UK: John Wiley & Sons Ltd, Jun. 2016.

[14] C. Cano, A. Pittolo, D. Malone, L. Lampe, A. M. Tonello, and A. G. Dabak, "State of the art in power line communications: From the applications to the medium," *IEEE J. Sel. Areas Commun.*, vol. 34, no. 7, pp. 1935–1952, Jul. 2016.

[15] V. R. Cadambe and S. A. Jafar, "Degrees of freedom of wireless X networks," in *Proc. IEEE Int. Symp. Inf. Theory (ISIT)*, pp. 1268–1272, July 2008.

[16] M. A. Maddah-Ali, A. S. Motahari, and A. K. Khandani, "Communication over X channel: Signaling and multiplexing gain," Uni. Waterloo, Waterloo, ON, Canada, Tech. Rep. UW-ECE-2006-12, July 2006.

[17] M. A. Maddah-Ali, A. S. Motahari, and A. K. Khandani, "Communication over MIMO X channels: Interference alignment, decomposition, and performance analysis," *IEEE Trans. Inf. Theory*, vol. 54, no. 8, pp. 3457–3470, Aug. 2008.

[18] V. R. Cadambe and S. A. Jafar, "Interference alignment and degrees of freedom of the K-user interference channel," *IEEE Trans. Inf. Theory*, vol. 54, no. 8, pp. 971–975 , Aug. 2008.

[19] Y. Hua, Y. Ma, A. Gholian, Y. Li, A. C. Cirik, and P. Liang, "Radio self-interference cancellation by transmit beamforming, all-analog cancellation and blind digital tuning," *Elsevier Signal Process.*, vol. 108, pp. 322–340, Sept. 2014.

[20] D. J. van den Broek, E. A. M. Klumperink, and B. Nauta, "A self-interference cancelling front-end for in-band full-duplex wireless and its phase noise performance," in *Proc. IEEE Radio Freq. Integrated Circuits Symp. (RFIC)*, pp. 75–78, Nov. 2015.

[21] F. H. Gregorio, G. J. Gonzalez, J. Cousseau, T. Riihonen, and R. Wichman, "RF front-end implementation challenges of in-band full-duplex relay transceivers," in *Proc. European Wireless (EW)* pp. 1–6, June 2016.

[22] Y. Liu, X. Quan, W. Pan, and Y. Tang, "Digitally assisted analog interference cancellation for in-band full-duplex radios," *IEEE Commun. Lett.* , vol. 21, no. 5, pp. 1079–1082, Jan. 2017.

[23] M. Duarte, C. Dick, and A. Sabharwal, "Experiment-driven characterization of full-duplex wireless systems," *IEEE Trans. Wireless Commun.*, vol. 11, no. 12, pp. 4296–4307, Dec. 2012.

[24] E. Everett, A. Sahai, and A. Sabharwal, "Passive self-interference suppression for full-duplex infrastructure nodes," *IEEE Trans. Wireless Commun.*, vol. 13, no. 2, pp. 680–694, Feb. 2014.

[25] D. Bharadia and S. Katti, "Full duplex MIMO radios," in *Proc. 11th USENIX Conf. on Networked Systems Design and Implementation (NSDI)*, pp. 359–372, Apr. 2014.

[26] B. P. Day, A. R. Margetts, D. W. Bliss, and P. Schniter, "Full-duplex bidirectional MIMO: Achievable rates under limited dynamic range," *IEEE Trans. Signal Process.*, vol. 60, no. 7, pp. 3702–3713, July 2012.

[27] D. Kim, H. Lee, and D. Hong, "A survey of in-band full-duplex transmission: From the perspective of PHY and MAC layers," *IEEE Commun. Surveys Tut.*, vol. 17, no. 4, pp. 2017-2046, 2015.

[28] H. Sato, "The capacity of the Gaussian channel under strong interference," *IEEE Trans. Inf. Theory*, vol. 27, no. 6, pp. 786–788 , Nov. 1981.

[29] S. Annapureddy and V. V. Veeravalli, "Gaussian interference networks: Sum capacity in the low interference regime," in *Proc. Int. Symp. Inf. Theory (ISIT)*, pp. 255–259, 2008.

[30] G. Miao, J. Zander, K. W. Sung, and B. Slimane, *Fundamentals of Mobile Data Networks*, UK: Cambridge University Press, 2016.

[31] P. A. Brown, *Powerline communications network employing TDMA, FDMA and/or CDMA*. US Patent 6,144,292, Nov. 2000.

[32] S. A. Jafar, *Interference Alignment–A New Look at Signal Dimensions in a Communication Network*, Netherlands: Now Publishers, 2011.

[33] R. Tresch and M. Guillaud, "Cellular interference alignment with imperfect channel knowledge," in *Proc. IEEE Int. Conf. Commun. (ICC)*, pp. 1–5, June 2009.

[34] X. Xu, X. Chen, M. Zhao, S. Zhou, C.-Y. Chi, and J. Wang, "Power-efficient distributed beamforming for full-duplex MIMO relaying networks," *IEEE Trans. Veh. Technol.*, vol. 66, no. 2, pp. 1087–1103, Feb. 2017.

[35] A. Pascual-Iserte, D. P. Palomar, A. I. Perez-Neira, and M. A. Lagunas, "A robust maximin approach for MIMO communications with imperfect channel state information based on convex optimization," *IEEE Trans. Signal Process.*, vol. 54, no. 1, pp. 346–359, Jan. 2006.

[36] C. Han et al., "Green radio: Radio techniques to enable energy-efficient wireless networks," *IEEE Commun. Mag.*, vol. 49, no. 6, pp. 46–54, June 2011.

[37] J. Zander, "Performance of optimum transmitter power control in cellular radio systems," *IEEE Trans. Veh. Technol.*, vol. 41, no. 1, pp. 57–62, Feb. 1992.

[38] G. Miao, N. Himayat, G. Y. Li, and S. Talwar, "Distributed interference-aware energy-efficient power optimization," *IEEE Trans. Wireless Commun.*, vol. 10, no. 4, pp. 1323–1333, Apr. 2011.

[39] E. Ahmed, A. M. Eltawali, and A. Sabharwal, "Self-interference cancellation with phase noise induced ICI suppression for full-duplex system, in *Proc. IEEE Global Telecommun. Conf. (GLOBECOM)*, pp. 3384–3388, Dec. 2013.

[40] C. Lin I, C. Rowell, S. Han, Z. Xu, G. Li, and Z. Pan, "Toward green and soft: a 5G perspective," *IEEE Commun. Mag.*, vol. 52, no. 2, pp. 66–73, Feb. 2014.

[41] V. W. S. Wong, R. Schober, D. W. K. Ng, and L.-C. Wang, Eds., *Key Technologies for 5G Wireless Systems*, UK: Cambridge University Press, Mar. 2017.

[42] Z.-Q. Luo, W.-K. Ma, A. M.-C. So, Y. Ye, and S. Zhang, "Semidefinite relaxation of quadratic optimization problems," *IEEE Signal Process. Mag.*, vol. 27, no. 3, pp. 20–34, May 2010.

[43] M. Batros and T. N. Davidson, "Convex conic formulations of robust downlink precoder designs with quality of service constraints," *IEEE J. Sel. Areas Signal Process.*, vol. 1, no. 4, pp. 714–724, Dec. 2007.

[44] N. Vucic, H. Boche, and S. Shi, "Robust transceiver optimization in downlink multiuser MIMO systems with channel uncertainty," in *Proc. IEEE Int. Conf. Commun. (ICC)*, pp. 3516–3520, May 2008.

[45] E. Chiu, V. K. N. Lau, H. Huang, T. Wu, and S. Liu, "Robust transceiver design for K-pairs quasi-static MIMO interference channels via semi-definite relaxation," *IEEE Trans. Wireless Commun.*, vol. 9, no. 12, pp. 2094–2098, Dec. 2010.

[46] Md. J. Rahman, A. C. Cirik, and L. Lampe, "Power-efficient transceiver design for full-duplex MIMO multi-cell systems with CSI uncertainty," *IEEE Access*, vol. 5, pp. 22689-22703, 2017.

[47] A. C. Cirik, Md. J. Rahman, and L. Lampe, "Robust fairness transceiver design for a full-duplex MIMO multi-cell system," *in press, IEEE Trans. Commun.*, Nov. 2017.

[48] Md. J. Rahman and L. Lampe, "Robust transceiver optimization for underlay device-to-device communications," in *Proc. IEEE Int. Conf. Commun. (ICC)*, pp. 7695–7700, June 2015.

[49] Md. J. Rahman and L. Lampe, "Rate improvement in MIMO power line communications through interference alignment," *Submitted*, 2017.

[50] Md. J. Rahman and L. Lampe, "Interference alignment in power line communications," *(in press) Invited contribution in Encyclopedia of Wireless Networks (Section: Interference Characterization and Mitigation)*, S. Shen, X. Lin, and K. Zhang, Eds. Germany: Springer, 2017, 8 pages.

[51] Md. J. Rahman and L. Lampe, "Interference alignment for MIMO power line communications," in *Proc. IEEE Intl. Symp. Power Line Commun. and Its Applications (ISPLC)*, pp. 71–76, Mar. 2015.

[52] L. Lampe, Md. J. Rahman, and H. E. Saffar, "Characteristics of power line networks: Diversity and interference alignment," in *Proc. IEEE Int. Symp. on Power Line Commun. and Its Applications (ISPLC)*, pp. 1–6, 2017.

[53] J. Zhang, O. Taghizadeh, and M. Haardt, "Transmit strategies for full-duplex point-to-point systems with residual self-interference," in *Proc. Int. ITG Workshop on Smart Antennas (WSA 2013)*, pp. 1–8, Mar. 2013.

[54] T. M. Kim, H. J. Yang, and A. Paulraj, "Distributed sum-rate optimization for full-duplex MIMO system under limited dynamic range," *IEEE Signal Process. Lett.*, vol. 20, no. 6, pp. 555–558, June 2013.

[55] S. Huberman and T. Le-Ngoc, "Full-duplex MIMO precoding for sum-rate maximization with sequential convex programming," *IEEE Trans. Veh. Technol.*, vol. 64, no. 11, pp. 5103–5112, Nov. 2015.

[56] A. C. Cirik, R. Wang, Y. Hua, and M. Latva-aho, "Weighted sum-rate maximization for full-duplex MIMO interference channels," *IEEE Trans. Commun.*, vol. 63, no. 3, pp. 801–815, Mar. 2015.

[57] A. C. Cirik, R. Wang, Y. Rong, and Y. Hua,"MSE-based transceiver designs for full-duplex MIMO cognitive radios," *IEEE Trans. Commun.*, vol. 63, no. 6, pp. 2056–2070, June 2015.

[58] A. Cirik, O. Taghizadeh, A. Liu, L. Lampe, and R. Mathar, "Sum-power minimization under rate constraints in full-duplex MIMO interference-channels," *21st Int. ITG Workshop on Smart Antennas (WSA)*, pp. 151–155, Mar. 2017.

[59] O. Taghizadeh, A. Cirik, R. Mathar, and L. Lampe, "Sum power minimization for TDD-enabled full-duplex bi-directional MIMO systems under channel uncertainty," *European Wireless*, pp. 412–417, May 2017.

[60] D. Nguyen, L.-N. Tran, P. Pirinen, and M. Latva-aho, "Precoding for full duplex multiuser MIMO systems: Spectral and energy efficiency maximization," *IEEE Trans. Signal Process.*, vol. 61, no. 16, pp. 4038–4050, Aug. 2013.

[61] D. Nguyen, L. Tran, P. Pirinen, and M. Latva-aho, "On the spectral efficiency of full-duplex small cell wireless systems," *IEEE Trans. Wireless Commun.*, vol. 13, no. 9, pp. 4896–4910, Sept. 2014.

[62] S. Li, R. Murch, and V. Lau, "Linear transceiver design for full-duplex multiuser MIMO system," *IEEE Int. Conf. Commun. (ICC)*, pp. 4921–4926, June 2014.

[63] J. M. B. da Silva Jr, G. Fador, and C. Fischione, "On the spectral efficiency and fairness in full-duplex cellular networks," *IEEE Int. Conf. Commun. (ICC)*, pp. 1–6, May 2017.

[64] A. C. Cirik, O. Taghizadeh, L. Lampe, R. Mathar, and Y. Hua, "Linear transceiver design for full-duplex multi-cell MIMO systems," *IEEE Access*, vol. 4, pp. 4678–4689, Aug. 2016.

[65] P. Aquilina, A. Cirik, and T. Ratnarajah, "Weighted sum rate maximization in full-duplex multi-user multi-cell MIMO networks," *IEEE Trans. Commun.*, vol. 64, no. 4, pp. 1590–1608, Jan. 2017.

[66] H. H. M. Tam, H. D. Tuan, and D. T. Ngo, "Successive convex quadratic programming for quality-of-service management in full-duplex MU-MIMO multicell networks," *IEEE Trans. Commun.*, vol. 64, no. 6, pp. 2340–2353, June 2016.

[67] S. Goyal, P. Liu, and S. S. Panwar, "User selection and power allocation in full duplex multi-cell networks," *IEEE Trans. Veh. Technol.*, vol. 66, no. 3, pp. 2408–2422, Mar. 2017.

[68] S. Boyd, L. Xiao, A. Mutapic, and J. Mattingley, "Sequential convex programming," Notes for EE364b, Stanford University, Jan. 2007. Available online: http://ww.stanford.edu/class/ee364b/.

[69] N. Vucic, S. Shi, and M. Schubert, "DC programming approach for resource allocation in wireless networks," in *Proc. Int. Symp. Modeling and Optimization in Mobile, Ad Hoc, and Wireless Net. (WiOpt)*, pp. 380–386, July 2010.

[70] J. Kaleva, A. Tölli, and M. Juntti, "Weighted sum rate maximization for interfering broadcast channel via successive convex approximation," in *Proc. IEEE Global Telecommun. Conf. (GLOBECOM)*, pp. 3838–3843, Dec. 2012.

[71] H. Pennanen, A. Tölli, J. Kaleva, P. Komulainen, and M. Latva-aho, "Decentralized linear transceiver design and signaling strategies for sum power minimization in multi-cell MIMO system," *IEEE Trans. Signal Process.*, vol. 64, no. 7, pp. 1729–1743, Apr. 2016.

[72] A. C. Cirik, M. C. Filippou, and T. Ratnarajah, "Transceiver design in full-duplex MIMO cognitive radios under channel uncertainties," *IEEE Trans. Cognitive Commun. Net.*, vol. 2, no. 1, pp. 1–14, March 2016.

[73] S. Xiao, X. Zhou, G. Y. Li, and W. Guo, "Robust resource allocation in full-duplex cognitive radio networks," *IEEE Global Commun. Conf. (GLOBECOM)*, pp. 1–7, Dec. 2016.

[74] R. Feng, Q. Li, Q. Zhang, and J. Qin, "Robust secure beamforming in MISO full-duplex two-way secure communications," *IEEE Trans. Vehicular. Tech.*, vol. 65, no. 1, pp. 408–414, Jan. 2016.

[75] Y. Sun, D. W. K. Ng, J. Zhu, and R. Schober, "Multi-objective optimization for robust power efficient and secure full-duplex wireless communication systems," *IEEE Trans. Wireless Commun.*, vol. 15, no. 8, pp. 5511–5526, Aug. 2016.

[76] M. R. Abedi, N. Mokari, H. Saeedi, and H. Yanikomeroglu, "Robust resource allocation to enhance physical layer security in systems with full-duplex receivers: Active adversary," *IEEE Trans. Wireless Commun.*, vol. 16, no. 2, pp. 885–899, Feb. 2017.

[77] A. C. Cirik, Y. Rong, and Y. Hua, "Achievable rates of full-duplex MIMO radios in fast fading channels with imperfect channel estimation", *IEEE Trans. Signal Process.*, vol. 62, pp. 3874–3886, Aug. 2014.

[78] A. C. Cirik, S. Biswas, S. Vuppala, and T. Ratnarajah, "Robust transceiver design for full duplex multi-user MIMO systems," *IEEE Wireless Commun. Lett.*, vol. 5, no. 3, pp. 260–263, Jun. 2016.

[79] A. Ghosh, J. Zhang, J. G. Andrews, and R. Muhamed, *Fundamentals of LTE.* Englewood Cliffs, NJ, USA: Prentice-Hall, 2010.

[80] H. Tang, Z. Ding and B. C. Levy, "Enabling D2D communications through neighbor discovery in LTE cellular networks," *IEEE Trans. Signal Process.*, vol. 62, no. 19, pp. 5157–5170, Oct. 2014.

[81] K. Lee, W. Kang, and H.-J. Choi, "A practical channel estimation and feedback method for device-to-device communication in 3GPP LTE system," in *Proc. 8th ACM Int. Conf. on Ubiquitous Inf. Management and Commun. (ICUIMC)*, Jan. 2014.

[82] W. Namgoong, "Modeling and analysis of nonlinearities and mismatches in AC-coupled direct-conversion receiver," *IEEE Trans. Wireless Commun.*, vol. 4, pp. 163–173, Jan. 2005.

[83] H. Suzuki, T. V. A. Tran, I. B. Collings, G. Daniels, and M. Hedley, "Transmitter noise effect on the performance of a MIMO-OFDM hardware implementation achieving improved coverage," *IEEE J. Sel. Areas Commun.*, vol. 26, pp. 867–876, Aug. 2008.

[84] Q. Shi, M. Razaviyayn, Z.-Q. Luo, and C. He, "An iteratively weighted MMSE approach to distributed sum-utility maximization for a MIMO interfering broadcast channel," *IEEE Trans. Signal Process.*, vol. 59, no. 9, pp. 4331–4340, Apr. 2011.

[85] D. Nguyen and M. Krunz, "Power-efficient spatial multiplexing for multi-antenna MANETs," *IEEE Int. Conf. Commun. (ICC)*, pp. 4016–4020, June 2012.

[86] K. T. Truong and R. W. Heath Jr., "Joint transmit precoding for the relay interference broadcast channel," *IEEE Trans. Veh. Technol.*, vol. 62, no. 3, pp. 1201–1215, Mar. 2013.

[87] E. Chiu, V. K. N. Lau, H. Huang, T. Wu, and S. Liu, "Robust transceiver design for K-pairs quasi-static MIMO interference channels via semidefinite relaxation," *IEEE Trans. Wireless Commun.*, vol. 9, no. 12, pp. 3762–3769, Dec. 2010.

[88] A. Scaglione, P. Stoica, S. Barbarossa, G. B. Giannakis, and H. Sampath, "Optimal designs for space-time linear precoders and decoders," *IEEE Trans. Signal Process.*, vol. 50, no. 5, pp. 1051–1064, May 2002.

[89] D. P. Palomar, J. M. Cioffi, and M. A. Lagunas, "Joint Tx-Rx beamforming design for multicarrier MIMO channels: A unified framework for convex optimization," *IEEE Trans. Signal Process.*, vol. 51, no. 9, pp. 2381–2401, Sept. 2003.

[90] Y. Ye and E. Tse, "An extension of Karmarkar's projective algorithm for convex quadratic programming," *Mathematical Programming*, pp. 157–179, 1989.

[91] X. Zhang, D. P. Palomar, and B. Ottersten, "Statistically robust design of linear MIMO transceivers," *IEEE Trans. Signal Process.*, vol. 56, no. 8, pp. 3678–3689, Aug. 2008.

[92] M. B. Shenouda and T. N. Davidson, "On the design of linear transceivers for multiuser systems with channel uncertainty," *IEEE J. Sel. Areas Commun.*, vol. 26, no. 6, pp. 1015–1024, Aug. 2008.

[93] V. Havary-Nassab, S. Shahbazpanahi, A. Grami, and Z. Q. Luo, "Distributed beamforming for relay networks based on second-order statistics of the channel state information," *IEEE Trans. Signal Process.*, vol. 56, no. 9, pp. 4306–4316, Sept. 2008.

[94] G. Zheng, S. Ma, K. Kit Wong, and T.-S. Ng, "Robust beamforming in cognitive radio," *IEEE Trans. Wireless Commun.*, vol. 9, no. 2, pp. 570–576, Feb. 2010.

[95] J. Maurer, J. Jalden, D. Seethaler, and G. Matz, "Vector perturbation precoding revisited," *IEEE Trans. Signal Process.*, vol. 59, no. 1, pp. 315–328, Jan. 2011.

[96] L. Zhang, Y.-C. Liang, Y. Xin, and H. V. Poor, "Robust cognitive beamforming with partial channel state information," *IEEE Trans. Wireless Commun.*, vol. 8, no. 8, pp. 4143–4153, Aug. 2009.

[97] E. A. Gharavol, Y.-C. Liang, and K. Mouthaan, "Robust linear transceiver design in MIMO ad hoc cognitive radio networks with imperfect channel state information," *IEEE Trans. Wireless Commun.*, vol. 10, no. 5, pp. 1448–1457, May 2011.

[98] Y. Zhang, E. DallAnese, and G. B. Giannakis, "Distributed optimal beamformers for cognitive radios robust to channel uncertainties," *IEEE Trans. Signal Process.*, vol. 60, no. 12, pp. 6495–6508, Dec. 2012.

[99] J. Wang and D. P. Palomar, "Worst-Case robust MIMO transmission with imperfect channel knowledge," *IEEE Trans. Signal Process.*, vol. 57, no. 8, pp. 3086–3100, Aug. 2009.

[100] J. Wang and D. Palomar, "Robust MMSE precoding in MIMO channels with pre-fixed receivers," *IEEE Trans. Signal Process.*, vol. 58, no. 11, pp. 5802–5818, Nov. 2010.

[101] R. A. Horn and C. R. Johnson, *Matrix Analysis*. Cambridge, UK: Cambridge University Press, 1985.

[102] M. Biguesh, S. Shahbazpanahi, and A. B. Gershman, "Robust downlink power allocation in wireless cellular systems," *EURASIP J. Wireless Commun. Net.*, no. 2, pp. 261–272, Dec. 2004.

[103] 3GPP, TR 36.828, "Further enhancements to LTE time division duplex (TDD) for downlink-uplink (DL-UL) interference management and traffic adaptation (Release 11)," June 2012.

[104] DUPLO project, "System scenarios and technical requirements for full-duplex concept," Deliverable D1.1. [Online]. Available: http://www.fp7-duplo.eu/index.php/deliverables.

[105] J. Liu, F. Gao, and Z. Qiu, "Robust transceiver design for downlink multiuser MIMO AF relay systems," *IEEE Trans. Wireless Commun.*, vol. 14, no. 4, pp. 2218–2231, Apr. 2015.

[106] A. Wiesel, Y. C. Eldar, and S. Shamai, "Linear precoding via conic optimization for fixed MIMO receivers," *IEEE Trans. Signal Process.*, vol. 54, pp. 161–176, Jan. 2006.

[107] A. Tolli, M. Codreanu, and M. Juntti, "Minimum SINR maximization for multiuser MIMO downlink with per BS power constraints," *IEEE Wireless Commun. Net. Conf.*, pp. 1144–1149, Mar. 2007.

[108] Y.-F. Liu, Y.-H. Dai, and Z.-Q. Luo, "Max-min fairness linear transceiver design for a multi-user MIMO interference channel," *IEEE Trans. Signal Process.*, vol. 61, no. 9, pp. 2413–2423, May 2013.

[109] D. Lee, G. Li, and S. Tang, "Intercell interference coordination for LTE systems," *IEEE Trans. Veh. Technol.*, vol. 62, no. 9, pp. 4408–4420, Nov. 2013.

[110] D. Lee, G. Y. Li, X. L. Zhu and Y. Fu, "Multistream multiuser coordinated beamforming for cellular networks with multiple receive antennas," *IEEE Trans. Vehicular Techn.*, vol. 65, no. 5, pp. 3072–3085, May 2016.

[111] S. S. Christensen, R. Agarwal, E. Carvalho, and J. M. Cioffi, "Weighted sum rate maximization using weighted MMSE for MIMO-BC beamforming design," *IEEE Trans. Wireless Commun.*, vol. 7, pp. 4792-4799, Dec. 2008.

[112] A. Tajer, N. Prasad, and X.-D. Wang, "Robust linear precoder design for multicell downlink transmission," *IEEE Trans. Signal Process.*, vol. 59, no. 1, pp. 235–251, Jan. 2011.

[113] S. Haykin, *Adaptive Filter Theory*, 5th ed., Prentice Hall, 2013.

[114] E. Karipidis, N. D. Sidiropoulos, and Z.-Q. Luo, "Quality of service and max-min fair transmit beamforming to multiple cochannel multicast groups," *IEEE Trans. Signal Process.*, vol. 56, pp. 1268–1279, Mar. 2008.

[115] E. Dahlman, S. Parkvall, J. Skold, and P. Beming, "3G Evolution: HSPA and LTE For Mobile Broadband," 2nd ed. Netherlands: Elsevier, 2008.

[116] C. Hoymann et al., "A lean carrier for LTE," *IEEE Commun. Mag.*, vol. 51, no. 2, pp. 74–80, Feb. 2013.

[117] U.S. Federal Communications Commission, "Notice of proposed rule making and order," ET Docket No 03-222, Dec. 2003.

[118] S. Haykin, "Cognitive radio: Brain-empowered wireless communications," *IEEE J. Sel. Areas Commun.*, vol. 23, no. 2, pp. 201–220, Feb. 2005.

[119] K. Doppler, M. Rinne, C. Wijting, C. B. Ribeiro, and K. Hugl, "Device-to-device communication as an underlay to LTE-advanced networks," *IEEE Commun. Mag.*, vol. 47, no. 12, pp. 42–49, Dec. 2009

[120] W. O. Oduola, L. Xiangfang, Q. Lijun, and H. Zhu, "Power control for device-to-device communications as an underlay to cellular system," in *Proc. IEEE Int. Conf. Commun. (ICC)*, pp. 5257–5262, June 2014.

[121] X. Qu and C. G. Kang, "An effective interference alignment approach for device-to-device communication underlaying multi-cell interference network," in *Proc. IEEE ICT Convergence*, pp. 219–220, Oct. 2012

[122] H. E. Elkotby, K. M. F. Elsayed, and M. H. Ismail, "Exploiting interference alignment for sum rate enhancement in D2D-enabled cellular networks," in *Proc. IEEE Wireless Commun. Net. Conf. (WCNC)*, pp. 1624–1629, Apr. 2012.

[123] X. Li, Y. Ren, H. Gao, and T. Lv, "Opportunistic interference alignment approach in device-to-device communications underlaying cellular networks," in *Proc. European Signal Process. Conf. (EUSIPCO)*, pp. 1838–1842, Dec. 2016.

[124] L. Yang, W. Zhang, and S. Jin, "Interference alignment in device-to-device LAN underlaying cellular networks," *IEEE Trans. Wireless Commun.*, vol. 14, no. 7, pp. 3715–3723, July 2015.

[125] W. Y. Shin, M. Kim, H. Yi, A. Kim, and B. C. Jung, "Degrees of freedom based on interference alignment with imperfect channel knowledge," *IEICE Trans. Commun.*, vol. E94, no. 12, pp. 3579–3582, Dec. 2011.

[126] J. Thukral and H. Bolcskei, "Interference alignment with limited feedback," in *Proc. IEEE Proc. Int. Symp. Inf. Theory (ISIT)*, pp. 1759–1763, July 2009.

[127] L. T. Berger, A. Schwager, P. Pagani, and D. Schneider, *MIMO Power Line Communications: Narrow and Broadband Standards, EMC, and Advanced Processing*. USA: CRC Press, Feb. 2014.

[128] K. Gomadam, V. R. Cadambe, and S. A. Jafar, "A distributed numerical approach to interference alignment and applications to wireless interference networks," *IEEE Trans. Inf. Theory*, vol. 57, no. 6, pp. 3309–3322, Jun. 2011.

[129] D. Rende, A. Nayagam, K. Afkhamie, L. Yonge, R. Riva, D. Veronesi, F. Osnato, and P. Bisaglia, "Noise correlation and its effect on capacity of inhome MIMO power line channels," in *Proc. IEEE Intl. Symp. Power Line Commun. and Its Applications (ISPLC)*, pp. 60–65, Apr. 2011.

[130] A. Pittolo, A. M. Tonello, and F. Versolatto, "Performance of MIMO PLC in measured channels affected by correlated noise," in *Proc. IEEE Intl. Symp. Power Line Commun. and Its Applications (ISPLC)*, pp. 261–265, Mar. 2014.

[131] A. Schwager, W. Bschlin, H. Hirsch, P. Pagani, N. Weling, J. L. G. Moreno, and H. Milleret, "European MIMO PLT field measurements: Overview of the ETSI STF410 campaign and EMI analysis," in *Proc. IEEE Intl. Symp. Power Line Commun. and Its Applications (ISPLC)*, pp. 298–303, Mar. 2012.

[132] "Setup and statistical results of MIMO PLT channel and noise measurements," *ETSI TR 101 562-3 V1.1.1*, 2012.

[133] T. Gou, C. Wang, and S. A. Jafar, "Aiming perfectly in the dark-blind interference alignment through staggered antenna switching," *IEEE Trans. Signal Process.*, vol. 59, no. 6, pp. 2734–2744, Mar. 2011.

[134] S. A. Jafar, "Blind interference alignment," *IEEE J. Sel. Topics Signal Process.*, vol. 6, no. 3, pp. 216–227, Feb. 2012.

[135] L. T. Berger, A. Schwager, P. Pagani, and D. M. Schneider, "MIMO power line communications," *IEEE Commun. Surveys Tut.*, vol. 17, no. 1, pp. 106–124, 2015.

[136] D. Schneider, J. Speidel, L. Stadelmeier, and D. Schill, "Precoded spatial multiplexing MIMO for inhome power line communications," in *IEEE Global Commun. Conf. (GLOBECOM)*, pp. 1–5, Nov. 2008.

[137] F. Versolatto and A. Tonello, "An MTL theory approach for the simulation of MIMO power-line communication channels," *IEEE Trans. Power Del.*, vol. 26, no. 3, pp. 1710–1717, Jul. 2011.

[138] F. Gruber and L. Lampe, "On PLC channel emulation via transmission line theory," in *Proc. IEEE Intl. Symp. Power Line Commun. and Its Applications (ISPLC)*, pp. 178–183, Mar. 2015.

[139] T. Banwell and S. Galli, "On the symmetry of the power line channel," in *Proc. Intl. Symp. Power Line Commun. and Its Applications (ISPLC)*, pp. 325–330, Apr. 2001.

[140] L. Lampe and A. J. H. Vinck, "Cooperative multihop power line communications, in *Proc. IEEE Intl. Symp. Power Line Commun. and Its Applications (ISPLC)*, pp. 1–6, Mar. 2012.

[141] A. Tölli, H. Pennanen, and P. Komulainen, "Decentralized minimum power multi-cell beamforming with limited backhaul signaling," *IEEE Trans. Wireless Commun.*, vol. 10, no. 2, pp. 570–580, Feb. 2011.

[142] Z. Xu and T. Zemen, "Time-variant channel prediction for interference alignment with limited feedback," *IEEE Int. Conf. Commun. (ICC)*, pp. 653–658, June 2014.

[143] S. Teodoro, A. Silva, R. Dinis, and A. Gameiro, "Low-bit rate feedback strategies for iterative IA-precoded MIMO-OFDM-based systems," *The Scientific World Journal*, vol. 2014, Article ID 619454, 11 pages, 2014. doi:10.1155/2014/619454

Appendix A

Appendix for Additional Publications

A.1 Additional Publications from Ph.D. Research (not included in this thesis)

- Md. Jahidur Rahman and Lutz Lampe, "Robust MSE-based Transceiver Optimization for Downlink Cellular Interference Alignment," in *Proceedings of IEEE International Conference on Communications (ICC), Track: Cognitive Radio and Networks*, pp. 4624–4629, Sept. 2015.

- Md. Jahidur Rahman, Moslem Noori, and Lutz Lampe, "A Low-Complexity Design for Robust SINR Fairness in MIMO Interference Networks," in *Proceedings of IEEE Wireless Communications and Networking Conference (WCNC), Track: PHY and Fundamentals*, pp. 64–69, Mar. 2015.

Appendix B

Appendix for Chapter 3

B.1 Replacement of the Unit Norm Constraint in (3.16)

We recognize that the new (restrictive) constraint contains the phase information, where the original constraint unit norm constraint does not contain any phase information. However, we also note that the phase information in the new constraint does not change the objective function in (3.18) nor other constraints in (3.20) and (3.21). To show this, let us consider that $(\mathbf{V}^X_{i_k,m})^*,\ i_k \in \mathcal{I},\ m \in \mathcal{M},\ X \in \{\mathrm{UL}, \mathrm{DL}\}$ is the optimal solution of the problem in (3.18)–(3.21) obtained using the new restrictive constraint. Since the new restrictive constraint involves a phase rotation, let us consider that there is a phase rotation, $e^{j\theta^X_{i_k,m}},\ i_k \in \mathcal{I},\ m \in \mathcal{M},\ X \in \{\mathrm{UL}, \mathrm{DL}\}$ to the optimal solution if one were to use the original unit norm constraint. If we can show that the new optimal solution, $(\mathbf{V}^X_{i_k,m})^* e^{j\theta^X_{i_k,m}}$, does not change the optimization objective or other constraints, we can claim that $(\mathbf{V}^X_{i_k,m})^*$ is also optimal solution of the original problem.

Note that the optimization objective in (3.18), and constraints (3.20) and (3.21) involve quadratic forms of the optimization variables, $\mathbf{V}^X_{i_k,m}$. Therefore, once we replace them with $(\mathbf{V}^X_{i_k,m})^* e^{j\theta^X_{i_k,m}}$, the phase information $e^{j\theta^X_{i_k,m}}$ that is involved with $(\mathbf{V}^X_{i_k,m})^*$ will vanish. Therefore, we conclude that the new constraint does not impact

the optimization objective nor other constraints.

B.2 Proof of Convergence of Algorithm 1

Let $f(\mathbf{V}, \mathbf{U})$ be the optimization objective in (3.18). Then, for any feasible value of $\mathbf{V}$ and $\mathbf{U}$ (i.e., constraints are satisfied), the Lagrangian $\mathcal{L}(\mathbf{V}, \mathbf{U}, \boldsymbol{\lambda}, \boldsymbol{\Delta})$ in (3.18) is equal to $f(\mathbf{V}, \mathbf{U})$. Since $\mathcal{L}(\mathbf{V}, \mathbf{U}, \boldsymbol{\lambda}, \boldsymbol{\Delta})$ is convex for $\mathbf{V}$ when all other variables are fixed, a feasible optimal precoding matrix $\mathbf{V}^{*,[n]}$ at the nth iteration will be the minimum of the objective with respect to a given receive filter $\mathbf{U}^{[n]}$, i.e.,

$$\mathcal{L}\left(\mathbf{V}^{*,[n]}, \mathbf{U}^{[n]}, \boldsymbol{\lambda}, \boldsymbol{\Delta}\right) = \min_{\mathbf{V}} \mathcal{L}\left(\mathbf{V}, \mathbf{U}^{[n]}, \boldsymbol{\lambda}, \boldsymbol{\Delta}\right). \tag{B.1}$$

The same observation can be made for the receive filter, $\mathbf{U}$, i.e.,

$$\mathcal{L}\left(\mathbf{V}^{[n]}, \mathbf{U}^{*,[n+1]}, \boldsymbol{\lambda}, \boldsymbol{\Delta}\right) = \min_{\mathbf{U}} \mathcal{L}\left(\mathbf{V}^{[n]}, \mathbf{U}, \boldsymbol{\lambda}, \boldsymbol{\Delta}\right). \tag{B.2}$$

Combining observations made in (B.1) and (B.2), we can make the following inequality statement:

$$\begin{aligned} \mathcal{L}\left(\mathbf{V}^{*,[n+1]}, \mathbf{U}^{*,[n+1]}, \boldsymbol{\lambda}, \boldsymbol{\Delta}\right) &\leq \mathcal{L}\left(\mathbf{V}^{*,[n]}, \mathbf{U}^{*,[n+1]}, \boldsymbol{\lambda}, \boldsymbol{\Delta}\right) \\ &\leq \mathcal{L}\left(\mathbf{V}^{*,[n]}, \mathbf{U}^{[n]}, \boldsymbol{\lambda}, \boldsymbol{\Delta}\right). \end{aligned} \tag{B.3}$$

If we iterate between computing optimal precoding matrix and receive filter, (B.3) guarantees that the Lagrangian is always updated with an equal or smaller value. The Lagrangian with any feasible value of $\mathbf{V}$ and $\mathbf{U}$ is lower bounded by zero; therefore, the algorithm guarantees that the objective function converges to a limit point.

Appendix C

Appendix for Chapter 4

C.1 ABCD Matrix Representation

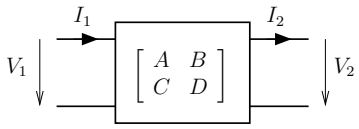

Figure C.1: ABCD-matrix representation of a two-port network.

The ABCD-matrix representation of a two-port network relates the voltages and currents identified in Fig. C.1 as

$$\begin{bmatrix} V_1 \\ I_1 \end{bmatrix} = \begin{bmatrix} A & B \\ C & D \end{bmatrix} \begin{bmatrix} V_2 \\ I_2 \end{bmatrix} . \tag{C.1}$$

The same ABCD parameters can be used when input and output are swapped, i.e., transmission in the other direction is considered. Then we have

$$\begin{bmatrix} V_2 \\ -I_2 \end{bmatrix} = \frac{1}{AD - BC} \begin{bmatrix} D & B \\ C & A \end{bmatrix} \begin{bmatrix} V_1 \\ -I_1 \end{bmatrix} . \tag{C.2}$$

If the reciprocity property holds, $AD - BC = 1$ is true. Hence, in this case (C.2)

simplifies to

$$\begin{bmatrix} V_2 \\ -I_2 \end{bmatrix} = \begin{bmatrix} D & B \\ C & A \end{bmatrix} \begin{bmatrix} V_1 \\ -I_1 \end{bmatrix} . \tag{C.3}$$

We note that reciprocity can be assumed for power line networks, where the overall ABCD-matrix is a cascade of reciprocal ABCD matrices, e.g. [139].

C.2 Property of the PLC Keyhole Channel

We consider the model in Fig. 4.11 and assume that either nodes n_1 and n_2 are transmitting simultaneously, or that source and load impedance are identical for those two nodes, so that $Z_1 = Z_{1,\mathrm{S}}$ and $Z_2 = Z_{2,\mathrm{S}}$. In this appendix, we show that then the ratio of the channel frequency responses H_{13} and H_{23} is independent of the network elements located between node n_B and node n_3.

From (4.29) and (4.30) we can write the ratio as

$$\frac{H_{13}}{H_{23}} = \frac{H_{1B}}{H_{2B}} . \tag{C.4}$$

Let us consider the numerator H_{1B} first. Starting from (4.26) we obtain

$$H_{1B} = \frac{1}{A_1 + C_1 Z_{1,\mathrm{S}} + (B_1 + D_1 Z_{1,\mathrm{S}})/Z_{1B}} \tag{C.5}$$

$$\overset{(a)}{=} \frac{1}{A_1 + C_1 Z_{1,\mathrm{S}} + (B_1 + D_1 Z_{1,\mathrm{S}}) \left(\frac{1}{Z_{B2}} + \frac{1}{Z_{B3}} \right)} \tag{C.6}$$

$$\overset{(b)}{=} \frac{1}{(B_1 + D_1 Z_{1,\mathrm{S}}) \left(\frac{1}{Z_{B1}} + \frac{1}{Z_{B2}} + \frac{1}{Z_{B3}} \right)} , \tag{C.7}$$

where (a) follows from substituting Z_{1B} using (4.25) and (b) from (4.24). Applying

the same transformations to H_{2B} leads to

$$H_{2B} = \frac{1}{(B_2 + D_2 Z_{2,\mathrm{S}}) \left(\frac{1}{Z_{B2}} + \frac{1}{Z_{B1}} + \frac{1}{Z_{B3}} \right)} \,. \tag{C.8}$$

Finally, substituting (C.7) and (C.8) into (C.4) gives us

$$\frac{H_{13}}{H_{23}} = \frac{H_{1B}}{H_{2B}} = \frac{B_2 + D_2 Z_{2,\mathrm{S}}}{B_1 + D_1 Z_{1,\mathrm{S}}} \,, \tag{C.9}$$

which only depends on the parameters of the network elements between nodes n_1 and n_B and nodes n_2 and n_B, respectively.